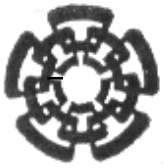


**Centro de Investigación y de Estudios Avanzados del Instituto Politécnico Nacional**

UNIDAD ZACATENCO
DEPARTAMENTO DE FÍSICA


# “Estudio del proceso de dispersión luz-axion”

**Tesis que presenta**


## Ivan Pérez Castro


para obtener el Grado de

Maestro en Ciencias

en la Especialidad de

Física

Director de tesis: **Dr. Abdel Pérez Lorenzana**

Ciudad de México Enero, 2024

CENTRO DE INVESTIGACION Y DE ESTUDIOS AVANZADOS
DEL INSTITUTO POLITECNICO NACIONAL

UNIT ZACATENCO
PHYSICS DEPARTMENT

# "Study of the light-axion scattering process"

**Thesis submitted by**

**Ivan Pérez Castro**

In order to obtain the

Master of Science

degree, speciality in

Physics

Supervisor: **Dr. Abdel Pérez Lorenzana**

Mexico City January, 2024.

*“Life need not be easy, provided only that it is not empty.”*
-**Lise Meitner**

# Dedicatoria

*Dedico esta tesis con profundo agradecimiento y cariño a mi madre, Carolina Castro Castro. Su inquebrantable apoyo ha sido la luz que iluminó cada paso de esta travesía académica, convirtiendo esta etapa de mi vida en una experiencia no solo educativa, sino también enriquecedora y amena. Su amor y aliento han sido el motor que ha impulsado mi perseverancia. Gracias por ser mi inspiración constante y por ser la fuerza que hizo posible este logro.*

# Agradecimientos

A mi gran amigo Héctor Hugo Aguilera Trujillo, quiero expresar mi profundo agradecimiento por la invaluable ayuda que me ha brindado y por todo lo que me ha enseñado en los últimos años, especialmente durante nuestras extensas discusiones sobre física. Sin duda, mi experiencia en el Cinvestav ha sido increíble gracias a la oportunidad de conocerle.

A Miguel Alfonso Zapata de la Cruz, a quien agradezco por su continuo apoyo a lo largo de los últimos años y, en particular, durante el inicio mi trayectoria en la maestría. Aprecio enormemente los buenos momentos y su contribución significativa para ayudarme a obtener mi primer trabajo.

A mis queridos amigos Uriel Aquino Moreno, Pablo Fajardo Gutiérrez y Rubén Velázquez, agradezco sinceramente todos estos años de amistad y los momentos memorables compartidos. Sin duda, muchos de mis mejores días han sido a su lado.

Agradezco a mi amigo Joshua Lara por el tiempo y el apoyo que me brindó. Sin su orientación, es probable que no habría logrado completar este trabajo.

A mi otro grupo de buenos amigos del Cinvestav, en especial a Erick García Rodríguez, le agradezco por sus brillantes ideas compartidas y el apoyo brindado para mi ingreso a la maestría, de quien aprendí las bases de la electrodinámica. A Noé Tepec Tinoco, le expreso mi agradecimiento por todo el respaldo ofrecido a lo largo de la vida y, sobre todo, por orientarme en la toma de decisiones en momentos difíciles. A mi amigo Oscar Isaac Pérez Ruiz, le doy las gracias por mostrarme que se puede equilibrar el trabajo y disfrutar de la vida, una lección en la que aún estoy trabajando.

A mi hermana Nancy Pérez Castro, mi agradecimiento por soportar pacientemente las horas dedicadas a hablar de física y por el apoyo que ha brindado en mi carrera académica. A mi pequeña hermana Ruth Pérez Castro, le aprecio el esfuerzo que hace para no aburrirse cuando le comparto historias y conceptos relacionados con la física.

A mi reciente amigo Fabián Nieto Castellanos, gracias por todo el apoyo en mis últimos proyectos durante la maestría. A las personas que ya no están, un especial recuerdo para la Srta. Galván por los momentos gratos que compartimos en el pasado.

Agradezco al Consejo Nacional de Humanidades Ciencias y Tecnologías (CONAHCyT) por el apoyo económico que recibí para la realización de mis estudios de maestría con la beca ref: 799763.

Al Cinvestav y, en especial, al Departamento de Física, agradezco el espacio brindado para llevar a cabo mi trabajo. Quiero destacar especialmente a Mariana del Castillo Sánchez por su increíble apoyo en todos los trámites burocráticos y su paciencia durante mis estudios.

Al Dr. Pablo Roig Garcés, mi profundo agradecimiento por el invaluable conocimiento que ha compartido conmigo y por todo el apoyo que he recibido de su parte durante mi estadía en la maestría. Asimismo, agradezco al Dr. Omar Miranda Romagnoli por su apoyo en la presentación de este trabajo y por sus consejos a lo largo de mi trayectoria académica.

Finalmente, deseo extender mi sincero agradecimiento al Dr. Abdel Pérez Lorenzana, mi asesor, por el tiempo y la dedicación brindados durante la realización de esta tesis de maestría, así como por el continuo apoyo que he recibido a lo largo de mi trayectoria académica. Además, al Dr. Tonatiuh Matos Chassin, le agradezco la propuesta de explorar el proceso de dispersión presentado en esta tesis.

# Abstract

The ΛCDM model has had great success in explaining the observed large-scale structures of the Universe, as well as the main properties of galaxies that form within dark matter haloes. At scales larger than $1\,\mathrm{Mpc}$, the observed structure is consistent with cold dark matter particles interacting purely through gravitational force. However, at scales smaller than $1\,\mathrm{Mpc}$, where structure formation becomes strongly nonlinear, problems arose within the ΛCDM model, known as "Small-scale problems".

To address these problems, solutions have been proposed that involve modifications to the linear predictions through the nature of the dark matter particle, such as Warm Dark Matter (WDM). On the other hand, to solve the Strong CP problem, an additional pseudo-goldstone boson called axion is introduced to the Standard Model of Particle Physics, whose only non-derivative coupling is with the topological QCD charge and is suppressed by the scale $f_a$. The axion is postulated as a good candidate for dark matter, and certain small-scale problems can be addressed by imposing conditions on its De'Broglie wavelength in terms of its mass $m_a$ and velocity $v_a$.

By relaxing the QCD axion constraints, one can have more general classes of dark matter models with Axion-Like Particles (ALPs), which arise in various extensions of the Standard Model.

In this thesis, the coupling between an axion and two photons is utilized to study their interaction in a way different from the usual approach, establishing the photon-axion scattering process at the tree level. This process follows the kinematics of the well-known Compton scattering process, and the thesis focuses on examining what occurs in the low-energy and high-energy scattering regimes. Although the cross-section of this process is expected to be very small, the relevance lies in the abundance of axions in the universe, which could lead to the observation of this process in astrophysical events. For example, the interaction of photons with the halo of axions that surrounds our galaxy. We provide strong evidence that renders this interaction negligible.

# Contents

# Introduction

In recent decades, advances in astronomical observations and high-energy experiments have provided valuable information about our Universe. One of the most significant enigmas is the presence of non-baryonic energy components in the cosmos. Conventionally, these components are divided into two categories: dark matter and dark energy. Dark energy shares similarities with Einstein's cosmological constant, which drives the accelerated expansion of today's universe. Although accelerated expansion has been confirmed by observations, the existence of a constant energy density is still subject to debate.

On the other hand, the existence of dark matter is becoming increasingly evident. The total density of matter in the universe, measured through various methods [1], turns out to be 5-6 times greater than the density of baryon matter obtained by observing the abundance of light elements [2]. This suggests that a large fraction of the cosmic matter density is composed of a non-baryonic component. This conclusion is further confirmed by the recent accurate measurement of the cosmic microwave background (CMB) by the WMAP satellite [3]. These observations strongly support the existence of non-baryonic matter, which interacts virtually only through gravitational force with ordinary matter.

The existence of dark matter cannot be explained within the framework of the standard model of particle physics. This fact motivates us to consider some new physics beyond the standard model. So far, several models of dark matter particles have been proposed [see, for example, [2] for a review]. One of the most intriguing candidates is the axion [4] [5]. The axion is a hypothetical particle that arises as a consequence of the Peccei-Quinn (PQ) mechanism, possibly the simplest solution to the strong CP problem of quantum chromodynamics (QCD) [6]. This mechanism introduces a global symmetry $U(1)_{\rm PQ}$ (called PQ symmetry) that must spontaneously break at some high energy scale (larger than the electroweak scale). The spontaneous breaking of this global symmetry predicts the existence of a (pseudo) Nambu-Goldstone boson, identified as the axion.

Initially, the axion was not considered a candidate for dark matter when it was proposed. In the original model, the axion was "visible" and provided some predictions for laboratory experiments. Unfortunately, no signal was observed, and the prototype axion model was discarded shortly after its proposal. However, it was argued that models with symmetry breaking at higher energies could still evade experimental constraints. The key is that interactions between axions and other fields are suppressed by a large factor of the symmetry breaking scale, about $\frac{1}{f_a}$. These models are known as "invisible" axions due to the smallness of their coupling with matter. This invisibility carries a cosmological consequence: coherent, quasi-stable fields of oscillating axions play a role in the dark matter of the universe [7] [8]. Furthermore, since these axions are produced non-thermally, they are "cold" in the sense of being highly non-relativistic. This property aligns with the cold dark matter scenario motivated by the study of large-scale structure formation [9].

The behavior of dark matter axions is closely related to the early history of the universe. In particular, the cosmological phase transition associated with spontaneous symmetry breaking provides some implications for the physics of axion dark matter. There are two relevant phase transitions: the PQ phase transition, corresponding to the spontaneous breaking of the $U(1)_{\rm PQ}$ symmetry, and the QCD phase transition, corresponding to the spontaneous breaking of the chiral symmetry of quarks. Axions are produced at the PQ phase transition and then gain mass due to the non-perturbative ef-

fect at the QCD phase transition. A notable feature of this sequence of phase transitions is the prediction of the formation of topological defects (see [10] for a review).

In this thesis, a general coupling between the axion or axion-like particles with two photons is studied, caused by its mixing with neutral pions in the context of quantum chromodynamics. This coupling provides the basis for studying the Compton scattering process using an ALP/Axion instead of an electron at the tree level. The differential cross-section is examined and the conditions under which this process is relevant for astrophysical calculations are reviewed. This relevance is closely linked to the mode of production of axions since the mass ranges allowed for the axion to influence the phenomenology of this process. Furthermore, the possibility of having inverse Compton scattering in this scenario is discussed, providing a more complete view of the astrophysical implications of the interaction between axions and photons.

# Chapter 1
# Standard Model

*"I think nature's imagination Is so much greater than man's, she's never going to let us relax."*
— **Richard P. Feynman**

The Standard Model of Particle Physics simply known as the Standard Model (SM) groups together two important models: Quantum Chromodynamics (QCD) and the Glashow, Weinberg, and Salam model for electroweak interactions (sometimes called the Electroweak Standard Model). To date, the SM has had great success due to its great predictive scope and various successes in various experiments.

The Standard Model can be divided into three sectors: that of gauge bosons, that of fermions, and that of Higgs. This model is itself a field theory based on the gauge symmetry group [11][12][13]

$$G_{SM} = SU(3)_C \times SU(2)_L \times U(1)_Y \,, \tag{1.1}$$

which is the direct product of the symmetry groups $SU(3)_C$ that describes the strong interactions and $SU(2)_L \times U(1)_Y$ that describes the electroweak interactions. Furthermore, the symmetry group of electromagnetic interactions $U(1)_{em}$ is a subgroup of the group $SU(2)_L \times U(1)_Y$ in this sense, we say that weak and electromagnetic interactions are unified or rather, partially unified. Some of the important characteristics of the interactions described by SM are: electromagnetic interactions have an infinite interaction range, while weak interactions are short range ($\sim 10^{-3}$ fm); this is because the weakly interacting carrier bosons have masses on the order of $80$ GeV, while strong interactions have an interaction range of $\sim 1$ fm.

This chapter presents an overview of the SM, with special emphasis on the $CP$ violation and the observations that indicate the incompleteness of this model.

## 1.1 The content of matter: a theory based on symmetry

The Standard Model consists of three fundamental sectors: the fermionic sector, the bosonic sector, and the scalar sector, also known as the Higgs sector.

In the first sector, all Standard Model fermions are considered to be organized in irreducible representations of the gauge symmetry group $G_{SM}$, as described in equation (1.1). This sector encompasses three generations, or what are commonly called flavors or families of fermions. These generations share identical properties, except for their masses. It is important to note that the inclusion of three fermion families in the theory is a phenomenological decision, since the Standard Model itself does not offer a prediction about the number of fermion generations. However, theoretical and experimental arguments can be used to justify this choice. For example, to satisfy the anomaly cancellation conditions, the left fermions must be grouped into doublets of $SU(2)_L$, implying the need for three families of fermions. Furthermore, recent measurements of the decay width of the $Z$ boson have allowed us to determine that the number of active neutrinos with masses less than $45$ GeV is $N_\nu = 2.9963 \pm 0.0074$ [14]. In the SM, neutrinos are initially considered to have

zero masses and do not have a right-hand chirality component. However, more than two decades ago it was confirmed that the masses of neutrinos are considerably small compared to the masses of other particles in the SM [15][16].

The bosonic sector includes several types of particles. First, we have the eight gluons $g_\alpha$, which play the role of gauge bosons in the context of the color group $SU(3)_C$. Additionally, the four gauge bosons are part of this sector: $W^\pm$, $Z^0$ and $\gamma$. The latter are the particles responsible for mediating the electroweak interactions through the $SU(2)_L$ and $U(1)_Y$ groups [17].

Regarding the physical properties of these gauge bosons, it is important to highlight that gluons are massless and electrically neutral, but they have a color charge. This distinctive feature implies that gluons not only interact with quarks but also exhibit self-interactions, which differentiates them from other particles in the Standard Model. The $W^\pm$ and $Z$ bosons are massive particles that also have mutual interactions between them. In particular, the $Z$ boson is electrically neutral, in contrast to the $W^\pm$ bosons, which carry an electric charge of $Q_{em} = \pm 1$, respectively. Finally, the $\gamma$ photon is characterized by being electrically neutral, having no mass, and lacking self-interactions.

Below, we will briefly describe the Standard Model. We identify fermion generations by their corresponding fermionic fields, denoted $\psi_i$, with $i = 1, 2, 3$, where $i$ represents the flavor or family index. The numbering of the families follows a hierarchy based on the magnitude of their masses, except for neutrinos, whose mass hierarchy is not yet known. Consequently, the first family is composed of the lightest fermions, and in the case of the electron, it is accompanied by its respective neutrino.

$$\begin{pmatrix} e \\ \nu_e \end{pmatrix} \qquad \text{and} \qquad \begin{pmatrix} u \\ d \end{pmatrix} . \tag{1.2}$$

The SM for a single family is a completely self-contained and self-consistent theory. However, in nature, we observe the existence of two other families, which are:

- second family

$$\begin{pmatrix} \mu \\ \nu_\mu \end{pmatrix} \qquad \text{and} \qquad \begin{pmatrix} c \\ s \end{pmatrix} . \tag{1.3}$$

- third family

$$\begin{pmatrix} \tau \\ \nu_\tau \end{pmatrix} \qquad \text{and} \qquad \begin{pmatrix} t \\ b \end{pmatrix} . \tag{1.4}$$

These families exhibit properties that resemble those of the first family and are integrated into the model without fully explaining the reason behind this phenomenal repetition. In this way, the Standard Model for three families is created, which continues to maintain its coherence and internal consistency. Importantly, the corresponding antiparticles are also included, leading to the formation of antifamilies.

The three generations of fermions that make up matter are divided into five unique gauge group representations, each identified by the following quantum numbers [11][12]:

$$\left(1, 2, -1\right), \quad \left(3, 2, \frac{1}{6}\right), \quad \left(1, 1, -1\right), \quad \left(3, 1, \frac{2}{3}\right), \quad \left(3, 1, -\frac{1}{3}\right) . \tag{1.5}$$

The terms inside the parentheses indicate the transformation properties when subjected to the actions of the groups $SU(3)_C$, $SU(2)_L$ and $U(1)_Y$. In this notation, electric charge is defined as follows

$$Q_{em} = T^3 + Y\,, \tag{1.6}$$

where $Y$ represents the hypercharge and $T^3$ is the projection on the weak isospin. The fermionic fields $\psi$ can be characterized by their right-hand chirality components $\psi_R$ and left-hand chirality $\psi_L$ as follows [12][18]

$$\psi_{R,L} = P_{R,L}\psi = \left(\frac{1 \pm \gamma_5}{2}\right)\psi, \quad \bar{\psi}_{L,R} = \bar{\psi}P_{R,L} = \bar{\psi}\left(\frac{1 \pm \gamma_5}{2}\right)\,. \tag{1.7}$$

In the context of the SM, it is important to note that the right and left fermions have different transformation properties when applied to the gauge group $G_{SM}$. For example, under the influence of the group $SU(2)_L$, the right and left fields are transformed as doublets and singlets, respectively. Therefore, we use the following notation

$$Q_L^i = \begin{pmatrix} u_L^i \\ d_L^i \end{pmatrix}, \quad l_L^i = \begin{pmatrix} \nu_L^i \\ e_L^i \end{pmatrix}\,. \tag{1.8}$$

And for the singlets

$$u_R^i, \quad d_R^i \quad \text{y} \quad l_R^i \tag{1.9}$$

here $i = 1, 2, 3$ are the indices that denote the generations, for example $u_L^i \in \{u_L, c_L, t_L\}$.

The subscripts $L$ and $R$ refer to the left and right chirality eigenstates, while the index $i = 1, 2, 3$ are the indices that denote the generations, for example, $u_L^i \in \{u_L, c_L, t_L\}$. In this notation, the quantum number assignment presented in the equation (1.5) is expressed as follows

$$l_L^i(1,2)_{-\frac{1}{2}}, \quad Q_L^i(2,3)_{\frac{1}{6}} \quad l_R^i(1,1)_{-1}, \quad u_R^i(1,1)_{\frac{2}{3}}, \quad d_R^i(3,1)_{-\frac{1}{3}}\,. \tag{1.10}$$

In the following table, we summarize what was discussed above [1].

| Family | $l_L^i(1,2)_{-\frac{1}{2}}$ | $Q_L^i(2,3)_{\frac{1}{6}}$ | $l_R^i(1,1)_{-1}$ | $u_R^i(1,1)_{\frac{2}{3}}$ | $d_R^i(3,1)_{-\frac{1}{3}}$ |
|---|---|---|---|---|---|
| 1 | $\begin{pmatrix}\nu_{eL}\\ e_L\end{pmatrix}$ | $\begin{pmatrix}u_L\\ d_L\end{pmatrix}$ | $e_R$ | $u_R$ | $d_R$ |
| 2 | $\begin{pmatrix}\nu_{\mu L}\\ \mu_L\end{pmatrix}$ | $\begin{pmatrix}c_L\\ s_L\end{pmatrix}$ | $\mu_R$ | $c_R$ | $s_R$ |
| 3 | $\begin{pmatrix}\nu_{\tau L}\\ \tau_L\end{pmatrix}$ | $\begin{pmatrix}t_L\\ b_L\end{pmatrix}$ | $\tau_R$ | $t_R$ | $b_R$ |

Table 1.1: Matter content of the Standard Model.

The matter content in the model, as presented in the table 1.1, encompasses the complete list of fields necessary to describe the interactions observed in elementary particles, together with the corresponding gauge fields. These charge assignments have been rigorously tested with the highest level of reliability for light fermions [2].

[1] This is a way to visualize the matter content of the standard model.

On the other hand, the Higgs sector induces a spontaneous breaking of the gauge symmetry, that is,

$$SU(3)_C \times SU(2)_L \times U(1)_Y \to SU(3)_C \times U(1)_{em}\,. \tag{1.11}$$

This spontaneous breaking of the electroweak symmetry is carried out through the so-called Higgs mechanism, which generates the masses of the electroweak gauge bosons and fermions, by the experimental values. Consequently, there is a new particle, the Higgs boson, which was discovered experimentally a decade ago [19][20]. On the other hand, one of the open problems in the Standard Model is knowing the representation of the Higgs boson that will manifest itself in the experiments. This is because the Higgs mechanism is not unique, and There are many representations of the Higgs boson that correctly describe the dynamics of the spontaneous breaking of the electroweak symmetry. However, the minimal version, included in the Standard Model, consists of a complex scalar doublet [13] [18]

$$\phi = \begin{pmatrix} \phi^+ \\ \phi^0 \end{pmatrix}\,, \tag{1.12}$$

where $\phi^+$ and $\phi^0$ are complex scalar fields, charged and neutral respectively. As mentioned above, this field $\phi$ is a singlet $SU(3)_C$, doublet of $SU(2)_L$ and has hypercharge $+1/2$.

The table 1.1 shows that neutrinos are fermions that lack strong, electromagnetic interactions (see Eq. (1.6)). This implies that neutrinos are singlets in the context of the group $SU(3)_C \times U(1)_{em}$. Additionally, active neutrinos, also known as neutrinos that participate in weak interactions, are found in lepton doublets. A notable feature of the Standard Model is that the gauge symmetry group $G_{SM}$ (c.f. Ec. (1.1)) and the matter content represented in the table 1.1 exhibit a global accidental symmetry [11][12]

$$G_{SM}^{Global} = U(1)_B \times U(1)_{L_e} \times U(1)_{L_\mu} \times U(1)_{L_\tau}\,, \tag{1.13}$$

where $U(1)_B$ is the symmetry associated with the baryon number and $U(1)_{L_e}, U(1)_{L_\mu}$ and $U(1)_{L_\tau}$ are the three symmetries of lepton flavor, with the total lepton number given by $L = L_e + L_\mu + L_\tau$. This symmetry is called accidental because it was not imposed, it is a consequence of the gauge symmetry group $G_{SM}$ and the representations of physical states.

## 1.2 The Lagrangian density of the Standard Model

The complete Lagrangian density of the SM, denoted $\mathcal{L}_{SM}$, is characterized as the most general renormalizable Lagrangian density that is consistent with both the gauge symmetry group $SU(3)_C \times SU(2)_L \times U(1)_Y$ as with the matter content previously described. Its construction is based on a sum of the following terms:

$$\mathcal{L}_{SM} = \mathcal{L}_{KG} + \mathcal{L}_{Kf} + \mathcal{L}_H + \mathcal{L}_Y + \mathcal{L}_{FG} + \mathcal{L}_{FP}\,, \tag{1.14}$$

where each term represents:

- $\mathcal{L}_{KG}$, corresponds to the kinetic energy of the gauge fields.
- $\mathcal{L}_{Kf}$, corresponds to the kinetic energy of the fermions.
- $\mathcal{L}_H$, corresponds to the kinetic and potential energy of the Higgs field.

- $\mathcal{L}_Y$, contains the terms of the Yukawa couplings.
- $\mathcal{L}_{FG}$, Lagrangian density that fixes the gauge.
- $\mathcal{L}_{FP}$, Faddeev-Popov Lagrangian density.

To preserve the gauge invariance of the kinetic terms against transformations of the gauge symmetry group $G_{SM}$, the covariant derivative must take the following form:

$$D_\mu = \partial_\mu - ig_s G_\mu^a T^a - igW_\mu^b \tau^b - ig' B_\mu Y \,, \tag{1.15}$$

In this context, the fields $G_\mu^a$ correspond to the eight gluons, $W_\mu^b$ represent the three intermediate bosons of the weak interactions, and $B_\mu$ is the hypercharge boson. The generators $T^a$ belong to the group $SU(3)_C$ of strong interactions and can be expressed through the Gell-Mann matrices, denoted as $\frac{1}{2}\lambda^a$ when applied to triplets. For their part, the generators $\tau^b$ belong to the group $SU(2)_L$ of weak interactions and are represented by the Pauli matrices, with the notation $\frac{1}{2}\sigma^b$, when applied to doublets. Finally, $Y$ refers to the charge associated with the group $U(1)_Y$ [21].

With the help of the covariant derivative, Eq. (1.15), the Lagrangian density of the Standard Model fields can be constructed as follows

$$\begin{aligned}\mathcal{L}_{SM} =& \bar{l}_L i\gamma^\mu D_\mu l_L + \bar{e}_R i\gamma^\mu D_\mu e_R + \bar{Q}_L^j i\gamma^\mu D_\mu Q_L + \bar{u}_R i\gamma^\mu D_\mu u_R + \bar{d}_R i\gamma^\mu D_\mu d_R \\ &+ (D^\mu\phi)^\dagger D_\mu\phi - \mu^2\phi^\dagger\phi - \lambda(\phi^\dagger\phi)^2 \\ &- Y_{ij}\bar{Q}_L^i \phi d_R^j - Y_{ij}\bar{Q}_L^i \tilde{\phi} u_R^j - Y_{ij}\bar{l}_L^i \phi e_R^j \\ &- \frac{1}{4}W_{\mu\nu}^a W^{a\mu\nu} - \frac{1}{4}B_{\mu\nu}B^{\mu\nu} - \frac{1}{4}G_{\mu\nu}^a G^{a\mu\nu} + \mathcal{L}_{FG} + \mathcal{L}_{FP}\,.\end{aligned} \tag{1.16}$$

The terms on the right side of the Lagrangian density $\mathcal{L}_{SM}$, Eq. (1.16), are broken down as follows:

- In the first row, we find the kinetic Lagrangian of the fermions, where $\gamma^\mu$ represents the Dirac matrices and $D_\mu$ the covariant derivative.
- The second row represents the kinetic and potential energy term of the Higgs field, with $\mu^2$ and $\lambda$ as real parameters.
- The third row corresponds to the Lagrangian of the Yukawa couplings, where the coefficients $Y_{ij}$ refer to the Yukawa coupling matrix elements, and $\tilde{\phi} = i\tau^2\phi^*$.
- Finally, the fourth line is related to the kinetic energy of the gauge fields and the Lagrangians $\mathcal{L}_{FG}$ and $\mathcal{L}_{FP}$.

The antisymmetric gauge tensors are constructed from the gauge fields as follows [22]

$$G_{\mu\nu}^a = \partial_\mu G_\nu^a - \partial_\nu G_\mu^a + g_s f^{abc} G_\nu^b G_\mu^c \tag{1.17}$$

$$W_{\mu\nu}^a = \partial_\mu W_\nu^a - \partial_\nu W_\mu^a + g\epsilon^{abc} W_\nu^b W_\mu^c, \tag{1.18}$$

$$B_{\mu\nu} = \partial_\mu B_\nu - \partial_\nu B_\mu\,. \tag{1.19}$$

In these expressions, the $W_{\mu\nu}^a$ are the antisymmetric gauge tensors constructed from the gauge fields $W_\mu^a(x)$ corresponding to the three generators of $SU(2)$; $\epsilon^{abc}$ is the structure constant of the group

$SU(2)$ and coincides with the Levi-Civita pseudotensor; $B_{\mu\nu}$ are the antisymmetric gauge tensors constructed from the gauge fields $B_\mu(x)$ associated with $U(1)$; $G^a_{\mu\nu}$ are the antisymmetric gauge tensors constructed from the eight fields $G^a_\mu(x)$ of the gluons, corresponding to the eight generators of $SU(3)$; $f^{abc}$ are the structure constants of the group $SU(3)$.

Additionally, it is important to note that

1. The Lagrangian density of the Standard Model ($\mathcal{L}_{SM}$) has 19 free parameters that must be determined experimentally [2].

2. The Lagrangian density for the scalar field $\phi$ must include terms up to order $\phi^4$ for the theory to be renormalizable [12][23].

3. The relative sign of the Higgs potential coupling constants $\mu$ and $\lambda$ is determined by the spontaneous breaking of gauge symmetry [18].

4. The Yukawa constants are elements of a matrix of dimensions $3 \times 3$ and are related to the masses and mixings of the fermions.

Before continuing with the explanation of each term of the Lagrangian density, Eq. (1.14), the next section will discuss in detail the spontaneous breaking of gauge symmetry. This approach aims to understand the Higgs mechanism and the discussion of the Goldstone Theorem, which will be fundamental in the development of this Thesis.

## 1.3 Spontaneous Symmetry Breaking and Goldtone's Theorem

In the electroweak sector of the Standard Model, the intermediate bosons of the interactions acquire mass, which leads to the vacuum state no longer invariant under the electroweak gauge group $SU(2)_L \times U(1)_Y$. In other words, the fact that the $W^\pm$ and $Z$ bosons become massive causes breaking of the electroweak gauge symmetry, which in turn invalidates the renormalizability of the theory [24]. To address this problem, the Higgs sector is introduced into the SM. The corresponding Lagrangian of the Higgs sector causes a spontaneous breaking of the electroweak gauge symmetry.

The phenomenon of spontaneous symmetry breaking, in quantum field theory, is seen from the Higgs potential, which is defined as [21]:

$$V(\phi) = \mu^2\phi^\dagger\phi + \lambda(\phi^\dagger\phi)^2\,, \tag{1.20}$$

where $\phi_j$ is a set of real fields, which are transformed according to some representation of the gauge symmetry group $G$ with $n$ generators, that is

$$\phi_j(x) \to \phi'_j(x) + i\epsilon_a(x)T^a_{jk}\phi_k(x), \quad a = 1, 2, \ldots, n\,. \tag{1.21}$$

In the potential $V(\phi)$, it is essential to require that $\lambda > 0$ so that the potential is lower bounded, which implies the existence of a fundamental state commonly called the vacuum state. The determination of the vacuum state involves the minimization of the potential $V(\phi)$. However, the location of the minimum is conditional on the sign of the parameter $\mu^2$, which leads us to consider two different situations:

In the first scenario, $\mu^2 > 0$ is considered, resulting in a vacuum state defined as $\phi_i = 0$. Consequently, the potential $V(\phi)$ remains invariant under the symmetry group $G$. In this case, the gauge symmetry $G$ is not broken, although the extreme value corresponds to a local maximum. For example, when the group $G$ coincides with the gauge group of the Electroweak Standard Model (ESM), the vacuum state preserves the symmetry $SU(2)_L \times U(1)_Y$, which means that a breaking the electroweak gauge symmetry. However, this situation is invalid from a physical point of view, since the existence of massive bosons contradicts the premise that $SU(2)_L \times U(1)_Y$ is not a vacuum symmetry.

In the second case, when $\mu^2 < 0$, the vacuum state is determined through the minimization of the potential $V(\phi)$, which gives rise to a non-trivial minimum. The minimum of $V(\phi)$ for the non-trivial case is:

$$\delta V(\phi) = \frac{\partial V}{\partial \phi_i}(\delta\phi_i) = \epsilon_a \frac{\partial V}{\partial \phi_i} T^a_{ij}\phi_j = 0\,. \tag{1.22}$$

From this equation, we deduce the expected value of the field $\phi$ in the vacuum state

$$\langle 0|\phi^\dagger\phi|0\rangle = \langle\phi^\dagger\phi\rangle_0 = -\frac{\mu^2}{2\lambda}\,. \tag{1.23}$$

From the previous expression, it is observed that the vacuum state is degenerate because there are multiple ways to satisfy it. However, quantum field theory demands that the ground state be unique. Therefore, by selecting one of these states as the vacuum state, symmetry breaking is induced. This phenomenon is known in the literature as the spontaneous breaking of gauge symmetry. The symmetry that lasts, or is not broken, depends on the choice of the vacuum state.

Deriving the Eq. (1.22) with respect to the field $\phi_i$ and evaluating in the empty state, we obtain:

$$\left.\frac{\partial^2 V}{\partial\phi_k^\dagger \partial\phi_i}\right|_{\phi_i=\langle\phi_i\rangle_0} = M^2_{ki} T^a_{ij}\langle\phi_j\rangle_0 = 0\,. \tag{1.24}$$

For the previous expression to be satisfied, two cases are considered:

1. When $T^a_{ij}\langle\phi_j\rangle_0 = 0$, the generator $T^a$ is classified as an intact or unbroken generator. The element of the group associated with $T^a$ maintains the empty state invariable, which is expressed as:

   $$e^{i\epsilon\cdot T}\langle\phi\rangle_0 = \langle\phi\rangle_0. \tag{1.25}$$

   In other words, the set of intact or unbroken generators forms a symmetry subgroup that preserves the vacuum state. As a result, the original symmetry group is broken into the symmetry subgroup that maintains the unaltered vacuum state.

2. When $T^a_{ij}\langle\phi_j\rangle_0 \neq 0$, the generator $T^a$ is classified as a broken generator, and $M^2_{ki}$ refers to the matrix of potential masses. This matrix must have at least one eigenvalue equal to zero. The previous statement corresponds to the **Goldstone Theorem**, which establishes that for every broken generator, there is a boson with a mass equal to zero, known as a Goldstone boson.

### Goldstone Teorem

The example above shows the importance of Goldstone's theorem in the Standard Model. The theorem states that if a Lagrangian density is invariant under a continuous symmetry group that has $n$ generators, and if its ground state is symmetric under a continuous group that contains $n'$ generators, then there should be $n - n'$ massless states in the spectrum of the theory [21][23][25].

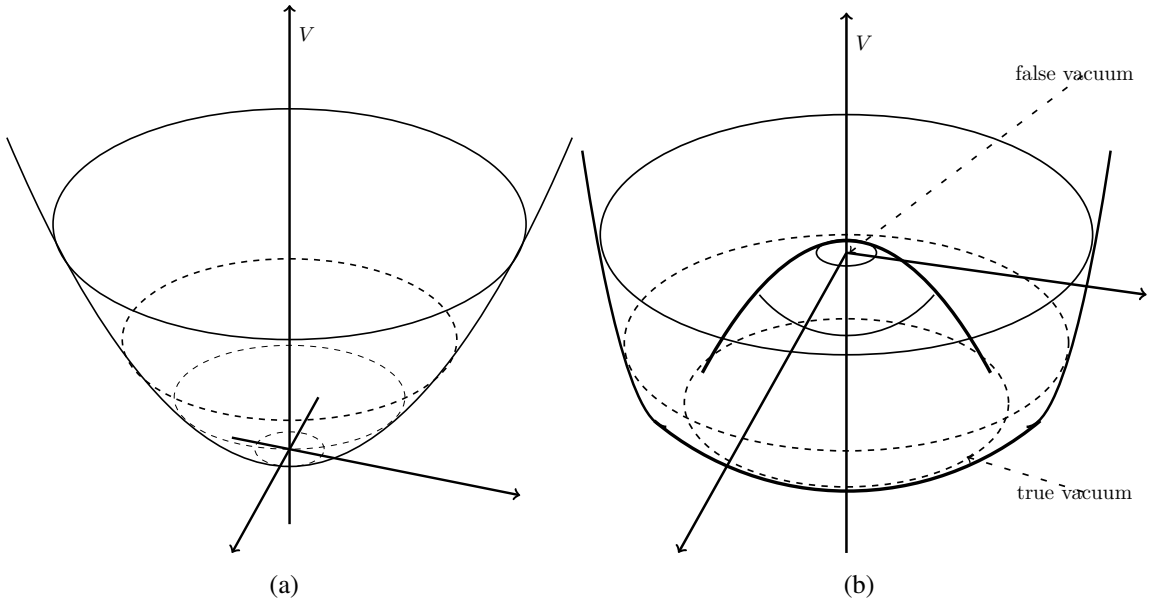


Figure 1.1: Higgs potential: (a) $\mu > 0$, single vacuum, (b) $\mu < 0$, false vacuum and true vacuum.

### 1.3.1 Higgs Mechanism

In the context of the ESM, the vacuum state is selected so that the remaining symmetry is compatible with the symmetry group of electrodynamics, which is $U(1)_{em}$. This means that the generator that remains without breaking the symmetry corresponds to the electric charge $Q_{em}$ [24].

For the Higgs mechanism, the field $\phi$ maps to a doublet of $SU(2)_L$ of the form:

$$\phi = \begin{pmatrix} \phi^+ \\ \phi^0 \end{pmatrix} = \frac{1}{\sqrt{2}} \begin{pmatrix} \phi_1 + i\phi_2 \\ \phi_3 + i\phi_4 \end{pmatrix} , \tag{1.26}$$

where $\phi_i$, $(i = 1, \ldots, 4)$, are real scalar fields. Thus, the Higgs potential given in Eq. (1.21) is invariant under the gauge transformation

$$\phi(x) \to \phi'(x) = e^{i\boldsymbol{\alpha}\cdot\boldsymbol{\tau}/2}\phi(x) , \tag{1.27}$$

here $\boldsymbol{\tau}$ is formed by the Pauli matrices and $\boldsymbol{\alpha}$ is a space-time function. The minimum of the Higgs potential, $V(\phi)$ for $\mu^2 < 0$, is

$$\langle 0|\phi^\dagger\phi|0\rangle = \langle\phi^\dagger\phi\rangle_0 = -\frac{\mu^2}{2\lambda} = \frac{v^2}{2} . \tag{1.28}$$

Depending on the actual fields, the term $\phi^\dagger\phi$ has the form

$$\phi^\dagger\phi = \frac{1}{2}\left(-\phi_1^2 + \phi_2^2 - \phi_3^2 + \phi_4^2\right) = \frac{v^2}{2} . \tag{1.29}$$

As can be seen, there is an infinite number of possible vacuum states, which correspond to the infinite number of values for the real fields that satisfy the relationship given in equation (1.30). Each of these vacuum states preserves the gauge symmetry $U(1)_{em}$, but not the electroweak gauge

symmetry. By choosing a particular direction in isospin space, spontaneous breaking of gauge symmetry is induced, following the scheme $SU(2)_L \times U(1)_Y \to U(1)_{em}$.

By selecting the direction in isospin space where $\phi_3 = v$ and $\phi_1 = \phi_2 = \phi_4 = 0$, the vacuum expectation value of $\phi$ takes the following form:

$$\langle\phi\rangle_0 = \frac{1}{\sqrt{2}}\begin{pmatrix}0\\ v\end{pmatrix}. \tag{1.30}$$

When a generator of the electroweak gauge group $(T_a, Y)$ acts on the vacuum state, it breaks the corresponding symmetry, i.e.

$$T^a\langle\phi\rangle_0 \neq 0\,, \quad Y\langle\phi\rangle_0 \neq 0\,. \tag{1.31}$$

On the other hand, when the generator of $U(1)_{em}$ ($Q_{em} = I_3 + Y$) acts on the vacuum state, it does not break,

$$Q_{em}\langle\phi\rangle_0 = \frac{1}{\sqrt{2}}Q\begin{pmatrix}0\\ v\end{pmatrix} = 0\,. \tag{1.32}$$

One implication of the spontaneous breaking of electroweak gauge symmetry is that the three electroweak gauge fields, namely $W^{\pm}$ and $Z^0$, acquire mass, which leads to these gauge fields acquiring longitudinal degrees of freedom. In this way, the three Goldstone bosons that were present in the theory before the spontaneous symmetry breaking re-emerge in the theory as the longitudinal degrees of freedom of the $W^{\pm}$ and $Z^0$ bosons [23].

## 1.4 Fermion masses and CP violation

Now, let's examine the part of the Lagrangian density of the ESM that refers to Yukawa couplings, known as the Lagrangian Yukawa density. This Lagrangian density is composed of terms that establish the relationship between the Higgs field and the quark and lepton fields.

In the interaction representation, the gauge interactions are diagonal and universal, meaning that they are described by a gauge coupling constant for each of the factors in the $G_{SM}$: $g_s$, $g$, and $g'$. According to this representation, the interaction eigenstates do not present gauge couplings between fermions of different generations, and mixtures between fermions of different flavors are prohibited [21]. However, the coupling of the Higgs field to fermions does not follow from the gauge invariance principle. Consequently, in this representation, the Yukawa couplings correspond to non-diagonal matrices. This implies that in the interaction representation, Yukawa couplings involve fermions of different generations. As a result, the interaction eigenstates are mixing and have no defined masses.

During the spontaneous breaking of gauge symmetry in the context of the Standard Model, $G_{SM}$, the Yukawa interactions generate the mass terms of the fermions. When considering the vacuum expectation value of the Higgs field, as described by the equation (1.30), the Yukawa Lagrangian density takes the following form [26]:

$$\mathcal{L}_Y^Q = -Y_{ij}^d\bar{Q}_L^i\phi d_R^j - Y_{ij}^u\bar{Q}_L^i\tilde{\phi}u_R^j - Y_{ij}^l\bar{l}_L^i\phi e_R^j - \text{h.c.} = -\bar{u}_L M_u u_R - \bar{d}_L M_d d_R - \bar{e}_L M_\ell e_R\,, \tag{1.33}$$

where $M_f$ $(f = u, d, \ell)$ are the mass matrices of the charged quarks and leptons. While

$$u = \begin{pmatrix}u\\ c\\ t\end{pmatrix}, \quad d = \begin{pmatrix}d\\ s\\ b\end{pmatrix}, \quad e = \begin{pmatrix}e\\ \mu\\ \tau\end{pmatrix}. \tag{1.34}$$

The mass matrices, obtained from the Yukawa couplings after symmetry breaking, are defined as [26]

$$(M_f)_{ij} = \frac{Y^f_{ij} v}{\sqrt{2}}\,, \tag{1.35}$$

where $v$ represents the vacuum expected value of the Higgs field and the $Y^f_{ij}$ are the elements of the Yukawa coupling matrix, which for the Standard Model correspond to complex matrices of $3 \times 3$. The most recent values for quark masses are shown in the table 1.2 [2].

| Familia | Quark | Masa |
|---|---|---|
| 1 | u | $2.16^{+0.49}_{-0.26}$ MeV |
| | d | $4.67^{+0.48}_{-0.17}$ MeV |
| 2 | c | $1.27 \pm 0.02$ GeV |
| | s | $93.4^{+8.6}_{-3.4}$ MeV |
| 3 | t | $172.69 \pm 0.30$ GeV |
| | b | $4.18^{+0.03}_{-0.02}$ GeV |

Table 1.2: Quark masses in the Standard Model.

The ESM does not provide predictions for the values of fermionic masses, instead, it is fitted to experimental measurements. The most recent values of the masses of charged leptons are found in reference [2]:

$$m_e = 0.51099895000 \pm 0.00000000015\,\text{MeV}\,, \tag{1.36}$$
$$m_\mu = 105.6583755 \pm 0.0000023\,\text{MeV}\,, \tag{1.37}$$
$$m_\tau = 1776.86 \pm 0.12\,\text{MeV}\,. \tag{1.38}$$

We will focus exclusively on the part of the Yukawa Lagrangian density related to the quark sector since this is the fundamental part of the development of this thesis. Since mixing between quarks of different generations is allowed, the mass matrices of these quarks are not diagonal in the interaction basis. This implies that the interacting eigenstates do not have clearly defined masses. In other words, in the interaction representation, fermions in general are not mass eigenstates. Therefore, it is necessary to diagonalize these matrices to find the mass eigenstates.

After symmetry breaking, the quark mass terms become

$$\mathcal{L}_{\text{masa}} = -\frac{v}{\sqrt{2}}\left(\bar{d}^i_L Y_{ij} d^j_R + \bar{u}^i_L Y_{ij} u^j_R\right) + \text{h.c.} = -\frac{v}{\sqrt{2}}\left(\bar{d}_L Y_d d_R + \bar{u}_L Y_u u_R\right) + \text{h.c.}\,, \tag{1.39}$$

where the last expression is in matrix form. To diagonalize the masses, we use that there are two diagonal matrices $M_d$ and $M_u$ and two unitary matrices $U_d$ and $U_u$ for which

$$Y_d Y_d^\dagger = U_d M_d^2 U_d^\dagger, \quad Y_u Y_u^\dagger = U_u M_u^2 U_u^\dagger\,. \tag{1.40}$$

The matrix $YY^\dagger$ is Hermitian and therefore has real eigenvalues. We can also write in a general way

$$Y_d = U_d M_d K_d^\dagger, \quad Y_u = U_u M_u K_u^\dagger\,, \tag{1.41}$$

for other unitary matrices $K_d$ and $K_u$. Therefore, the Yukawa couplings are

$$\mathcal{L}_{\text{masa}} = -\frac{v}{\sqrt{2}}\left(\bar{d}_L U_d M_d K_d^\dagger d_R + \bar{u}_L U_u M_u K_u^\dagger u_R\right) + \text{h.c.}\,. \tag{1.42}$$

Now we can freely change the basis of the right quarks with $d_R \to K_d d_R$ and $u_R \to K_u u_R$ and the left quarks with $u_L \to U_u u_L$ and $d_L \to U_d d_L$. This removes the matrices $U$ and $K$ from the Yukawa terms, leaving the diagonal mass matrices $M_u$ and $M_d$ [27]. This is known as going to the *basis of masses*. On this basis the mass terms in the Lagrangian density are simply

$$\mathcal{L}_{\text{masa}} = -\sum_j \left(m_j^d \bar{d}_L^j d_R^j + m_j^u \bar{u}_L^j u_R^j\right) + \text{h.c.}\,, \tag{1.43}$$

where $m_j^d$ and $m_j^u$ are the diagonal elements of $\frac{v}{\sqrt{2}}M_d$ and $\frac{v}{\sqrt{2}}M_u$, respectively . Note that there still exists a residual global symmetry $U(1)^6$ with six angles $\alpha_j$ and $\beta_j$, under which

$$d_L^j \to e^{i\alpha_j} d_L^j, \quad d_R^j \to e^{i\alpha_j} d_R^j, \quad u_L^j \to e^{i\beta_j} u_L^j, \quad u_R^j \to e^{i\beta_j} u_R^j\,. \tag{1.44}$$

Of course, this basis change also implies modifications in the kinetic terms of the Lagrangian density of the SM. In the original flavor basis, gauge boson interactions do not affect mixing between different quark families. When we perform the rotation $u_L \to U_u u_L$ and $d_L \to U_d d_L$, the couplings of $B_\mu$ and $W_\mu^3$ do not change, since they do not involve the mixing of up and down quarks [26]. The only elements that are sensitive to these rotations are the $W_\mu^\pm$ couplings. This leads to all relevant mixing effects being encapsulated in a single matrix, known as the CKM (Cabibbo–Kobayashi–Maskawa) matrix, which is defined as $V = U_u^\dagger U_d$.

The CKM matrix is a complex unitary matrix, which implies that it has a total of nine real degrees of freedom. If we consider that the CKM matrix, denoted as $V$, was a real matrix, we would be dealing with a matrix of dimension $3 \times 3$, which would imply the existence of three degrees of freedom corresponding to the angles of rotation. Consequently, we would have three angles and six phases in the matrix $V$.

However, we can take advantage of the $U(1)^6$ symmetry present in the equation (1.44), where the masses remain invariant, to set certain phases to zero. Under these transformations, the matrix $V$ generally changes. However, if all rotations are identical, that is, $\alpha_j = \beta_j = \theta$, then the matrix $V$ remains unchanged. Through this approach, we can eliminate only five phases in this way, resulting in a total of four remaining degrees of freedom. These four degrees of freedom consist of three angles, denoted $\theta_{12}$, $\theta_{23}$ and $\theta_{13}$, which correspond to the rotations in the flavor planes $ij$, and a phase, represented by $\delta$ [27].

### 1.4.1 Yukawa Couplings and CP Violation

The parity violation in the electroweak theory is an obvious consequence of the differences in coupling between left-chirality fields and right-chirality fields. This phenomenon is evident in nuclear beta decay, where the emission of electrons with left-hand chirality is consistently observed [28][29]. However, it is possible that, despite the lack of invariance under mirror reflection in the universe, this invariance could be maintained if it is accompanied by an exchange of particles and antiparticles, which is known as $CP$ invariance. Currently, we are aware that $CP$ invariance breaks

down in rare processes involving hadrons, which we call a weak violation of $CP$ [30][31]. Additionally, there is another potential form of $CP$ violation known as strong $CP$ violation, which is predicted theoretically but has not yet been observed experimentally, generating what is known as the strong $CP$ problem, which we will discuss in detail. in Chapter 3. In what follows, we will discuss the physics related to the $CP$ transformation.

The way $CP$ acts in spinor bilinears is [11][27]:

$$\bar{\psi}_i\psi_j(t,\mathbf{x}) \to +\bar{\psi}_j\psi_i(t,-\mathbf{x}), \tag{1.45}$$
$$\bar{\psi}_i\gamma_5\psi_j(t,\mathbf{x}) \to -\bar{\psi}_j\gamma_5\psi_i(t,-\mathbf{x}), \ . \tag{1.46}$$

Using the above we can determine which terms in the Lagrangian density of the SM could break the $CP$ symmetry. Remember that, in the flavor basis, the entire flavor structure is in the Yukawa matrices. Consider the up-type quark $(uct)$ mass terms

$$\begin{aligned}\mathcal{L}_{\text{Yukawa}} &= -\frac{v}{\sqrt{2}}\bar{u}_L Y_u u_R + \bar{u}_R Y_u^\dagger u_L \\ &= -\frac{v}{\sqrt{2}}\left(\bar{u}(Y_u + Y_u^\dagger)u + \bar{u}(Y_u - Y_u^\dagger)\gamma^5 u\right) \ .\end{aligned} \tag{1.47}$$

Under CP, $\bar{u}_i u_j \to \bar{u}_j u_i$ and $\bar{u}_i\gamma^5 u_j \to -\bar{u}_j\gamma^5 u_i$ ( along with $x \to -x$), so

$$\begin{aligned}\mathcal{L}_{\text{Yukawa}} &\to -\frac{v}{2\sqrt{2}}\left(\bar{u}(Y_u + Y_u^\dagger)^T u - \bar{u}(Y_u - Y_u^\dagger)^T\gamma^5 u\right) \\ &= -\frac{v}{2\sqrt{2}}\left(\bar{u}(Y_u^* + Y_u^{\dagger *})u - \bar{u}(Y_u^* - Y_u^{\dagger *})\gamma^5 u\right) \ .\end{aligned} \tag{1.48}$$

Thus, we see that the Lagrangian density is invariant under $CP$ if the coefficients are real.

Whether or not a matrix is real is not a basis-invariant statement. In fact, in the flavor basis where the interactions $W$ are diagonal in flavor and the mass matrix is complex (i.e., $V = 1$), there can still be a violation of $CP$. Conversely, even if the mass matrix were diagonal and $V$ was complex, violation of $CP$ might not occur if some residual chiral rotation could remove the phase. This is especially true if one of the quarks is massless. Therefore, it is beneficial to have a basis-independent measure to assess $CP$ violation.

Now, let us remember that we relate the Yukawa couplings to the diagonal mass matrices through Eq. (1.41) where

$$M_d = \frac{\sqrt{2}}{v}\text{diag}(m_d, m_s, m_b)\,, \tag{1.49}$$
$$M_u = \frac{\sqrt{2}}{v}\text{diag}(m_u, m_c, m_t)\,. \tag{1.50}$$

since $V = U_u^\dagger U_d$, if $U_u = U_d$, then $V = 1$, implying the absence of flavor violation or $CP$. Previously, we took advantage of the freedom to rotate the right fields without disturbing the weak interactions to eliminate $K_d$ and $K_u$. Equivalently, we could have performed rotations on $d_R$, i.e. $d_R \to K_d U_d^\dagger d_R$, and on $u_R$, i.e. $u_R \to K_u U_u^\dagger u_R$, from so that

$$Y_d = U_d M_d U_d^\dagger\,, \tag{1.51}$$
$$Y_u = U_u M_u U_u^\dagger\,, \tag{1.52}$$

which makes the Yukawa matrices Hermitian. Then, suppose that $Y_u$ and $Y_d$ are Hermitian, without loss of generality. If $Y_u$ and $Y_d$ could be diagonalized simultaneously, then $V = 1$ and there would be no violation of $CP$. Therefore, the $CP$ violation is completely hardcoded into the switch [27]

$$-iC = [Y_u, Y_d] = U_u M_u U_u^\dagger, U_d M_d U_d^\dagger = U_u \left(M_u V M_d V^\dagger\right) U_u^\dagger \,. \tag{1.53}$$

The matrix $C$ is traceless and Hermitian because $Y_u$ and $Y_d$ are Hermitian. Therefore, it is natural to look at its determinant as an invariant quantity in the basis

$$\det C = -\frac{16}{v^6}(m_t - m_c)(m_t - m_u)(m_c - m_u)(m_b - m_s)(m_b - m_d)(m_s - m_d)J \,, \tag{1.54}$$

where, for any $i, j, k$ and $l$,

$$\text{Im}\left[V_{ij} V_{kl} V_{il} V_{kj}\right] = J = \sum_{m,n} \epsilon_{ikm} \epsilon_{jln} \,, \tag{1.55}$$

where $\epsilon_i jk$ is the 3-index antisymmetric tensor. This can be expressed as

$$J = \text{Im}(V_{11} V_{22} V_{12} V_{21}) = -\text{Im}(V_{11} V_{32} V_{12} V_{31}) = \text{Im}(V_{22} V_{33} V_{23} V_{32}) = \dots \,, \tag{1.56}$$

here these products are equal due to the unitarity of the CKM matrix. $J$ is known as the *Jarlskog invariant*. In terms of the standard parameterization,

$$J = s_{12} s_{23} s_{31} c_{12} c_{23} c_{31} \sin\delta \,. \tag{1.57}$$

The important point about the Jarlskog invariant vanishes if and only if there is no violation of $CP$. That is, all weak CP violation in the Standard Model is proportional to Im$det[Y_u, Y_d]$.

This explanation is valid when the $CP$ violation mechanism is distinguished from the Higgs mechanism in the spontaneous breaking of gauge symmetry. Yukawa interactions are responsible for the masses of the fermions and constitute the only source of $CP$ violation in the ESM.

## 1.5 Beyond the Standard Model

Particle Physics has made notable achievements with the SM, a theory that describes elementary particles and their interactions in a surprisingly precise way. However, the SM is not a complete theory, and several shortcomings and limitations have been identified that highlight the need to seek an extension beyond this model. Below we will briefly explain two issues that suggest making this extension.

### 1.5.1 Why do we need Dark Matter?

Observations of the Cosmic Microwave Background (CMB) strongly suggest that the universe, at large scales, is virtually flat [32]. This results in an observed value of the current energy density, denoted as $\rho_0$, which is close to its critical value

$$\rho_0 \approx \rho_{\text{crit}} \equiv \frac{3H_0^2}{8\pi G_N} \approx 10^{-29}\,\text{g/cm}^3 \,, \tag{1.58}$$

corresponding to an average density of 10 protons per cubic meter; in Eq.(1.58), $H_0 \approx 70\,\text{km/s/Mpc}$ is the value of the Hubble constant today (i.e., the Hubble constant) and $G_N \approx 6.67\times10^{-11}\,\text{Nm}^2/\text{kg}^2$ is Newton's gravitational constant. This energy density is made up of various contributions [32]. Mainly (about $70\%$) Dark Energy (DE), which is responsible for the accelerated expansion of the universe, followed by Dark Matter (DM, about $26\%$), which is responsible for the gravitational collapse of the universe, ordinary matter (generally called "baryons" and which constitutes the remaining $4\%$) and, finally, the formation of the structures that we observe in the cosmos.

We can determine the amount of Dark Matter in the Universe, which is as follows

$$\Omega_{\text{DM}} \equiv \frac{\rho_{\text{DM},0}}{\rho_0} \approx 0.26\,, \tag{1.59}$$

where $\rho_{\text{DM},0}$ is the density of dark matter evaluated today [2]. The number in the Eq. (1.59) can be expressed in units more suitable for astrophysics and particle physics as follows:

$$\rho_{\text{DM},0} \approx 10^{10} M_\odot\,\text{Mpc}^3 \approx 10^{-6}\,\text{GeV cm}^3\,, \tag{1.60}$$

where $M_\odot \approx 2\times10^{30}\,\text{kg}$ is the mass of the Sun. We can get some clues about the microscopic nature of dark matter by trying to answer the following questions:

- Dark Matter is generally believed to be not "bright" in the sense that DM particles do not interact electromagnetically and therefore cannot scatter photons; in other words, they do not possess an electrical charge. However, the observations do not exclude that DM particles may have an extremely small electrical charge [33] or that they do so through other mechanisms.

- We know that dark matter must be gravitationally bound on scales at least as large as the size of a spherical dwarf galaxy ($dSph$). We can use this size to derive an upper limit on the de Broglie wavelength ($\lambda_{dB}$) of a DM particle and, consequently, a lower limit on its mass. Considering a dark matter particle of mass $m$ with a speed $v \approx 100\,\text{km/s}$, using the value of Planck's constant (which we recover for the moment) $h_{Pl} \approx 4\times10^{-15}\,\text{eV}\cdot\text{s}$, and the fact that, since the particle is non-relativistic, the de Broglie wavelength $\lambda_{dB} = h_{Pl}/(mv)$ is calculated as

  $$\lambda_{dB} \approx \frac{4\times10^{-15}}{10^2}\,\text{eV}\cdot\text{m}\cdot\text{s}^2\cdot\text{km} \approx 4\,\text{meV}\cdot\text{m}\,. \tag{1.61}$$

  This result implies that, for $\lambda_{dB} < 1\,\text{kpc} \approx 3\times10^{21}\,\text{cm}$, we need a mass $m > 10^{-22}\,\text{eV}$, which is not a very strict lower limit.

While the SM has been remarkably successful in describing particles and three of the four fundamental interactions that make up visible matter, it does not explain dark matter. The inclusion of a dark matter particle in an extension of the Standard Model is essential to address this cosmological challenge. This hypothetical particle could have weak or gravitational interactions with visible matter and would form large-scale structures in the universe, such as dark matter halos around galaxies.

[2] Generally a subscript 0 means, in cosmology, that the corresponding quantity is evaluated at present, that is, at the age of the universe $t_0$.

### 1.5.2 Problems in QCD theory

One of the most important outstanding issues is the need to address the problem of $CP$ violation in the context of strong interaction. To understand this question, we must first introduce some concepts solidly established in current physics. One of the most direct tests of invariance under time reversal $\mathcal{T}$ comes in single particle transitions [34][3]. Next, we will focus on a static quantity that describes a particle or state: the Electric Dipole Moment (EDM).

Let us consider a system, which could be an elementary particle, an atom, or a molecule, immersed in a weak electric field $\mathbf{E}$. The change in the energy of the system due to the external electric field can be decomposed into a power series of $\mathbf{E}$ as follows

$$\Delta\epsilon = d_i E_i + D_{ij} E_i E_j + \dots \,. \tag{1.62}$$

The coefficient of the linear term in $\mathbf{E}$ is called the electric dipole moment (EDM), while that of the quadratic term is known as the induced dipole moment. If an elementary particle possesses an EDM, this implies the violation of the parity $P$ and time reversal $\mathcal{T}$ symmetries. The EDM is a measure of charge polarization within a particle and is expressed as the expected value of an operator (for a system of charges)

$$\mathbf{d} = \sum_i \mathbf{r}_i e_i \,, \tag{1.63}$$

where $\mathbf{r}_i = \mathbf{r}_i^+ - \mathbf{r}_i^-$ is a relative vector that locates the charges on $\mathbf{r}_i^+$ in $\mathbf{r}_i^-$, while $e_i$ the respective charge. For parity conservation $P$ to be fulfilled, the following must happen

$$\langle N, s|\mathbf{d}|N, s\rangle = \langle N, s|P^\dagger P \mathbf{d} P^\dagger P|N, s\rangle = -\langle N, s|\mathbf{d}|N, s\rangle \,. \tag{1.64}$$

Therefore, the expected value of this operator must be zero. A non-zero expected value of this operator would imply that the dynamics acting on the particle violate parity symmetry.

In the early 1950s, Purcell and Ramsey used this argument to demonstrate the conservation of parity in nuclear forces [36][37]. At that time, the existing limit for the neutron EDM, obtained by Rabi, Havens, and Rainwater, as well as Fermi and Hughes, was $10^{-17}$ e cm [38][39].

After the parity violation was discovered in 1957, determining the EDM of the neutron was considered the ideal option to independently investigate such a violation. However, Landau, Lee, and Schwinger pointed out that a non-zero EDM would imply the violation of another symmetry: the time-reversal $\mathcal{T}$ and, therefore, the violation of $CP$ [29][40][41]. This is due to the condition that in a quantum field theory, conservation of symmetry $CP\mathcal{T}$ is imperative according to the CPT theorem [4].

It has often been mentioned that one of the attractive features of Quantum Chromodynamics (QCD) is that it "naturally" preserves baryon number, flavor, parity, and $CP$ symmetry. This was the consensus for a while until it was pointed out [43] that it is not entirely true.

From the Lagrangian density of QCD

$$\mathcal{L}_{QCD} = -\frac{1}{4} G^a_{\mu\nu} G^{a\mu\nu} + \bar{Q}_L i\gamma^\mu D_\mu Q_L + \bar{u}_R i\gamma^\mu D_\mu u_R + \bar{d}_R i\gamma^\mu D_\mu d_R - Y_{ij}\bar{Q}^i_L \phi d^j_R - Y_{ij}\bar{Q}^i_L \tilde{\phi} u^j_R \,, \tag{1.65}$$

[3] A prominent example of this is neutrino oscillations [35].

[4] For a rigorous proof of this theorem, see the following reference [42].

we can see that we can add a term constructed from the intensity tensor defined in (1.17): $\epsilon^{\mu\nu\rho\sigma}G^a_{\mu\nu}G^a_{\rho\sigma}$. This term is gauge invariant and has dimension $4$; therefore, there is no reason to exclude this term from $\mathcal{L}_{QCD}$. Quantum field theory teaches us to include every gauge-invariant four-dimensional operator in the Lagrangian density: loop corrections would induce its presence even if it is omitted from the original Lagrangian density unless it is prohibited by some symmetry other than the Lagrangian. must obey. So we must add the non-perturbative term to $\mathcal{L}_{QCD}$

$$\mathcal{L}_{\text{eff}} = \mathcal{L}_{\text{QCD}} + \frac{\theta g_s^2}{32\pi^2} G^a_{\mu\nu}\widetilde{G}^{a\mu\nu}\,, \tag{1.66}$$

where $\widetilde{G}^{a\mu\nu} := \frac{1}{2}\epsilon^{\mu\nu\rho\sigma}G^a_{\rho\sigma}$. The appearance of a term $G^a_{\mu\nu}\tilde{G}^{a\mu\nu}$ in the $\mathcal{L}_{eff}$ causes a serious problem. Because $G^a_{\mu\nu}\tilde{G}^{a\mu\nu}$, unlike $G^a_{\mu\nu}G^{a\mu\nu}$, violates both parity and invariance under time reversal [44]. This is called, somewhat carelessly, the "strong CP problem".

On the other hand, QCD with light quarks $u$ and $d$ in the limit of massless quarks, where $m_u$ and $m_d$ are much smaller than the QCD scale ($\Lambda_{\text{QCD}}$), appears to possess a global symmetry $U(2)_L \times U(2)_R$. Although the vector component $U(2)_{L+R}$ remains conserved even after quantum corrections, the axial part $SU(2)_{L-R}$ breaks spontaneously, giving rise to the pions, which initially are Goldstone bosons but they gain mass due to the non-zero masses of $m_u$ and $m_d$.

The puzzle arises when considering the symmetry $U(1)_{L-R}$, which cannot represent a valid symmetry, since it would lead to "parity doubling" that is not observed in nature. The assumption of its spontaneous breakdown should give rise to a fourth Goldstone boson, which is not found in the particle spectrum. This leads to the $U(1)_A$ problem in QCD [45].

The solution to this puzzle lies in the quantum anomaly in the axial flavor singlet current, which breaks chiral symmetry for massless quarks. Such an anomaly is known as the "triangle anomaly", is generated by a triangular fermionic loop diagram, and has been an important topic in theoretical physics [46][47][48]. However, the resolution of this $U(1)_A$ problem introduces the "Strong CP Problem", which will be stated more clearly in Chapter 3. The $U(1)_A$ and Strong $CP$ Problems become even more intertwined if weak interactions are also included. Since the gluonic operator $G^a_{\mu\nu}\widetilde{G}^{a\mu\nu}$ does not change flavor, we immediately suspect that its most notable impact would be to generate an EDM for neutrons. This is, in fact, the case, but establishing this connection more concretely requires a more sophisticated argument, which you can find in chapter 15 of [34]. By adding fields to the Standard Model to introduce the new anomalous $U(1)$ symmetry. This symmetry is named by its authors as Peccei-Quinn symmetry. If this $U(1)_{PQ}$ breaks down spontaneously, it will generate a new Goldstone boson, $a$. Taking $a = \bar{\theta}$ and the ground state has no effective effect of $\bar{\theta}$. The excitations around this void are known as axions and also provide a viable candidate for the dark matter particle.

In summary, the need to extend the Standard Model is important to our understanding of nature, and the problem of $CP$ violation in the context of strong interaction is one of the most intriguing and fundamental challenges presented. This has led us to establish a good candidate for dark matter. The search for this extension is essential to better understand the mysteries of the Universe and advance our knowledge of fundamental physics.

# Chapter 2
# Dark Matter

*"We have peered into a new world and have seen that it is more mysterious and more complex than we had imagined. Still, more mysteries of the universe remain hidden. Their discovery awaits the adventurous scientists of the future."*
**—Vera Rubin**

Throughout the history of science, the exploration of cosmic mysteries has been a constant search. As we advance our understanding of the universe, we encounter an enigma that challenges the very foundations of physics and cosmology: Dark Matter (DM).

In the vast expanses of space lurks a fundamental component of the cosmos that, for the most part, does not interact detectably with light. As a result, it remains invisible to our instruments and observations. In this chapter, we will lay out the problem of dark matter, exploring its impacts on cosmology and the theories that attempt to shed light on its true nature.

## 2.1 Evidence for the existence of Dark Matter

Today, cosmological models always incorporate a type of non-baryonic matter, which interacts electromagnetically extremely weakly or not at all with light, and which has a negligible speed in terms of structure formation. This form of matter is known generically as "Cold Dark Matter" (CDM).

Within the framework of the well-known Standard Model of Cosmology, called $\Lambda$CDM, dark matter represents $26.4\%$ of the critical density of the universe or $84.4\%$ of the total density of matter. However, as for its nature, we only know a small fraction of it, ranging between at least $0.5\%$ (given the behavior of neutrinos) and a maximum of $1.6\%$ (according to the combined cosmological constraints)[2]. Of all the non-baryonic matter content in the universe, we only fully understand the three neutrinos that are part of the Standard Model of particle physics. To date, the fundamental composition of the vast majority of dark matter remains unknown.

Assuming the validity of General Relativity [1], we can observe that dark matter is ubiquitously present in structures that They experience gravitational interactions. These structures range from the smallest known galaxies, as demonstrated in [50], to galaxies comparable in size to our Milky Way, as mentioned in [51], and extend even to groups and clusters of galaxies, as investigated in [52].

Below we will mention some observational evidence that shows us the existence of dark matter:

- **Galaxy rotation curves:** The velocities of stars do not decrease as they move away from the center, which would be expected if only visible matter were present. Instead, these curves reveal that the rotation speed remains constant or, in some cases, even increases in the farther regions. This observation points directly to the existence of a substantial amount of invisible

[1] There are various tests, such as the detection of gravitational waves that are conclusive proof of the solidity of the theory [49].

matter that provides the necessary additional gravity. This invisible matter is what we know as dark matter. The study of these rotation curves was one of the first observations that suggested the existence of DM [53].

- **Anisotropies in the Cosmic Microwave Background (CMB):** The study of cosmic background radiation, the afterglow of the Big Bang, provides information about the distribution of matter in the early universe. The anisotropies observed in this radiation are consistent with models that include both visible matter and dark matter. For example, detailed observations of the cosmic background radiation support anisotropies and features in the angular spectrum, which is consistent with the existence of visible matter and dark matter in the early universe [54].

- **Gravitational lenses:** Gravitational lensing is a phenomenon in which the gravity of a very massive object, such as a galaxy or galaxy cluster, bends the light from objects behind it. The amount of curvature observed is greater than would be explained by visible matter alone, suggesting the existence of dark matter contributing to this additional gravitational lensing [55] [56].

- **Galaxy Agglomerations:** The way galaxies are grouped into clusters and superclusters suggests the existence of a significant amount of invisible matter. Gravity generated solely by visible matter would not be able to hold these structures together at the observed speeds, as has been pointed out in several scientific studies [57].

According to the previous evidence, we must point out that dark matter has only been observed indirectly and it is said that it does not interact with electromagnetic light. Furthermore, dark matter does not emit detectable signals in the form of particles that our particle detectors can pick up. In contrast, visible matter is composed of atoms and particles that emit or reflect detectable particles, such as electrons, protons, and photons.

However, although DM is invisible to light and our particle detectors, we know it exists because of its gravitational influence. Gravity is the only known form of interaction that affects DM and visible matter equally. This gravitational influence is what has been presented as evidence. Additionally, cosmologists use computer simulations to study the evolution of the universe and how dark matter interacts with visible matter [58]. These simulations recreate the formation of large-scale structures and are supported by observational data, providing additional evidence for the existence of DM.

In summary, although we have not directly observed DM, its gravitational influence and its consistency with theoretical models supported by observational data provide us with strong evidence for its existence.

## 2.2 About the genesis of Dark Matter

The genesis of DM is an intriguing mystery in cosmology and astrophysics. As we explore the universe and study its phenomena, we are faced with overwhelming evidence for the existence of “invisible” matter that exerts significant gravitational influence. However, the origin and exact nature of this dark matter remain enigmas to be solved. In this section, we will explore the clues

and theories that have emerged over time to better understand the crucial role that DM plays in the structure and evolution of the universe.

In the early universe, dark matter generation can occur through thermal, non-thermal processes, or a combination of both, and can even arise due to asymmetries between particles and antiparticles. The thermal scenarios are [59][60]:

- **Freeze-out:** In the "freeze-out" scenario, DM particles are initially in thermal equilibrium with the early primordial universe. This means that the particles are constantly interacting, colliding, and annihilating each other. As the universe expands and cools, the rate of annihilation of dark matter particles decreases. This is because collisions become less frequent due to expanding space and cooling. At some point, the rate of annihilation becomes slower than the expansion of the universe, meaning that dark matter particles are no longer in thermal equilibrium with their surroundings. At this point, the abundance of DM is "frozen" at a specific value, determined by the previous annihilation rate. As a result, the final abundance of dark matter depends on the annihilation cross section (the probability that two particles annihilate when they collide) and the temperature of the universe at the time of the freeze-out.

- **Freeze-in:** In the "freeze-in" scenario, DM particles are generated from collision processes that never brought them into thermal equilibrium with the primordial universe. Over cosmic time, these dark matter particles are gradually created due to collisions and decays of lighter particles, without an abrupt "freezing" in their abundance occurring. In general, dark matter particles generated through freeze-in tend to have longer lifespans, meaning they can exist for an extended period before disintegrating or annihilating. This, in turn, can result in distinctive, detectable signals in particle experiments and cosmic observations.

In summary, "freeze-out" implies that dark matter particles cease to be in thermal equilibrium with the universe due to cooling and expansion, while "freeze-in" involves the gradual generation of dark matter particles through out-of-equilibrium processes throughout cosmic time. Both scenarios are important in understanding DM and its abundance in the Universe.

For completeness, it is important to mention that the production of DM can occur through processes that develop outside of thermal equilibrium. These processes may include the generation of DM through the decay of a "mother" particle into DM [61] or through gravitational effects. Another possibility is the existence of asymmetric DM, where the abundance of DM results from an asymmetry between DM particles and their corresponding antiparticles [62]. It is important to note that this asymmetry is not necessarily related to the asymmetry between baryon matter and antimatter. In this context, depending on the model and its thermal history, there may be a relationship between the masses of the dark matter particles and the mass of the proton. Several theories have been proposed arguing that baryogenesis can be explained by an asymmetry in the DM sector or vice versa [63].

## 2.3 Small-scale problems

The $\Lambda$CDM model has been remarkably successful in explaining the large-scale structures observed in the Universe, as well as the fundamental properties of galaxies formed within DM haloes [64]. Despite its effectiveness at large scales, the model faces challenges at scales below $\sim 1$ Mpc, where

structure formation becomes highly nonlinear. These challenges include three main problems: "the cusp-core problem", "the missing satellite problem" and "the too-big-to-fail problem". These problems initially arose when comparing theoretical predictions of dark matter simulations with observations, and while some solutions are found in baryon physics, such as supernova feedback, other challenges might require a modification or extension of the ΛCDM model.

1. **The cusp-core problem:** Observations seem to indicate an approximately constant dark matter density in the inner parts of galaxies, while cosmological computer simulations indicate steep power-law type behavior, namely $\rho(r) \propto r^{-\gamma}$, with $\gamma = 0.8 - 1.4$ [65][66]. This difference is known as "the core-cusp problem" and remains one of the unsolved problems in small-scale cosmology.

2. **The Missing Satellite Problem:** Broadly refers to the overabundance of predicted CDM subhaloes compared to the known satellite galaxies that exist in the Local Group [67]. Cosmological simulations predict hundreds or thousands of Milky Way-sized subhaloes, with masses that are, in principle, large enough to allow galaxy formation ($> 10^7 M_\odot$). But we observe less than $100$ satellite galaxies in our vicinity. One possible solution is that galaxy formation becomes less efficient in smaller haloes, preventing galaxy formation in smaller dark matter haloes. From that point of view, the question is to identify the source of feedback that makes small haloes dark and to identify any obvious mass scales where truncation in the efficiency of galaxy formation occurs.

3. **The too-big-to-fail problem:** This problem arises from observing fewer galaxies with large central densities ($\approx 10^{10} M_\odot$) than predicted by ΛCDM. Solutions may include baryon effects [68] or modifications to linear and nonlinear predictions, such as hot dark matter (WDM) or self-interacting dark matter particles (SIDM) [64].

The growing amount of data from the Milky Way and Andromeda satellites is used to constrain alternative DM models. Warm dark matter (WDM) models postulate particles with masses on the order of keV, while simulations Cosmological experiments with SIDM suggest that certain values of $\frac{\sigma}{m_{\text{SIDM}}} \approx (0.5 \times 10^{-21}\ \text{cm}^2/\ \text{g})$ could address challenges such as the core/cusp and the too-big-to-fail problem, leading to dark matter cores in dwarf galaxies with sizes of $(0.3 - 1.5)$ kpc [69]. However, observational constraints, especially in galaxy clusters, present additional challenges, highlighting the need for a $\sigma$ dependence on the particle velocity to resolve small-scale problems and meet the constraints observed at different ranges of speed [2].

## 2.4 Local density and velocity distribution

The density and distribution of dark matter in the Milky Way contain relevant dynamic information about our galaxy, especially important for experiments that seek to detect dark matter directly and indirectly. The "local density" of dark matter, denoted by $\rho_0$, refers to an average calculated within a volume spanning a few hundred parsecs in the vicinity of our solar system. The determination of $\rho_0$ from observations is performed using two classes of [70] methods. "Local measurements" are based on monitoring the vertical movement of tracer stars in the vicinity of the Sun. In contrast, "global measurements" extrapolate $\rho_0$ from the measured rotation curve, making use of additional assumptions about the shape of the galactic halo.

By comparing the extrapolated local density with that obtained from local measurements, it is possible to constrain the local configuration of the Milky Way halo. However, a major source of uncertainty in the estimate of $\rho_0$ comes from the contribution of baryons (stars, gas, stellar remnants) to the dynamical mass in the local neighborhood. For example, the motion of tracer stars, which is used in local measurements, is influenced by the total potential generated by both baryons and dark matter. To infer the additional contribution of dark matter, a robust baryon census is essential [71].

Recent determinations using global methods are in the range of $(0.2-0.6), \mathrm{GeV/cm^3}$ [72] [73] [74] [75] [76], in contrast, analyzes of local dark matter density from Data from the **Gaia** satellite provide values in the range of $(0.3-1.5), \mathrm{GeV/cm^3}$, depending on the type of stars used in the research [70].

Other observational quantities can be used that enter the DM phase space distribution and provide constraints on Milky Way mass models such quantities are the local circular velocity $v_c$ and the escape velocity $v_e$. Local circular velocity is measured by several methods, roughly divided into measurements of the Sun's velocity concerning an object assumed to be at rest concerning the galactic center or direct measurements of the local radial force. These methods return values of $v_c = (218-246)\,\mathrm{km/s}$. A recent estimate of the escape velocity, defined as the velocity above which objects are not gravitationally bound to our galaxy, is $v_e = 533^{+54}_{-41}\,\mathrm{km/s}$ [77].

An important fact is that the local velocity distribution of DM particles cannot be directly measured at present and is mainly derived from simulations. High-resolution simulations, focusing exclusively on DM, have revealed that the velocity distributions deviate significantly from a Maxwell-Boltzmann distribution. These simulations also evidence additional components above the predominant smooth distribution, including narrow peaks caused by tidal currents [78]. However, recent hydrodynamic simulations, incorporating baryons in Milky Way-like galaxies, have shown that these baryons have a non-negligible impact on the distribution of dark matter in the solar neighborhood [79].

Generally speaking, experiments typically employ the Simplest *Standard Halo Model (SHM)* as the basis for their data analysis. This model assumes an isotropic and isothermal sphere of dark matter particles with a density profile $\rho(r) \propto r^{-2}$. In this context, the velocity distribution is modeled as Maxwellian, with a velocity dispersion $\sigma_v = v_c/\sqrt{2}$. Although this distribution is formally defined to infinity, it is truncated at $v_e$ [80]. Surprisingly, recent hydrodynamic simulations have velocity distributions that are close to the Maxwell form, supporting the idea that the Standard Halo Model is a good approximation [81] [82] [83].

The primary purpose is to determine the velocity distribution from observations, taking advantage of data from the Gaia satellite to study various stellar populations, including those that share kinematics with dark matter (DM). It was recently revealed that the local stellar halo has two components: a weakly rotating quasi-spherical structure with metal-poor stars and an oblate, radially anisotropic structure of metal-rich stars, which arose due to accretion $(10^{11-12} M_\odot)$of a large dwarf galaxy about $(8-10)\times 10^9$ years ago [84]. Incorporating the anisotropic structure observed in the Gaia data an analytical expression for the velocity distribution can be established. The resulting local dark matter density is $(0.55 \pm 0.17)\,\mathrm{GeV/cm^3}$, with $30\%$ corresponding to the systematic error, while the circular rotation speeds and exhaust are set to $v_c = (233 \pm 3)\,\mathrm{km/s}$ and $v_e = 528^{+24}_{-25}\,\mathrm{km/s}$, respectively [85].

# Chapter 3
# Axions and Axion-like particles

*"Tapestries are made by many artisans working together. The contributions of separate workers cannot be discerned in the completed work, and the loose and false threads have been covered over. So it is in our picture of particle physics."*
**— Sheldon L. Glashow**

As we advance our understanding of the cosmos, the search for suitable candidates for dark matter has become an exciting and challenging field of study.

In this chapter, we will delve into a fascinating world of exotic particles that have been proposed as possible candidates for DM. Among these particles, one that has gained notoriety is the axion, a hypothetical particle that possesses unique properties that make it a strong contender to solve the mystery of DM. However, it is not alone in this quest. Similar particles, known as **Axion-Like Particles (ALPs)**, also figure prominently in this exploration. In the next few pages, we will explore the properties, characteristics, and potential evidence supporting the consideration of axions and ALPs as possible DM candidates.

## 3.1 The Strong CP problem

Next, we will explore one of the most likely sources of CP symmetry violation in the SM. As we mentioned earlier, the problems $U(1)_A$ and $CP$ Strong become even more intertwined by including the weak interactions.

Sometimes global chiral symmetries, such as $\psi \to e^{i\gamma_5\theta}\psi$, which are symmetries in a classical Lagrangian density, do not hold as symmetries in a quantum theory. In these cases, we say that the symmetries are "anomalous". As we will see, we can understand that these anomalies arise in situations in which a classical action remains invariant under a symmetry transformation, but the path integral measure does not. An illustrative example is when we apply a chiral transformation to a quark, which results in [27]

$$\int \mathcal{D}\overline{\psi}\mathcal{D}\psi \to \int \mathcal{D}\overline{\psi}\mathcal{D}\psi \left( i\theta \int \frac{g_s^2}{64\pi^2} \epsilon^{\mu\nu\rho\sigma} G^a_{\mu\nu} G^a_{\rho\sigma} \right) , \tag{3.1}$$

where $G^a_{\mu\nu}$ is the field strength given in eq. (1.17) for anything under which quarks are charged, $g_s$ is the corresponding charge, and $\epsilon^{\mu\nu\rho\sigma}$ is the Levi-Civita symbol with 4 indices [1]. For multiple generations, rotating by $\psi^i_R \to R^{ij}\psi^j_R$ and $\psi^i_L \to L^{ij}\psi^j_L$, the angle of rotation will be given by $\det(R^\dagger L) = re^{i\theta}$ for some $r \in \mathbb{R}$ [2].

The term $\epsilon^{\mu\nu\rho\sigma} G^a_{\mu\nu} G^a_{\rho\sigma}$ conserved the charge conjugation $C$ but violates both spatial parity $P$, temporal reversal $\mathcal{T}$ and therefore violates $CP$. To understand this in detail, let's take into account

[1] It is antisymmetric under exchange of two contiguous indexes.
[2] If the rotation is non-chiral $\theta = \det(R^\dagger L) = re^{i\theta} = 0$.

the following transformation laws under $CP$:

$$A_0^a(t,\mathbf{x}) \to -A_0^a(t,-\mathbf{x})\,, \qquad A_i^a(t,\mathbf{x}) \to A_i^a(t,-\mathbf{x})\,, \qquad \partial_0 \to \partial_0\,, \qquad \partial_i \to -\partial_i\,. \tag{3.2}$$

If both $CP$ and $P$ are violated, then the Lagrangian density has the following allowed terms

$$\mathcal{L}_{CPV} = \theta_{\text{QCD}}\frac{g_s^2}{64\pi^2}\epsilon^{\mu\nu\rho\sigma}G^a_{\mu\nu}G^a_{\rho\sigma} + \theta_2\frac{g^2}{64\pi^2}\epsilon^{\mu\nu\rho\sigma}W^a_{\mu\nu}W^a_{\rho\sigma} + \theta_1\frac{g'^2}{32\pi^2}\epsilon^{\mu\nu\rho\sigma}B_{\mu\nu}B_{\rho\sigma}\,. \tag{3.3}$$

Here, $G^a_{\mu\nu}$, $W^a_{\mu\nu}$ and $B_{\mu\nu}$ represent the intensity fields corresponding to the $SU(3)$, $SU(2)$ and $U(1)$ symmetries (see eq.(1.17)-ec.(1.18).). The inclusion of these terms in the theory is not only permitted, also it is necessary to do so. This is because these terms can originate through divergent corrections in the ultraviolet ($UV$) limit, and therefore the introduction of the parameters $\{\theta_i\}$ becomes necessary to regularize these divergences [34].

On the other hand, it is important to note that since the values of $\theta_i$ can change under chiral rotations, questions arise about whether these parameters can have observable consequences. This is because observations in physics must be independent of our choices of chiral phase conventions, which poses challenges in the interpretation of these terms and their possible implications for observable phenomena.

To see if the angles $\theta_i$ have observable consequences, let's check the Yukawa matrices, which can be written as (C.f. ec. (1.41))

$$Y_d = U_d M_d U_d^\dagger K_d^\dagger\,, \qquad\qquad Y_u = U_u M_u U_d^\dagger K_u^\dagger\,.$$

Extra factors $U_d^\dagger$ and $U_u^\dagger$ have been inserted here, without loss of generality. Then we can perform chiral rotations only on the right-hand fields to remove $K_d$ and $K_u$, and then perform non-chiral rotations to remove $U_d$ and $U_u$. The phase induced by the chiral rotations $K_d$ and $K_u$ is given by

$$\arg\det(K_dK_u) = -\arg[\det(M_dM_u)\det(Y_dY_u)] = -\arg\det(Y_dY_u)\,,$$

as $\det(M_dM_u) \in \mathbb{R}$. Then the $CP$ violating term after rotation is written as

$$\mathcal{L}_\theta = \bar\theta\frac{g_s^2}{32\pi^2}G^a_{\mu\nu}\widetilde{G}^{a\mu\nu}, \quad \text{with} \quad \bar\theta = \theta_{\text{QCD}} - \Delta\theta_{EW} \quad \text{and} \quad \widetilde{G}^{a\mu\nu} = \frac{1}{2}\epsilon^{\mu\nu\rho\sigma}G^a_{\rho\sigma}\,, \tag{3.4}$$

where

$$\Delta\theta_{EW} := \det(Y_dY_u)\,. \tag{3.5}$$

A chiral rotation moves the phase back and forth between $\theta_{\text{QCD}}$ and $\Delta\theta_{EW}$, leaving $\bar\theta$ unchanged. Therefore, $\bar\theta$ is an independent measure of the basis of $CP$ violation and may be physical. $\bar\theta$ is known as the **strong CP phase**. However, if $\det(M_dM_u) = 0$, that is, if any of the quark masses disappear, then $\bar\theta$ becomes non-physical again. We observe that the angles associated with $SU(2)$ and $U(1)$ can be completely eliminated by chiral rotations [3] [27]. Therefore, neither $\theta_2$ nor $\theta_1$ can have physical consequences.

[3] Rotating only the right-hand fields can make the Yukawa couplings real, but $\theta_2$ does not change with these rotations since the right-hand fields are not charged. Therefore, we can rotate the left-hand fields just to put $\theta_2$ into the Yukawa couplings and then rotate the right-hand fields to remove it. Therefore, there is no independent measure of the basis of $CP$ violation for $SU(2)$ and $\theta_2$ is not physical. Similarly, since neutrinos have no charge, we can rotate them to show that the $U(1)$ phase is unphysical.

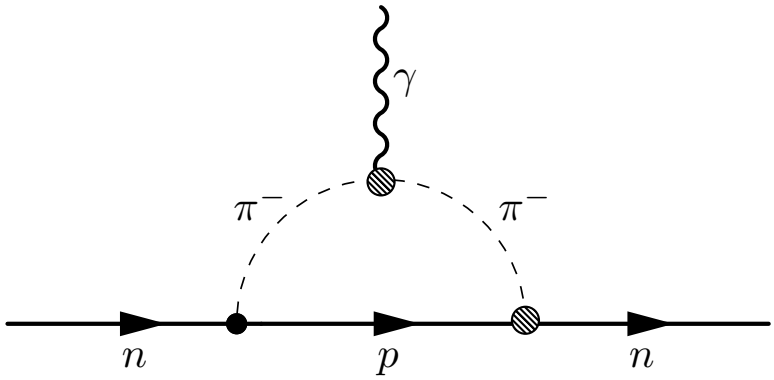


Figure 3.1: Feynman diagram of the main contribution to NEDM [6]. The black ball represents the CP flight effect and the striped balls represent the effective couplings.

We have observed that $\bar{\theta}$ is independent of the basis, and if none of the quark masses disappear, then it can be measured. However, as we indicated at the end of Chapter 1, this term does not appear in perturbation theory. To understand this, let us note that the quantum anomaly manifests itself in an equation where the divergence of the current is proportional to a gluonic field term [86]. This shows that the supposed $U(1)_A$ symmetry ($U(1)_A$ Problem, [45]) never existed from the beginning, even for light quarks, and only three Goldstone bosons are predicted in the isotopic spin limit [43]. So we can write

$$G^a_{\alpha\beta}\widetilde{G}^{a\alpha\beta} = \partial_\mu K^\mu\,, \qquad\qquad K^\mu := \epsilon^{\mu\nu\rho\sigma}\left(A^a_\nu G^a_{\rho\sigma} - \frac{g_s}{3} f^{abc} A^a_\nu A^b_\rho A^c_\sigma\right)\,,$$

showing that $G^a_{\alpha\beta}\widetilde{G}^{a\alpha\beta}$ is a total derivative, where $K^\mu$ is known as the **Chern-Simons current** [87]. Total derivatives never contribute to perturbation theory, since Feynman's rule would have a factor of the sum of all the moments entering the vertex minus the moments leaving it, resulting in a factor of zero. Therefore, $\bar{\theta}$ can only have physical consequences through non-perturbative effects [86].

### 3.1.1 Neutron Electric Dipole Moment

The term $G^a_{\mu\nu}\widetilde{G}^{a\mu\nu}$ does not change the flavor, and although we cannot calculate the effect of $\bar{\theta}$ directly in QCD, we can make accurate quantitative predictions using the chiral Lagrangian density. The chiral Lagrangian density is a nonlinear sigma model in which the pions are embedded in a compound field $U(x) = \exp 2i\pi^a(x)\tau^a/f_\pi$, being $f_\pi$ the decay constant of the neutral-pion [27].

One of the most important consequences of this model is that the neutron acquires an Electric Dipole Moment (EDM) proportional to $\bar{\theta}$. The neutron and proton form an isospin doublet, so their couplings to the pion must be of the form

$$\mathcal{L}_{\pi NN} = \pi^a \bar{\psi}\left(i\gamma^5 g_{\pi NN} + \bar{g}_{\pi NN}\right)\tau^a\psi\,, \tag{3.6}$$

where $\psi$ is the proton-neutron isospin doublet. The first term is the ordinary Yukawa coupling to pseudoscalar pions, which gives rise to the Yukawa potential that describes the strong nuclear force

between nucleons. The second term violates $CP$ and must be proportional to $\bar{\theta}$. Upgrading isospin to $SU(3)$, it can be shown that [88] [4]

$$\bar{g}_{\pi NN} = -\frac{m_u m_d}{F_\pi(2m_s - m_u - m_d)(m_u + m_d)}(M_\Xi - M_N)\bar{\theta} \approx 0.038\bar{\theta}\,, \tag{3.7}$$

or a more updated value $\bar{g}_{\pi NN} \approx 0.023\bar{\theta}$ [6]. It can be compared with $g_{\pi NN} = 13.4$ [88]. Pion loops with the $CP$ violation at the vertex $\bar{g}_{\pi NN}$ generate a Neutron Electric Dipole Moment (NEDM). These loops are UV divergent. Cutting off the UV divergences into $m_N$ gives [88]

$$d_N = \frac{m_N}{4\pi^2} g_{\pi NN}\bar{g}_{\pi NN} \ln\frac{m_N}{m_\pi} e = (5.2 \times 10^{-16}\, e \cdot \text{cm})\bar{\theta}\,. \tag{3.8}$$

Therefore, using the upper bound value for the NEDM $|d_N| < 2.9 \times 10^{-26} e \cdot \text{cm}$ [90], so $\bar{\theta} < 10^{-10}$ or with updated values [6]

$$\bar{\theta} < 0.7 \times 10^{-11}\,. \tag{3.9}$$

*The smallness of $\bar{\theta}$ despite the large number of $CP$ violation in the weak sector* is known as the **Strong CP problem**.

### 3.1.2 About Strong CP problem solution

A symmetry-based solution to the $U(1)_A$ problem is considered natural. The Eqs. (3.4) with $\bar{\theta}$ provide an example. If one of the quark masses $m_q$ vanishes ($\det(M_u M_d) = 0$), leading to a chiral symmetry, then the non-physical phase $\alpha_i$ can be used to tune $\bar{\theta}$ to zero. However, no symmetry protects $m_q = 0$, since chiral symmetry is anomalous.

One could argue for some "pragmatic" solution. Assuming that $\bar{\theta}$ can in general be renormalized to any value, including zero. This is technically correct; however, setting $\bar{\theta}$ to a value less than $10^{-11}$ by hand is considered highly "unnatural".

- A priori there is no reason why $\theta_{\text{QCD}}$ and $\Delta\theta_{\text{EW}}$ should be practically zero.
- Even if $\theta_{\text{QCD}} = 0 = \Delta\theta_{\text{EW}}$ were established by decree, the quantum corrections to $\Delta\theta_{\text{EW}}$ are usually much larger than $10^{-9}$ and ultimately divergent [34].
- Expecting $\theta_{\text{QCD}}$ and $\Delta\theta_{\text{EW}}$ to cancel so that $\theta$ is small enough would require fine-tuning of a type that it would have to appear even to a skeptic as unnatural; since $\theta_{\text{QCD}}$ reflects the dynamics of the strong sector and $\Delta\theta_{\text{EW}}$ that of the electroweak sector.

Over the years, a solution to the Strong $CP$ Problem has been sought, and various proposals have emerged. In some of these solutions, evolution with the Renormalization-Group (RG) scale of $\bar{\theta}$ plays an important role. In particular, they try to fix $\bar{\theta}$ at some RG scale and take advantage of the fact that, in the Standard Model (SM), evolution with the RG scale of $\bar{\theta}$ occurs to 7-loops [91]. If $\bar{\theta}$ is set to 0 at some high scale and the Effective Field Theory (EFT) down to low energies is simply the SM, then $\bar{\theta}$ will remain very small at low energies, so it can be effectively ignored.

[4] For the values known at that time $\frac{m_u}{m_d} = 0.38 \pm 0.13$, $\frac{m_d}{m_s} = 0.045 \pm 0.011$ [89] and $\ln\frac{m_N}{m_\pi} = 1.9$ [88] or the mass term of the nucleon $m_N \sim 1\,\text{GeV}$.

The general assumption is that anything that is not prohibited by symmetries will not be null, so we claim that at 7-loops there is likely to be a non-null correction. The evolution with the Renormalization-Group (RG) scale of $\bar{\theta}$ is derived from the only other $CP$ violation phase in the SM, $\delta_{\text{CKM}}$. This relationship can be understood by treating $\bar{\theta}$ and $\delta_{\text{CKM}}$ as spurions [5] of the $CP$ symmetry. Furthermore, this evolution must respect the flavor symmetries $SU(3)_Q \times SU(3)u^c \times SU(3)_{d^c}$ of the SM.

Solutions to the strong $CP$ problem that use CP symmetry are typically called Nelson-Barr models [93] [94]. These models postulate that $CP$ is a good symmetry in the ultraviolet (UV) so that both the CKM and $\theta_{\text{QCD}}$ angles vanish. However, since CKM is observed to be large, while $\bar{\theta}$ is observed as small, these models are carefully constructed so that the breakdown of $CP$ generates a large CKM angle, while corrections to $\bar{\theta}$ are small. On the other hand, the QCD axion is probably the simplest solution: an additional pseudo-goldstone boson is introduced into the Standard Model, whose only non-derivative coupling is with the QCD topological charge [43] and is suppressed by the scale $f_a$, called the axion decay constant. This coupling allows the effects of the $CP$ violation angle $\theta$ to be redefined through a change of the axion field, thus ensuring that its vacuum expectation value (VEV) cancels out. Furthermore, it produces a mass for the axion of $\mathcal{O}(m_\pi f_\pi / f_a)$.

## 3.2 Peccei-Quinn Symmetry and Axions

As we have argued, $\bar{\theta} \leq \mathcal{O}(10^{-11})$ [6] could hardly arise accidentally. A particularly intriguing proposal is to reinterpret a physical quantity that is normally taken as a constant, as a dynamic degree of freedom that adjusts to a desired value in response to forces acting on it [7]. R. Peccei and H. Quinn complemented the Standard Model with a global $U(1)_{\text{PQ}}$ symmetry [96] [97], now called Peccei-Quinn symmetry, which is axial and has the following properties:

- It is a symmetry of the classical theory.
- It is subject to an axial anomaly; that is, it breaks down explicitly due to non-perturbative effects, reflecting the complexity of the QCD ground state.
- It also breaks spontaneously.

The original model that predicts the axion was proposed by Weinberg and Wilczek [4] [5], based on the idea of Peccei and Quinn [96] [97]. This formulation is known as the Peccei-Quinn-Weinberg-Wilczek (PQWW) model, or the "visible" axion model. In this framework, the axion field is identified as a phase direction of the Standard Model Higgs field. The need to introduce two (or more) Higgs doublets arises because the axion degree of freedom does not exist in the theory with a single Higgs doublet.

[5] Spurions are frequently used in Quantum Field Theory (QFT) to formally restore explicitly broken symmetries. In doing so, the calculation proceeds by requiring complete symmetry, and only at the end of the calculation is the original form of the breaking term reintroduced into the spurion field. This is a very efficient way to make evident how breakdown terms affect physical quantities [92].

[6] Originally the estimate was at $\bar{\theta} \leq \mathcal{O}(10^{-9})$ [34].

[7] An early example is provided by the original theory by Kaluza-Klein that invokes a six-dimensional space-time "manifold", where two of them are dynamically compactified and therefore lead to the quantization of electric and magnetic charge [95].

In the minimal version, we designate the two Higgs doublets as $\phi_1$ and $\phi_2$. We assign the charges $U(1)_{\rm PQ}$, $\beta_1$ and $\beta_2$, to the Higgs doublets and the quarks so that:

$$U(1)_{\rm PQ}: \quad \phi_1 \to e^{i\epsilon\beta_1}\phi_1\,, \quad \phi_2 \to e^{i\epsilon\beta_2}\phi_2\,, \tag{3.10}$$

$$u_L \to e^{i\epsilon\beta_2/2}u_L\,, \quad u_R \to e^{-i\epsilon\beta_2/2}u_R\,, \tag{3.11}$$

$$d_L \to e^{i\epsilon\beta_1/2}d_L\,, \quad d_R \to e^{-i\epsilon\beta_1/2}d_R\,, \tag{3.12}$$

where $\epsilon$ is an arbitrary constant parameter. Yukawa couplings for quarks become

$$\mathcal{L}_y = -y_u\bar{q}_L\phi_2 u_R - y_d\bar{q}_L\phi_1 d_R + \text{h.c.}\,. \tag{3.13}$$

Both PQ and electroweak symmetries are spontaneously broken when the two Higgs doublets acquire the vacuum expectation values.

$$\langle\phi_1^0\rangle = v_1, \quad \langle\phi_2^0\rangle = v_2, \quad v = \sqrt{v_1^2 + v_2^2} \approx 246\,\text{GeV}\,. \tag{3.14}$$

The axion in the PQWW model is considered "visible" in the sense that it makes observable predictions in laboratory experiments. However, theoretical predictions of the PQWW axion conflict with the experimental limits on the decay rate of $J/\Psi$ and $\Upsilon$ [98], as well as the decay of $K^+$ [99]. Other experiments, such as nuclear deexcitations and particle beam experiments, also contradict the predictions of the PQWW model [100]. These results initially seemed to rule out the original PQWW model. Subsequently, some variant models were proposed that avoided the $J/\Psi$ and $\Upsilon$ decay constraints [101] [102], but these models were also excluded by $\pi^+$ decay experiments [103] and beam experiments of electrons [104].

### 3.2.1 The Invisible Axion and representative models

The problem of the original PQWW model can be avoided if the PQ symmetry is broken at some energy scale $\eta$, which is higher than the electroweak scale $v \approx 246\,\text{GeV}$, since the couplings of axions with other particles are suppressed by $1/\eta$ [105].

This fact motivates the formulation of the "invisible" axion model. In this approach, the axion is not the phase direction of the Higgs doublet of the standard model. It is necessary to introduce a scalar field that is singular under $SU(2)_L \times U(1)_Y$, whose phase would be identified as the axion.

We denote the singular scalar field under $SU(2)_L \times U(1)_Y$ as $\Phi$ and designate it as the Peccei-Quinn field. Under the transformation $U(1)_{\rm PQ}$, it undergoes the following change:

$$U(1)_{\rm PQ}: \quad \Phi \to e^{i\epsilon}\Phi\,. \tag{3.15}$$

Here, we choose the PQ charge of $\Phi$ to be the unit [8]. We propose a potential for $\Phi$ as

$$V(\Phi) = \frac{\lambda}{4}(|\Phi|^2 - \eta^2)^2\,, \tag{3.16}$$

the PQ field takes the expected value of the void $|\Phi| = \eta$, and the phase direction of the axion field is identified as $\Phi \propto \exp(ia/\eta)$. The experimental limitations can be circumvented if $\eta$ is large enough compared to the electroweak scale.

[8] Alternatively, one can assign the PQ charge $Q_\Phi$ such that $\Phi \to e^{iQ_\Phi\Phi}$, $a \to a + f_a$, and $f_a = Q_\Phi\eta$.

The PQ field $\Phi$ cannot have direct couplings with the quarks of the standard model, since they acquire mass when $\Phi$ takes the value expected from the vacuum. To address the QCD anomaly, additional fields need to be incorporated into the standard model sector. Below we present two well-known examples:

- **KSVZ model**
  In the Kim-Shifman-Vainshtein-Zakharov (KSVZ) model [105] [106], the QCD anomaly is obtained by introducing a heavy quark $Q$, which has a Yukawa coupling with the PQ field:

  $$\mathcal{L}_Q = -y_Q \bar{Q}_L \Phi Q_R + \text{h.c.}\,. \tag{3.17}$$

  Under the symmetry $U(1)_{\text{PQ}}$, the heavy quark transforms as:

  $$U(1)_{\text{PQ}}: \quad Q_L \to e^{i\epsilon/2} Q_L, \quad Q_R \to e^{-i\epsilon/2} Q_R\,. \tag{3.18}$$

  In this model, only $\Phi$ and $Q$ have charge under $U(1)_{\text{PQ}}$. In particular, the axion does not interact with electrons. Such a model is called the "hadronic axion" model [107].

- **DFSZ Model**
  The Dine-Fischler-Srednicki-Zhitnisky (DFSZ) model [108] [109] realizes the QCD anomaly without introducing a heavy quark. The trick is to assume two Standard Model Higgs doublets, $\phi_1$ and $\phi_2$. Light quarks couple directly to $\phi_1$ and $\phi_2$ via the Yukawa terms (3.13), but not to the PQ field $\Phi$. The PQ field couples to the two Higgs doublets through the scalar potential:

  $$\begin{aligned} V(\phi_1, \phi_2, \Phi) =& \lambda_1 \frac{1}{4}(\phi_1^\dagger \phi_1 - v_1^2)^2 + \lambda_2 \frac{1}{4}(\phi_2^\dagger \phi_2 - v_2^2)^2 + \lambda \frac{1}{4}(|\Phi|^2 - \eta^2)^2 \\ &+ (a\phi_1^\dagger \phi_1 + b\phi_2^\dagger \phi_2)|\Phi|^2 + c(\phi_1 \cdot \phi_2 \Phi^2 + \text{h.c.}) + d|\phi_1 \cdot \phi_2|^2 + e|\phi_1^\dagger \phi_2|^2\,. \end{aligned} \tag{3.19}$$

  The Lagrangian is invariant under the PQ symmetry transformation $U(1)_{\text{PQ}}$:

  $$\begin{aligned} U(1)_{\text{PQ}}: \quad & \phi_1 \to e^{-i\epsilon}\phi_1, \quad \phi_2 \to e^{-i\epsilon}\phi_2\,, \\ & u_L \to u_L, \quad u_R \to e^{i\epsilon} u_R\,, \\ & d_L \to d_L, \quad d_R \to e^{i\epsilon} d_R\,, \end{aligned} \tag{3.20}$$

  along with (3.15). The axion field is a linear combination of the phases of three scalar fields $\phi_1^0$, $\phi_2^0$ and $\Phi$.

Of course, the purpose of these models is to solve the strong CP problem, therefore, we will explain the mechanism that solves this problem.

### 3.2.2 The Peccei-Quinn mechanism

R. Peccei and H. Quinn proposed the theory that naturally explains the smallness of $\bar{\theta}$ [96] [97]. The essence of his idea consists of the following:

1. Introduce a field $a$, which we call the axion field. It is a singlet of $SU(2)_L$.

2. Assume that there exists a global axial symmetry $U(1)$, which we call Peccei-Quinn (PQ) symmetry, and that this symmetry $U(1)_{\text{PQ}}$ is spontaneously broken at some scale of energy greater than the QCD scale $\Lambda_{\text{QCD}} \approx \mathcal{O}(100\ \text{MeV})$.

3. Impose appropriate PQ charges on the quarks so that an anomaly $U(1)_{\text{PQ}}$-$SU(3)_C$ exists.

The dynamical degree of freedom $a$ can be identified as a Nambu-Goldstone boson associated with spontaneous symmetry breaking $U(1)_{\text{PQ}}$ [4] [5]. The symmetry $U(1)_{\text{PQ}}$ acts as a displacement in the field

$$U(1)_{\text{PQ}} : a \to a + \epsilon\eta\,, \tag{3.21}$$

where $\eta$ is an arbitrary constant parameter and the energy scale of spontaneous symmetry breaking $U(1)_{\text{PQ}}$. According to assumption 3, the current $U(1)_{\text{PQ}}$ is not conserved due to the anomaly:

$$\partial_\mu j^\mu_{\text{PQ}} = \frac{g_s^2}{32\pi^2} C_Q G^a_{\mu\nu} \widetilde{G}^{a\mu\nu}\,, \tag{3.22}$$

where $C_Q$ is a constant determined by the model charge assignment. This implies that the Lagrangian density must be transformed according to (3.21) as

$$\delta\mathcal{L} = \frac{g_s^2}{32\pi^2} C_Q G^a_{\mu\nu} \widetilde{G}^{a\mu\nu}\,. \tag{3.23}$$

Then, the low energy effective Lagrangian density can be written as:

$$\mathcal{L}^{\text{Low}}_{\text{eff}} = -\frac{1}{4} G^a_{\mu\nu} G^{a\mu\nu} + \frac{1}{2}\partial_\mu a \partial^\mu a + \frac{g_s^2}{32\pi^2}\frac{a}{f_a} G^a_{\mu\nu}\widetilde{G}^{a\mu\nu} + \bar{\theta}\frac{g_s^2}{32\pi^2} G^a_{\mu\nu}\tilde{G}^{a\mu\nu} + \dots\,, \tag{3.24}$$

where the ellipses correspond to possible terms containing derivatives of $a$, and $f_a := \frac{\eta}{C_Q}$ is called **axion decay constant**. The eq. (3.24) shows that the observable parameter $\bar{\theta}_{\text{eff}}$ is determined by the value of the axion field: $\bar{\theta}_{\text{eff}} := \frac{a}{f_a} + \bar{\theta}$.

If there is no term that violates the $CP$ except for the term proportional to $\bar{\theta}_{\text{eff}}$, the effective potential for the axion field is minimized by $\bar{\theta}_{\text{eff}} = 0$, and therefore the strong CP problem is solved. Let's see that this proposal is appropriate.

The effective potential $V(a)$ for the axion field is obtained by integrating the gluon field into the path integral in Euclidean spacetime:

$$\exp\left\{-\int d^4x V(a)\right\} = \left|\int \mathcal{D}A \exp\left\{-\int d^4x \left[\frac{1}{4} G_{a\mu\nu} G^{\mu\nu}_a - i\frac{g_s^2}{32\pi^2}\frac{a+\bar{\theta}f_a}{f_a} G^a_{\mu\nu}\widetilde{G}^{a\mu\nu}\right]\right\}\right|\,, \tag{3.25}$$

where we have ignored the kinetic energy of the axion field. Using the Schwarz inequality [9], we find that

$$\begin{aligned}
\exp\left\{-\int d^4x V(a)\right\} &\le \int \mathcal{D}A \left|\exp\left\{-\int d^4x \left[\frac{1}{4} G_{a\mu\nu} G^{\mu\nu}_a - i\frac{g_s^2}{32\pi^2}\frac{a+\bar{\theta}f_a}{f_a} G^a_{\mu\nu}\widetilde{G}^{a\mu\nu}\right]\right\}\right| \\
&= \int \mathcal{D}A \exp\left\{-\int d^4x \frac{1}{4} G_{a\mu\nu} G^{\mu\nu}_a\right\} \\
&= \exp\left\{-\int d^4x V(a = -\bar{\theta}f_a)\right\}\,.
\end{aligned} \tag{3.26}$$

[9] $\left|\int d^4x f\right| \le \int d^4x\, |f|$.

Therefore, $\int d^4x V(a) \geq \int d^4x V(a = -\bar{\theta} f_a)$. We dynamically deduce that the value of $\bar{\theta}_{\text{eff}} = \frac{\langle a \rangle}{f_a} + \bar{\theta} = 0$ is a minimum of the effective potential for the axion field, where $\langle a \rangle$ the VEV of the axion field. The excitations around this void are known as **axions**. Furthermore, since the potential is generated by integrating the gluon field, the height of the potential is given approximately by the QCD scale $\sim \Lambda^4_{\text{QCD}}$.

In short, spontaneous symmetry breaking will give rise to Goldstone bosons called axions. Since $U(1)_{\text{PQ}}$ is axial, it exhibits a triangular anomaly leading to a coupling of the axion field with $G^a_{\mu\nu}\widetilde{G}^{a\mu\nu}$, as indicated in [34][44]:

$$\mathcal{L}a = \left(\frac{a}{f_a} + \bar{\theta}\right) \frac{1}{32\pi^2} G^a_{\mu\nu}\widetilde{G}^{a\mu\nu} \,. \tag{3.27}$$

This, in turn, generates mass for the axion; more importantly, it transforms the quantity $\bar{\theta}$ into a dynamic quantity that depends on the axion field. The potential due to non-perturbative dynamics induces a vacuum expectation value for the axion such that $\bar{\theta} \approx 0$ [44].

We have written both the term $\theta$ and the axion coupling to demonstrate a simple trick that shows how the axion is coupled. As can be seen in this interaction, the axion follows an anomalous symmetry:

$$a \to a + \alpha f_a, \quad \bar{\theta} \to \bar{\theta} - \alpha \,. \tag{3.28}$$

This symmetry dictates how the axion can attach to particles. For example, any non-derivative axion interaction can be obtained by noting that where we have a coupling $\theta$, we can replace it with $\theta + a/f_a$. Derivative couplings are more complicated because $\partial\theta = 0$, so they are not accompanied by a corresponding coupling of $\theta$. QCD axion UV terminations will occasionally generate other couplings [44]:

$$\mathcal{L}_{\text{int}} = \frac{a}{f_B}\frac{1}{32\pi^2} B_{\mu\nu}\widetilde{B}^{\mu\nu} + \frac{a}{f_W}\frac{1}{32\pi^2} W^a_{\mu\nu}\tilde{W}^{a\mu\nu} \,. \tag{3.29}$$

Axions with these additional couplings are still called a QCD axion as long as the axion still has the coupling shown in Eq. (3.27). Due to the anomalous symmetry structure of the axion and the topological nature of the $\theta$ spurion, these couplings must be there initially, or they are not generated by evolution with RG.

The purpose of introducing the axion was to solve the Strong CP Problem, so we will see how the axion sets the electric dipole moment (neutron EDM) to zero. Using low-order chiral perturbation theory for the pion and neutron presented in [110], we can shown that [44]:

$$d_N \propto \frac{\langle a \rangle}{f_a} + \bar{\theta} = 0 \,. \tag{3.30}$$

Therefore, once the axion relaxes to the minimum of its potential, it dynamically sets the electric dipole moment of the neutron to zero. As stated, the QCD axion solves the Strong $CP$ Problem, since the entire CP breakdown in QCD is dictated by the $\bar{\theta}$ spurion. An important fact is that, once all quark generations are included, the CKM matrix has a $CP$ violation phase that can break $CP$ and shift the axion potential away from having the electric dipole moment of the neutron equal to zero. This effect is estimated to have a size of $\frac{\langle a \rangle}{f_a} + \bar{\theta} \sim 10^{-18} - 10^{-20}$ [111].

### 3.2.3 The axion quality problem

The Axion Quality Problem arises because, despite the existence of a well-defined anomalous symmetry associated with the axion couplings, as shown in Eq. (3.27), there is no proper symmetry linked to this. This lack of appropriate symmetry properties gives rise to two problems, which together are called the Axion Quality Problem [112] [113]:

1. Quantum gravity is postulated to violate all ungauged symmetries [114]. Thus, even if anomalous symmetry is imposed, gravitational effects will break it, resulting in the axion acquiring a separate mass term. This prevents the axion from centering around a zero EDM of the neutron, thus reintroducing the problem.

2. Effective Field Theories (EFTs) are constructed by specifying the particle and symmetry content of the problem [115], and then writing out each coupling allowed by the symmetry. Due to the lack of symmetry properties of the axion, it is not possible to form the axion coupling in Eq. (3.27) without also including several other couplings.

There are various ways to approach the Axion Quality Problem, broadly classified into theories where $U(1)_{\text{PQ}}$ is an accidental symmetry, theories where $U(1)_{\text{PQ}}$ comes from gauge symmetries in 5 dimensions, and examples from string theory [116]. However, none of these approaches comes close to the elegance of axion EFT. The complexity of the models required to justify elegant EFT often goes unnoticed in discussions of the axion.

## 3.3 Variations of the Axion of QCD and ALPs

The QCD axion EFT stands out for its elegance and simplicity. Their coupling to gluons and their mass are intrinsically linked, while couplings to fermions and photons depend on the model in question. As the exploration of diverse frontiers has gained momentum, two fundamental variations of the QCD axion have been investigated.

In the first variation, couplings to fermions and photons are observed that are considerably larger than anticipated. The second case breaks the mass-neutron coupling relationship. The QCD axion coupling to fermions, $f_Q$, and photons, $g_{a\gamma\gamma}$, can be much larger or smaller than $f_a$:

$$\frac{g_{a\gamma\gamma}a}{4}F_{\mu\nu}\widetilde{F}^{\mu\nu}, \quad \frac{\partial_\mu a}{f_Q}Q^\dagger\sigma^\mu Q\,. \tag{3.31}$$

Making $f_Q$ significantly smaller than $f_a$ turns out to be an arduous task, since the evolution of the renormalization network (RG) tends to bring $f_Q$ a within a loop factor of $f_a$ [44]. Similarly, reducing $g_{a\gamma\gamma}$ drastically below $\frac{1}{f_a}$ is complicated due to the mixing with pions that couples the axion to the photons [117] [111].

$$g_{a\gamma\gamma} \propto \frac{\alpha}{2\pi}\left(\frac{1}{f_{\text{UV}}} - \frac{1.92(4)}{f_a}\right)\,, \tag{3.32}$$

where $f_{\text{UV}}$ is the model-dependent coupling, and the second term comes from QCD. Photon couplings parametrically smaller than $f_a$ are only achievable if the two terms cancel. This cancellation occurs accidentally in some GUTs where $f_{\text{UV}} = \frac{f_a}{2}$ [118] and can happen if the Casimirs of the UV quarks are chosen to give $f_{\text{UV}} \sim \frac{f_a}{1.92}$ [119] [120]. There is no known way to get $g_{a\gamma\gamma}$ parametrically small without fine-tuning.

### 3.3.1 Axion-Like Particles

Unless complex models are accepted, the relation $g_{a\gamma\gamma} \sim \frac{1}{f_a}$ is valid for the QCD axion. As a consequence, mass and photon coupling, which are the most accessible of the axion couplings to investigate, are interrelated. Through this coupling, numerous experiments have been dedicated to the search for the QCD axion, although $g_a\gamma\gamma$ is completely decoupled from Strong $CP$ problem. The main reason for this search lies in the possibility of finding various particles that present the effective coupling of a scalar particle with two photons. These particles emerge in various extensions of the standard model and are called Axions-Like Particles (ALPs).

ALP-fermion couplings have some model dependence, since they depend on the $U(1)$ charge assignments for the fermions, in [121] you can find a description of what the general expectations are for these couplings in theories with several fields of axions. and an underlying GUT. While coupling with photons is generally present in ALP models, therefore, we will say that ALPs are particles that have the Lagrangian density expressed as:

$$\mathcal{L}_{\text{ALP}} = \frac{1}{2}\partial_\mu a \partial^\mu a + \frac{1}{2}m_a^2 a^2 - g_{a\gamma\gamma}\frac{a}{4}F_{\mu\nu}\widetilde{F}^{\mu\nu} \tag{3.33}$$

The mass of these particles may or may not come from the confinement of another gauge group. Due to the absence of coupling to gluons [10], mass and coupling to photons are completely independent of each other. There are motivations from string theory that suggest why these new particles may exist [123].

## 3.4 ALPs and Axions as Dark Matter

One of the attractive features of the axion is that it can also be dark matter, thus simultaneously addressing two fundamental problems [7] [8]. The abundance of axions as dark matter can originate from both the misalignment mechanism and topological defects. In this section, we will explore the properties of axions and ALPs in the context of their possible role as dark matter.

### 3.4.1 Production of Axions and ALPs

Axions and ALPs are stable particles and their interactions with ordinary matter are strongly suppressed. Consequently, if the relic abundance of these axions matches the current abundance of dark matter, there is a possibility of explaining the presence of dark matter in the universe through these axions. To assess whether axions can adequately explain the current abundance of dark matter, it is necessary to closely examine the mechanisms that govern their production in the early stages of the universe.

The cosmological scenario is different between the case where inflation occurred after the PQ phase transition (scenario I) and the case where inflation occurred before the PQ phase transition (scenario II). For scenario I, the quantum fluctuations of the axion field generated in the inflationary stage impose a constraint on some model parameters. On the other hand, for scenario II, we must take into account the evolution of topological defects such as strings and domain walls. Since these

[10] For light axions, since there are models in which heavy axions are expected and their coupling with gluons may be present [122].

topological defects produce an additional population of axions, the composition of the axion dark matter is different for each of the scenarios. In this section, we mainly consider the cosmological aspects of axions produced by distinct mechanisms.

**Thermal production: Freeze-out**

If the temperature of the primordial plasma is high enough, axions are generated from the thermal bath of the Quantum Chromodynamics (QCD) plasma. Thermal axion production is modeled using the standard freeze-out scenario [124] [125]. The thermal axion number density $n_a^{th}$ follows the Boltzmann equation

$$\frac{dn_a^{th}}{dt} + 3Hn_a^{th} = \Gamma(n_a^{eq} - n_a^{th}), \tag{3.34}$$

where $\Gamma = \sum_i n_i \langle \sigma_i v \rangle$ is the interaction rate, $n_i$ is the number density of species $i$, $\langle \sigma_i v \rangle$ is the thermal cross section average, and $H$ is the Hubble parameter defined in (A.7). $n_a^{eq}$ is the equilibrium number density of axions, obtained using the Bose-Einstein distribution [125]

$$n_a^{eq} = \frac{\zeta(3)}{\pi^2} T^3, \tag{3.35}$$

where $\zeta(3) = 1.20206...$ and $g = 1$ has been used for axions. Choosing a normalization $Y \equiv n_a^{th}/s$, where $s$ is the entropy density:

$$s = \frac{2\pi^2}{45 g_s^*} T^3 \,. \tag{3.36}$$

The Eq. (3.34) can be written as

$$x \frac{dY}{dx} = \Gamma H (Y_{eq} - Y) \,, \tag{3.37}$$

where $x = \frac{f_a}{T}$ and $Y_{eq} = \frac{n_a^{eq}}{s} \approx \frac{0.27}{g_*}$. In these equations, the approximation $g_{s^*} \approx g_*$ constant has been used, for simplicity.

The thermal mean interaction rate $\Gamma$ is calculated in [125] and includes three elementary processes:

1. $a + g \leftrightarrow q + \bar{q}$,
2. $a + q \leftrightarrow g + q$ and $a + \bar{q} \leftrightarrow g + \bar{q}$,
3. $a + g \leftrightarrow g + g$,

here $g$ is a gluon and $q(\bar{q})$ is a light quark (anti-quark). The result of the analysis in [125] is

$$\Gamma \approx 7.1 \times 10^{-6} \frac{T^3}{f_a^2} \,. \tag{3.38}$$

Since $H \propto T^2$, the following quantity turns out to be constant

$$k \equiv x \frac{\Gamma}{H} \,. \tag{3.39}$$

Let's define the quantity $y \equiv Y/Y_{eq}$, and we reduce the eq. (3.37) to

$$x^2 \frac{dy}{dx} = k(1-y)\,, \tag{3.40}$$

which has a solution

$$y(x) = 1 - Ce^{k/x}\,, \tag{3.41}$$

where $C$ is a constant of integration. The axions decouple from the QCD plasma at $x = k$ ($\Gamma = H$). After this, the number of axions becomes almost constant. The temperature at decoupling $T_D$ is obtained from the condition $x = k$, which gives

$$T_D = 2 \times 10^{11}\,\text{GeV} \left(\frac{f_a}{10^{12}\,\text{GeV}}\right)^2 . \tag{3.42}$$

The relic abundance of axions depends on the thermal history of the universe. For simplicity, let us assume that the PQ symmetry is broken after inflation if $T_R > f_a$, where $T_R$ is the heating temperature after inflation.

We can consider the following possibilities: (i) $T_R > f_a > T_D$, (ii) $T_R > T_D > f_a$, (iii) $T_D > T_R > f_a$, (iv) $T_D > f_a > T_R$, (v) $f_a > T_D > T_R$, (vi) $f_a > T_R > T_D$. The Eq. (3.41) is rewritten as:

$$y(x) = 1 - e^{k(1/x-1)}\,, \tag{3.43}$$

where the initial condition $y(x=1) = 0$ can be imposed so that axions do not exist at $T = f_a$. We require that the deviation of the thermal spectrum at the time of decoupling be less than $5\%$.

$$\frac{Y_D}{Y_{eq}} = y(x=k) = 1 - e^{k(1/k-1)} > 0.95\,, \tag{3.44}$$

where $Y_D$ is the value of $Y$ at decoupling. We obtain:

$$k = \frac{f_a}{T}\frac{\Gamma}{H} > 5.0 \times \left(\frac{10^{12}\text{GeV}}{f_a}\right) > 4\,. \tag{3.45}$$

This corresponds to the condition [126]

$$f_a < 1.2 \times 10^{12}\text{GeV}\,. \tag{3.46}$$

In other words, if Eq. (3.46) is satisfied, the axions enter thermal equilibrium before decoupling from the plasma. On the other hand, for cases (ii) and (iii), the axions never enter thermal equilibrium [125].

Since the PQ symmetry is broken before inflation for cases (iv), (v), and (vi), we must use a different initial condition than the one used in (i). Choosing the initial condition $y(x) = 0$ at $T = T_R$. This leads to the solution:

$$y(x) = 1 - e^{k(1/x - 1/x_R)}\,, \tag{3.47}$$

with $x_R \equiv f_a/T_R$. For cases (iv) and (v), the axions never enter thermal equilibrium, and we obtain:

$$y(\infty) = 1 - e^{-k/x_R}\,, \tag{3.48}$$

where $k/x_R = T_R/T_D < 1$. On the other hand, for case (vi), the axions could enter thermal equilibrium, but the condition for thermalization (3.45) is replaced by:

$$\frac{k}{x_R} = \frac{T_R}{T_D} > 4\,. \tag{3.49}$$

The relic abundance of thermal axions for case (i) or (vi) is:

$$n_a^{th}(t_0) = Y_{eq} s_0 = 0.27 g_*(T_D) s_0 = 7.8\,\mathrm{cm}^{-3}(100 g_*(T_D))\,, \tag{3.50}$$

Where $s_0$ is the entropy density at present, and $g_*(T_D)$ is the number of radiative degrees of freedom at the time of decoupling. The present density of thermal axions is:

$$\Omega_{a,th}h^2 = \frac{m_a n_{th_a}(t_0)}{\rho_{c,0}/h^2} = 4.44\times 10^{-9}\frac{100 g_*(T_D)}{(10^{12}\mathrm{GeV}/f_a)}\,, \tag{3.51}$$

Here, $\rho_{c,0}$ is the current critical density. The population of thermal axions is too small to explain dark matter for the typical value of the decay constant $f_a \sim 10^9 - 10^{12}$ GeV [127] [128]. Therefore, other mechanisms are proposed.

### Non-Thermal Production: Misalignment

The nonthermal production of axions is estimated by investigating the evolution of the background field. Let us consider the theory with the complex scalar field $\Phi$ (the PQ field) whose Lagrangian density is given by

$$\mathcal{L} = -\frac{1}{2}|\partial_\mu \Phi|^2 - V(\Phi)\,, \tag{3.52}$$

where the potential $V(\Phi)$ is defined by the equation (3.16). When $U(1)_{\mathrm{PQ}}$ breaks spontaneously, the axion field $a(x)$ is identified as the phase direction of the complex scalar field $\Phi$ such that

$$\Phi = \eta e^{ia(x)/\eta}. \tag{3.53}$$

The evolution of the axion field in the expanding FRW Universe (see A.1) is governed by the equation [129]

$$\ddot{a}(x) + 3H\dot{a}(x) - \frac{\nabla^2}{R^2(t)}a(x) + \frac{dV(a)}{da} = 0, \tag{3.54}$$

where $F(t)$ is the scale factor of the universe. Substituting the effective potential for the axion field into $V(a) = V_{\mathrm{QCD}}(a) + V_{\mathrm{grav}}(a)$, where [130]

$$V_{\mathrm{QCD}}(a) = m_a^2 f_a^2\left(1 - \cos\left(\frac{a}{f_a}\right)\right)\,, \tag{3.55}$$

while $V_{\mathrm{grav}}(a)$ is the unknown gravitational contribution, and is considered negligible [131]. Assuming that $a$ is small compared to $f_a$, we obtain

$$\ddot{a}(x) + 3H\dot{a}(x) - \frac{\nabla^2}{R^2(t)}a(x) + m_a^2 a(x) = 0\,. \tag{3.56}$$

We define the time $t_1$ in which the condition is satisfied

$$m_a(T_1) = 3H(t_1)\,. \tag{3.57}$$

where $T_1$ is the temperature at time $t_1$, and $H(t_1)$ is the Hubble parameter at that time.

Some years ago, Wantz and Shellard [132] presented the temperature dependence of $m_a$, which is valid at all temperatures within the interacting instanton liquid model [133]. Using this dependence, it can be argued, by observing the comparative scale of the Hubble parameter concerning mass and time $t_1$, that each mode that is outside the horizon up to $t \approx t_1$ is frozen, as shows in $\widetilde{a}(t, \mathbf{k}) = C_1(\mathbf{k}) + C_2(\mathbf{k})t^{-1/2}$ [11]. When the axion mass term becomes non-negligible $t > t_1$, they begin to oscillate with a frequency $m_a$. We call these modes zero modes and denote them as $a_0$. The evolution of $a_0$ is described by the equation $\ddot{a}_0 + 3H\dot{a}_0 + m_a^2 a a_0 = 0$.

### Misalignment: ALP Dark Matter

In a Friedmann-Robertson-Walker (FRW) universe, the equation of motion for ALP dark matter is described by [44]

$$\ddot{a} + 3H\dot{a} + m_a^2 a = 0\,. \tag{3.58}$$

It is generally considered a radiation-dominated universe where $H = 1/(2t)$. We assume that the axion has an initial field value $a = a_0$. In the early universe, Eq.(3.58) describes an overdamped harmonic oscillator, and we approximate it as

$$a = a_0\,, \quad H \gg m_a\,. \tag{3.59}$$

In the late universe, Eq.(3.58) describes an underdamped harmonic oscillator. Using the WKB approximation, we find that in the distant future,

$$a = \left(\frac{R(H = m_a)}{R(t)}\right)^{3/2} A_0 \cos(m_a t)\,, \quad H \ll m_a\,, \tag{3.60}$$

where $R$ is the scale factor. When estimating the numerical abundance of ALPs, we apply Eq.(3.59) and Eq. (3.60) when $3H > m_a$ and $3H < m_a$, respectively, ignoring the regime crossing. Using these approximations, we have $A_0 \approx a_0$.

It is notable that at late times, the axion behaves as cold non-relativistic matter, and its energy density decreases by

$$\rho(t) = \rho(H = m_a)\left(\frac{R(H = m_a)}{R(t)}\right)^3\,. \tag{3.61}$$

Furthermore, its energy is found through the Fourier transformation to be equal to its mass. Thus, we have a production mechanism for cold dark matter (CDM) that works even when the particle is much lighter than the keV scale. This is an impressive achievement since generally, dark matter with a mass below one keV behaves like hot dark matter.

The energy density of the Standard Model (SM) and the ALP when the ALP begins to behave like CDM is

$$\rho_{\text{SM}} \sim H^2 M_p^2 \sim m_a^2 M_p^2, \quad \rho_a \sim m_a^2 a_0^2\,. \tag{3.62}$$

[11] What is the axion field in Fourier space.

Here $M_p$ is the Planck mass scale. Requiring the ALP to represent all dark matter ($\rho_{\text{DM}} \sim T^3\text{eV}$) results in

$$a_0^2 \sim \frac{eV M_p^{3/2}}{m_a^{1/2}}\,. \tag{3.63}$$

As long as the initial value of ALP satisfies this condition, it will constitute all dark matter. Importantly, this is a simplification, as misalignment is also present when PQ symmetry is restored. In this case, the initial angle is random and can be averaged over all Hubble patches. The inhomogeneity in the axion initial angle leads to a different phenomenology.

**Misalignment: Axion Dark Matter**

The density estimate for axion dark matter is very similar to that of ALP DM but with one critical difference. The mass of the axion changes with time [132]. As a result, it is necessary to be careful about the lack of energy conservation.

The mass of the axion comes from thermal instantons [107], and through dimensional analysis, it is established [12] [44]

$$V \sim m_u m_d m_s T e^{-8\pi^2/g_3^2(T)} \cos\left(\frac{a}{f_a}+\theta\right) \sim m_u m_d m_s \Lambda^9 T^8 \cos\left(\frac{a}{f_a}+\theta\right)\,. \tag{3.64}$$

As a result, the temperature dependence of the axion is

$$m_a(T)^2 \sim \frac{m_u m_d m_s f_a^2 \Lambda^9 T^8}{f_a^2}\,. \tag{3.65}$$

Finally, before beginning to establish the DM abundance of the axion, we roughly specify the initial conditions for the axion. We take $a_0 = \theta_0 f_a$. Because the axion is a periodic field, we work with the misalignment angle $\theta_0$. The generic assumption people make is that $\theta_0 \sim \mathcal{O}(1)$, simply due to our affinity for numbers $\mathcal{O}(1)$. In some cases, the initial angle can be estimated in an inflationary context. Inflation will cause the expected value of the axion to change by about an amount $\sim H$ each Hubble time in the form of a random walk. This leads to inflation populating every value of $\theta_0$. Depending on how the measurement problem is approached, this may even lead to predictions for the value of $\theta_0$.

Another effect of inflation that changes the expected value of the axion is the existence of inhomogeneities between various Hubble patches. As a result, different Hubble patches will have different dark matter densities, leading to well-known isocurvature constraints if $H/f_a$ is not small enough [134] [135].

The equations of motion for the axion are

$$\ddot{a} + 3H\dot{a} + m_a^2(T)a = 0. \tag{3.66}$$

Comparing the energy densities of axion and dark matter at $T \sim \Lambda_{\text{QCD}} \sim 100\,\text{MeV}$, where conservation of energy in axions becomes a good approach:

$$\rho_a \sim \theta_0^2 \Lambda_{\text{QCD}}^4 \frac{m_a(T_c)}{m_a}\frac{\Lambda_{\text{QCD}}}{T_c^3} \sim \theta_0^2 \Lambda_{\text{QCD}}^4 \frac{f_a \Lambda_{\text{QCD}}}{T_c M_p} \sim \rho_{\text{DM}} \sim \text{eV}\ \Lambda_{\text{QCD}}^3, \tag{3.67}$$

[12] We are interested in the mass of the axion around temperatures between 100 MeV and 1 GeV, since in this range the QCD acts like the three-flavor QCD

where we have used $m_a^2 f_a^2 \sim \Lambda_{\text{QCD}}^4$. Solving the equation (3.67), we find that $T_c \sim$ GeV and $f_a \sim 10^{11}$ GeV [44].

The misalignment mechanism operates when the $PQ$ symmetry is broken during inflation and is never restored after inflation. Inflation results in the same initial conditions being seen everywhere. The topological mechanism operates when the $PQ$ symmetry is restored either during inflation or after inflation [136] [137] [138] and we will not talk about it since to talk about the production mechanisms is to motivate Axions and ALPs as dark matter.

### 3.4.2 Axion/ALPs couplings with photons

The interactions of the invisible axion with other particles have already been discussed previously and discussed in detail in [119]. The terminology surrounding axions can be slightly confusing in the extensive literature; Therefore, we clarify:

- QCD Axion: Solve the strong $CP$ problem.
- ALP: Does not solve the strong $CP$ problem.
- Axion: Must be determined by context. If the reader encounters the word "axion," he or she must discern from the context whether it solves the strong $CP$ problem.

Therefore, we will use the word "axion" to refer to both the QCD Axion and an ALP. We understand axions to be the hypothetical light bosons (sub-eV) predicted in some extensions of the standard model of particle physics. One of the most interesting couplings for axion detection [139][140] [141] [142] is its effective coupling with two photons. In astrophysical environments composed of high-energy gamma rays and turbulent magnetic fields, the existence of ALPs can modify the energy spectrum of gamma rays for sufficiently large coupling between axions and photons. This modification would result in an irregular behavior of the energy spectrum in a limited range.

Axions interact with photons due to effective coupling

$$\mathcal{L}_{a\gamma\gamma} = -\frac{1}{4} g_{a\gamma\gamma} a F_{\mu\nu} \widetilde{F}^{\mu\nu} \,, \tag{3.68}$$

where $F_{\mu\nu}$ is the field tensor of the photon and $\widetilde{F}^{\mu\nu} = \frac{1}{2} = \epsilon^{\mu\nu\ rho o\sigma} F_{\rho\sigma}$ is its dual, with $\epsilon^{0123} = +1$ and $g_{a\gamma\gamma}$ is coupling constant. The axion-photon coupling is parameterized by [13]

$$g_{a\gamma\gamma} = \frac{\alpha}{2\pi f_a} c_{a\gamma\gamma} \,, \tag{3.69}$$

where $\alpha = \frac{e^2}{4\pi}$ is the fine structure constant. The numerical coefficient $c_{a\gamma\gamma}$ is defined as

$$c_{a\gamma\gamma} := \frac{E}{C_Q} - \frac{2}{3}\left(\frac{4+Z}{1+Z}\right) \,, \tag{3.70}$$

with $C_Q$ being the color anomaly, as presented in equation (3.22), and $E$ being the electromagnetic anomaly. In the KSVZ model, $\frac{E}{C_Q} = 0$, while in the DFSZ model, $\frac{E}{C_Q}$ depends on the charge

[13] For the QCD axion

assignment of the leptons [143]. Here $Z = \frac{m_u}{m_d} \approx 0.48$ is the ratio between the up quark mass and the down quark mass [6].

Due to coupling with photons, the axion can decay into two photons with a decay width (see B.2)

$$\Gamma_\gamma = \frac{g_{a\gamma\gamma}^2 m_a^3}{64\pi} = \frac{\alpha^2}{256\pi^3 c_{a\gamma\gamma}^2} m_a^3 \left( \frac{f_a}{2.2 \times 10^{12}\ \text{GeV}} \right)^5 , \tag{3.71}$$

where we have used the equation $m_a \approx 6 \times 10^{-6}\,\text{eV} \left( \frac{10^{12}\,\text{GeV}}{f_a} \right)$ and $c_{a\gamma\gamma} = 1$ for simplicity. The axion half-life exceeds the age of the Universe, $t_0 \approx 10^{17}$ sec, for $f_a \lesssim 10^5$ GeV. Therefore, the invisible axion is practically stable, which motivates us to consider it as the dark matter of the Universe.

The interesting thing about this coupling is that in astrophysics extraordinary conditions more favorable for the interaction between axons and photons could arise, and their traces could become visible. There are three types of imprints of this type.

- The two-photon coupling described in Equation (15.54) allows stars like our Sun to produce axions by transforming a photon into an axion. The solar flux of axions can be searched directly by the inverse process that transforms an axion into a photon. A strong magnetic field $\mathbf{B}$ can stimulate axion $\rightarrow$ photon conversion, where the virtual photon affects the interaction with an inhomogeneous magnetic field in a cavity. Available microwave technology allows for impressive experimental sensitivity.

- There may also be indirect astrophysical signatures, as axion emission entails a loss of energy and thus provides a cooling mechanism in stellar evolution. Not surprisingly, its greatest impact comes in the lives of red giants and supernovae, such as SN 1987a. The actual limits depend on the model, whether a KSVZ or DFSZ axion, but relatively moderately. In summary, astrophysics tells us that if axions exist, we have [144]:

$$m_a < 10^{-2}\text{eV}\,. \tag{3.72}$$

Various bounds for axion parameters have been established in recent years.

| Mass Range $m_a$[eV] | Upper limit of $g_{a\gamma\gamma}$[GeV$^{-1}$] | Observation |
|---|---|---|
| $15 \times 10^{-9} < m_a < 60 \times 10^{-9}$ | $< 2.1 \times 10^{-11}$ | PKS 2155-304 [145] |
| $5 \times 10^{-10} < m_a < 5 \times 10^{-9}$ | $< 5 \times 10^{-12}$ | NGC 1275 [146] |
| $m_a < 10^{-13}$ | $< 2.6 \times 10^{-12}$ | M87 [147] |
| $0.6 \times 10^{-9} < m_a < 4 \times 10^{-9}$ | $< 10^{-11}$ | PKS 2155-304 [148] |
| $5 \times 10^{-10} < m_a < 5 \times 10^{-7}$ | $(2 \times 10^{-11} - 6 \times 10^{-11})$ | Mrk 421 [149] |
| $1 \times 10^{-8} < m_a < 2 \times 10^{-7}$ | $< 3 \times 10^{-11}$ | Mrk 421 [150] |
| $m_a < 1 \times 10^{-12}$ | $(6 - 8) \times 10^{-13}$ | NGC 1275 [151] |

Table 3.1: Upper limits of $g_{a\gamma\gamma}$ for different ranges of $m_a$.

The limit that we find interesting to analyze is $g_{a\gamma\gamma} < 0.66 \times 10^{-10}\,\text{GeV}^{-1}$ for $m_a < 0.02$ eV at the $2\sigma$ level [152]. Coincidentally, exactly the same limit has been deduced from the analysis of some particular stars in globular clusters [153].

# Chapter 4
# Generalized Compton scattering

*"The only laws of matter are those that our minds must fabricate and the only laws of mind are fabricated for it by matter."*
**—James C. Maxwell**

*In this chapter, we will be using conventional units due to the interest of the topic in astrophysics.*

A noteworthy situation to consider in nature is the passage of a particle in a photon gas such that the particle can scatter photons. In the most general case, we have a gas of photons with differential number density

$$dn = n(\epsilon, \mathbf{i}_\Omega) d\epsilon d\Omega \,, \tag{4.1}$$

which is the number of photons per unit volume with energies within $d\epsilon$, moving in the direction defined by the unit vector $\mathbf{i}_\Omega$ and the solid angle element $d\Omega$. In the most general case, we can consider the distribution of *scattering particles* $dn_s = n_s(\epsilon_1, \mathbf{i}_{\Omega_s}) dE_s d\Omega_s$ passing through a gas of photons and we wonder: what is the total spectrum of "Compton photons" scattered per unit volume and time $dN_1/dtdV d\epsilon_1 d\Omega_1$?

We will focus on trying to solve this problem with a series of simplifications that result in certain limiting cases that correspond to conditions in some astrophysics problems [1]. The simplifications we will make are listed below, where we work in the reference system where the scattering particle rests.

- (*Low energy*) The photon energy before scattering in the reference frame where the electrons are at rest must be $\epsilon' \ll m_s c^2$ [2].
- (*High energy*) The photon energy before scattering in the reference frame where the electrons are at rest must be $\epsilon' \gg m_s c^2$ [3].

In the usual Compton scattering process, an electron $e^-$ is considered at rest and free (it could even be inside some metal but weakly bound). Then, a radiation beam is incident upon it, and a scattering process occurs, which must be considered as an inelastic collision [4] between a photon and the electron to explain the experimental results. We can generalize this situation by considering that the scattering particle of mass $m_s$ is not necessarily at rest.

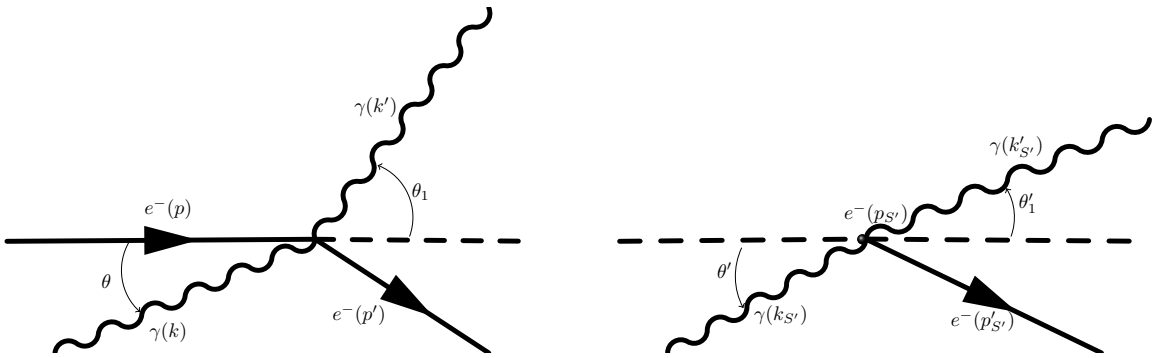


Figure 4.1: Pictorial representation of Compton scattering with electrons: (a) Laboratory reference frame, (b) Reference frame where the electron is at rest.

## 4.1 Relativistic kinematics of Compton scattering

Consider the collision between a photon and a particle of mass $m_s$ with which it can interact (for example, an electron). We have the following $4$-momenta before the collision in the reference frame, which we will call

$$p^\mu = \gamma m_s (c, \mathbf{v}) \,, \tag{4.2}$$

$$k^\mu = \frac{\epsilon}{c} (1, \mathbf{i_k}) \ , \tag{4.3}$$

where $\mathbf{i_k}$ indicates the direction of propagation of the incident photon and $\gamma = (1-\beta^2)^{-1/2}$ with $\beta = \frac{v}{c}$, such that $|\mathbf{v}| = v$. After the collision, we have the following $4$-momenta in the reference system of the *laboratory*

$$p'^\mu = \gamma' m_p (c, \mathbf{v}') \,, \tag{4.4}$$

$$k'^\mu = \frac{\epsilon_1}{c} (1, \mathbf{i_{k'}}) \ , \tag{4.5}$$

where $\mathbf{i_{k'}}$ indicates the direction of propagation of the scattered photon and $\gamma' = (1-\beta'^2)^{-1/2}$ with $\beta' = \frac{v'}{c}$, such that $|\mathbf{v}'| = v'$. From the conservation of $4$-momentum and using the dispersion relations $p^2 = p'^2 = m_s^2 c^2$ (for the particle of mass $m_p$) and $k^2 = k'^2 = 0$ (for the photon)

$$p \cdot k' + k \cdot k' = p \cdot k \,. \tag{4.6}$$

With this equation, we can establish a relationship between the energy of the scattered photon and the energy of the incident photon. To do this, we note that the scalar products of the involved

[1]When the particles that scatter photons are electrons, for example.

[2]This is in agreement with the Thomson limit established with electrons, in which the scattering cross-section is independent of the energy of the incident photon.

[3]When the scattering particle is an electron, this condition is known as the Klein-Nishina extreme limit.

[4]In an elastic collision the total kinetic energy of the system is conserved and there is no energy loss, while in an inelastic collision such as Compton scattering, there is energy loss and the total kinetic energy of the system is not conserved.

4-momenta are

$$p \cdot k' = p_\mu k'^\mu = \gamma m_s \epsilon_1 \left(1 - \frac{\mathbf{v}}{c} \cdot \mathbf{i}_{\mathbf{k}'}\right) , \tag{4.7}$$

$$k \cdot k' = k_\mu k'^\mu = \left(\frac{\epsilon}{c}\right)\left(\frac{\epsilon_1}{c}\right)(1 - \mathbf{i}_{\mathbf{k}} \cdot \mathbf{i}_{\mathbf{k}'}) , \tag{4.8}$$

$$p \cdot k = p_\mu k^\mu = \gamma m_s \epsilon \left(1 - \frac{\mathbf{v}}{c} \cdot \mathbf{i}_{\mathbf{k}}\right) . \tag{4.9}$$

We define the dispersion angle $\Theta$ by the relation $\mathbf{i}_{\mathbf{k}} \cdot \mathbf{i}_{\mathbf{k}'} = \cos\Theta = \cos(\theta_1 - \theta)$, that is, the angle is measured with respect to the direction of the incident photon. Furthermore, we can define the following angles (see Fig. 4.1(a), which illustrates photon-electron scattering).

$$\mathbf{v} \cdot \mathbf{i}_{\mathbf{k}'} = v \cos\theta_1 , \tag{4.10}$$

$$\mathbf{v} \cdot \mathbf{i}_{\mathbf{k}} = v \cos\theta . \tag{4.11}$$

So the equation (4.6) is written as

$$\gamma m_s \epsilon_1 \left(1 - \frac{v}{c}\cos\theta_1\right) + \left(\frac{\epsilon}{c}\right)\left(\frac{\epsilon_1}{c}\right)(1 - \cos(\theta_1 - \theta)) = \gamma m_s \epsilon \left(1 - \frac{v}{c}\cos\theta\right) . \tag{4.12}$$

Then the energy of the scattered photon is (with $\beta = \frac{v}{c}$)

$$\epsilon_1 = \frac{\epsilon(1 - \beta\cos\theta)}{\left[(1 - \beta\cos\theta_1) + \left(\frac{\epsilon}{\gamma m_s c^2}\right)(1 - \cos(\theta_1 - \theta))\right]} . \tag{4.13}$$

Note that the expression (4.13) is valid even when $v = 0$, which implies that $\gamma = 1$. In such a case, $\theta_1 - \theta \to \theta'_1 - \theta'$ is the scattering angle, resulting in $m_s = m_e$ (electron mass).

$$\epsilon'_1 = \frac{\epsilon'}{\left[1 + \left(\frac{\epsilon'}{m_e c^2}\right)(1 - \cos(\theta'_1 - \theta'))\right]} . \tag{4.14}$$

In this situation, we work in the reference frame $S'$ where the electron is at rest, therefore $\epsilon_1 \to \epsilon'_1$ and $\epsilon \to \epsilon'$.

Taking into account that this process is carried out in a vacuum, the relations $\lambda'\nu' = c$ ($\epsilon'_1 = h\nu'_1$) and $\lambda'_1\nu'_1 = c$ ($\epsilon' = h\nu'$) are fulfilled, in addition, $\theta'_1 - \theta' \to \theta'$ [5], so we can write

$$\lambda' - \lambda = \frac{h}{m_e c}(1 - \cos\theta'_1) , \tag{4.15}$$

which is the usually known formula for the Compton scattering by an electron at rest.

Usually, the Compton wavelength is defined for the electron as $\lambda c := \frac{h}{m_e c}$. *An important fact to note is that this Compton wavelength must be comparable to or greater than the wavelength of the incident photon for this type of scattering to be observed in the reference system $S'$* [6]. If this condition is not met, the electron simply acts as a radiator that scatters the incoming radiation. This type of scattering is known as Thomson scattering.

[5] Without loss of generality, we can set the angle of incidence of the photon to $\theta' = 0$.

[6] For example, for x-ray $\lambda = (0.01 - 10)$ nm, we have $\frac{\Delta\lambda}{\lambda} \sim \frac{\lambda_c}{\lambda} \sim (2.4 \times 10^{-4} - 0.24)$.

Then we observe that this effect happens if $\epsilon' > m_e c^2$, a process in which the radiation is "cooled" by transferring the energy of the photon to the electron, resulting in $\epsilon' < \epsilon'_1$.

In general, the expression (4.13) shows how we can exchange energy between a scattering particle and a radiation field (photons). Let us consider the case in which $\epsilon \ll \gamma m_s c^2$ has a relativistic scattering particle and a low-energy photon. Under these conditions

$$\frac{\epsilon_1}{\epsilon} = \frac{1-\beta\cos\theta}{1-\beta\cos\theta_1}\,, \tag{4.16}$$

or equivalently

$$\frac{\epsilon_1-\epsilon}{\epsilon} = \beta\left[\frac{\cos\theta-\cos\theta_1}{1-\beta\cos\theta_1}\right] = \beta(\cos\theta-\cos\theta_1)(1+\beta\cos\theta_1+(\beta\cos\theta_1)^2+\cdots)\,. \tag{4.17}$$

To first order, the frequency changes go like $\beta$, however, if the angles $\theta$ and $\theta_1$ are distributed randomly, a photon can gain energy, this process is called **Inverse Compton Scattering (ICS)**.

## 4.2 Relationship between the Laboratory frame and the scattering particle´s rest frame

We will explore how measurements in the laboratory reference system ($S$) are related to the reference system where the scattering particle (with mass $m_s$) is at rest ($S'$). To do this, let's assume that in $S$, this particle moves along the $x$-axis, and consider that in $S'$, we have $\epsilon_1 \to \epsilon'_1$ and $\epsilon \to \epsilon'$. The equation (4.14) can then be written as

$$\epsilon'_1 = \frac{\epsilon'}{\left[1+\left(\frac{\epsilon'}{m_s c^2}\right)(1-\cos(\theta'_1-\theta'))\right]}\,. \tag{4.18}$$

Since in the reference frame $S$, the scattering particle moves with speed $v = v\hat{e}_x$, and in the reference frame $S'$ it is at rest. The components of a 4-vector $q^\mu$ are related by a Lorentz boost as follows

$$\begin{pmatrix} q^0_{S'} \\ q^1_{S'} \\ q^2_{S'} \\ q^3_{S'} \end{pmatrix} = \begin{pmatrix} \gamma & -\beta\gamma & 0 & 0 \\ -\beta\gamma & \gamma & 0 & 0 \\ 0 & 0 & 1 & 0 \\ 0 & 0 & 0 & 1 \end{pmatrix} \begin{pmatrix} q^0_S \\ q^1_S \\ q^2_S \\ q^3_S \end{pmatrix}\,. \tag{4.19}$$

In particular, to analyze dispersion, we can examine the $x-y$ spatial plane and the 4-momenta $k^\mu = \frac{\epsilon}{c}(1,\cos\theta,\sin\theta,0)$ and $k^\mu_{S'} = \frac{\epsilon'}{c}(1,\cos\theta',\sin\theta',0)$. In this way, we obtain the equations:

$$\epsilon' = \gamma\epsilon(1-\beta\cos\theta)\,, \tag{4.20}$$

$$\epsilon'\cos\theta' = \gamma\epsilon(-\beta+\cos\theta)\,, \tag{4.21}$$

$$\epsilon'\sin\theta' = \epsilon\sin\theta\,. \tag{4.22}$$

The last two equations indicate that the incident angle $\theta'$ at $S'$ is determined by

$$\tan\theta' = \frac{\sin\theta}{\gamma(\cos\theta-\beta)}\,. \tag{4.23}$$

### 4.2.1 Ultrarelativistic scatterers

If we consider very relativistic scattering particles, that is, $\gamma \gg 1$, we have the following approximation for the value of $\beta$ (which tends to 1).

$$\gamma = \frac{1}{\sqrt{1-\beta^2}} \quad \Rightarrow \quad \gamma^2 = \frac{1}{(1-\beta)(1+\beta)} \approx \frac{1}{2}\frac{1}{1-\beta}\,, \tag{4.24}$$

of the above $\beta \approx 1 - \frac{1}{2}\gamma^{-2}$. Furthermore, if $\theta'$ is very small, $\beta \approx 1$, then

$$\tan\theta' \approx -\gamma^{-1}\cot\left(\frac{\theta}{2}\right)\,. \tag{4.25}$$

This last equation indicates that for ultrarelativistic particles, upon passing into the system at rest, *the scattering particle "sees" the photons incident on it in the opposite direction to its movement, forming a semi-aperture cone* $\sim 1/\gamma$.

For the extreme cases we have

- $\theta = 0$, we have that the incident photon energy is such that

$$\epsilon' = \gamma\epsilon(1-\beta) \approx \gamma\epsilon\left(\frac{1}{2}\gamma^{-2}\right) = \epsilon/2\gamma\,. \tag{4.26}$$

- $\theta = \pi$, the energy of the photon incident on $S'$ must be

$$\epsilon' = \gamma\epsilon(1+\beta) \approx 2\gamma\epsilon\,. \tag{4.27}$$

From the above we establish

$$\epsilon'_{min} = \epsilon/2\gamma\,, \tag{4.28}$$

$$\epsilon'_{max} = 2\gamma\epsilon\,. \tag{4.29}$$

We note that photons with $\theta = 0$ produce a small recoil and are of little relevance, while the most relevant are those for which $\theta = \pi$, which are those of frontal "collision". Furthermore, in the system $S'$ (this implies that $\tan\theta' \approx 0$ and in turn $\theta' \to \pi - \theta' \approx 0$, see Fig. 4.2).

$$\epsilon'_1 = \frac{\epsilon'}{1 + (\frac{\epsilon'}{m_s c^2})(1-\cos\theta'_1)}\,. \tag{4.30}$$

In a similar way to that used in subsection **1.2.2** we can establish the relationship of the 4-vectors between the reference systems $S$ and $S'$ by means of a Lorentz boost.

$$\begin{pmatrix} q^0_S \\ q^1_S \\ q^2_S \\ q^3_S \end{pmatrix} = \begin{pmatrix} \gamma & \beta\gamma & 0 & 0 \\ \beta\gamma & \gamma & 0 & 0 \\ 0 & 0 & 1 & 0 \\ 0 & 0 & 0 & 1 \end{pmatrix} \begin{pmatrix} q^0_{S'} \\ q^1_{S'} \\ q^2_{S'} \\ q^3_{S'} \end{pmatrix}\,. \tag{4.31}$$

When taking into account the observation of what the collision looks like, $\theta' \to \pi - \theta'_1$, to maintain the measurement in the reference system angle of the particle.

The 4-momenta $k'^{\mu} = \frac{\epsilon_1}{c}(1, \cos\theta_1, \sin\theta_1, 0)$ and $k'^{\mu}_{S'} = \frac{\epsilon'_1}{c}(1, \cos(\pi-\theta'_1),\ sin(\pi-\theta'_1), 0)$ (see Fig.4.2).

$$\epsilon_1 = \gamma\epsilon'_1(1 + \beta\cos(\pi - \theta'_1)) \approx \gamma\epsilon'_1(1 - \beta\cos\theta'_1)\,. \tag{4.32}$$

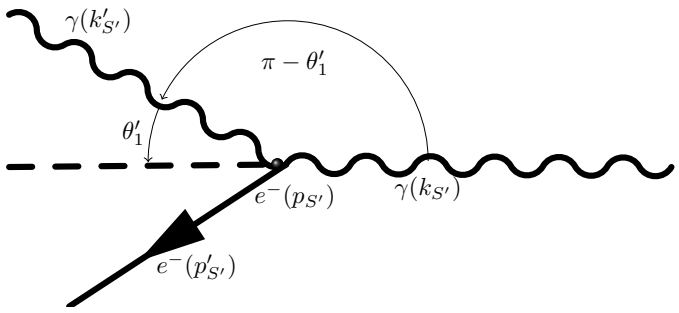


Figure 4.2: Pictorial representation of Compton scattering with ultrarelativistic electrons in the electron rest frame, corresponding to a head-on collision in the laboratory frame.

**About the Thomson limit and the Klein-Nishina extreme limit**

From the equation (4.32) we can analyze what happens with the Thomson limit, in which $\epsilon' \ll mc^2$, which implies that $\epsilon'_1 \approx \epsilon'$, which implies that the scattering particle is given a very small recoil in the scattering.

In the Laboratory reference system $\epsilon_{1max} \approx 2\gamma\epsilon'_{1max}$ according to the eq.(4.32), and using the result determined in (4.29)

$$\epsilon_{1max} \approx 4\gamma^2\epsilon\,. \tag{4.33}$$

This maximum corresponds to a head-on collision of the electron and the photon, however, the energy of the scattered photon remains small compared to the energy of the electron, so the electron loses little energy. In contrast to the Klein-Nishina limit $\epsilon' \gg mc^2$, by eq.(4.32)

$$\epsilon_1 \approx \gamma\epsilon'_1(1-\beta\cos\theta'_1) = \gamma\frac{\epsilon'(1-\beta\cos\theta'_1)}{[1+(\epsilon'/mc^2)(1-\cos\theta'_1)]} = \gamma mc^2\frac{(1-\beta\cos\theta'_1)}{[(mc^2/\epsilon')+(1-\cos\theta'_1)]}\,,$$

therefore

$$\epsilon_{1max} \approx \gamma mc^2\frac{1-\beta\cos\theta'_1}{1-\cos\theta'_1} \sim \gamma mc^2\,. \tag{4.34}$$

In the following graph, we have a comparison of the maximum energies obtained by the photons scattered in the Thomson limit and in the extreme Klein-Nishina limit from $\gamma = 1$ ($\beta = 0$) to $\gamma = 2$ ($\beta \approx 0.86$). In summary we have the following

- *In the Thomson limit, when the electron enters a photon gas and scatters losing only a small fraction of energy in each scattering, so there should be many of these.*
- *In the Klein-Nishina limit, when the electron enters a photon gas and scatters, losing a large fraction of energy from the first scattering, that is why this case is more relevant.*

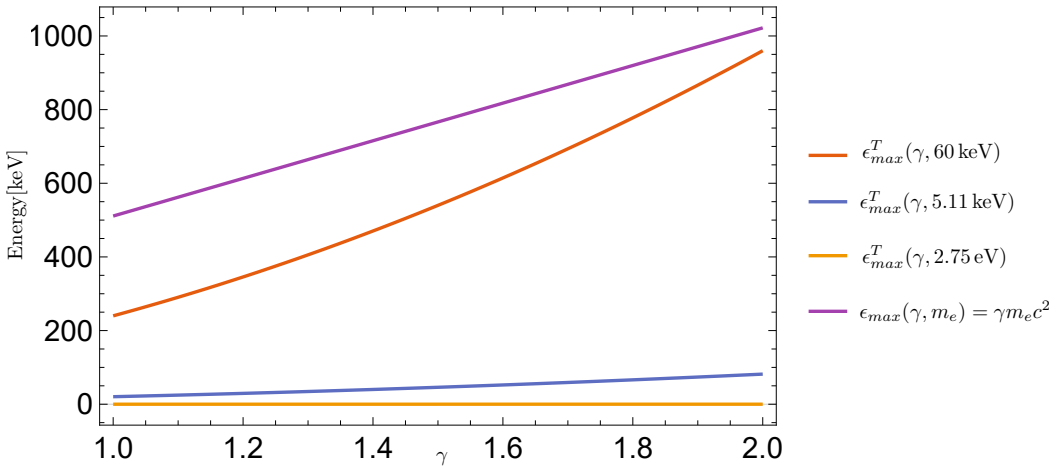


Figure 4.3: Maximum energy of the scattered photon in the extreme Klein-Nishina limit $\epsilon_{max}(\gamma, m_e)$ vs that found in the Thomson limit $\epsilon^T_{max}(\gamma, \epsilon)$ in the $S$ system for electron scattering. For comparison, we use visible light $(2.75, \mathrm{eV})$ and X rays $(60, \mathrm{keV})$. The emitted X rays will scatter favorably forward, as will photons generated through positron annihilation $(511, \mathrm{keV})$.

## 4.3 Total Compton spectrum

The process called inverse Compton scattering was introduced in 1947 by Follin as a mechanism for the energy loss of cosmic ray electrons. It was investigated by Feenberg and Primakoff[154] as well as by Donahue[155] in this context. This process was proposed as a source of energetic photons by Savedoff[156] and by Felten and Morrison[157]. Since then, it has received considerable attention from this perspective.

### 4.3.1 Energy distribution of photons scattered through Compton scattering

Most calculations of scattered photon spectra were initially made using a fairly simple approximation: It has been observed that the average energy transferred to a photon in a Compton collision is proportional to the initial energy of the photon and the square of the energy of the electron. This square dependence on the electron energy is reminiscent of the synchrotron radiation process. For this reason, the spectrum of radiated photons for a single electron energy is approximated by a peak function $\delta$ in the average radiated energy. This spectrum is then folded into the electron energy distribution to produce the resulting photon spectrum. While this method gives satisfactory results for synchrotron spectra, it is now known that inverse Compton spectra differ enough to raise some doubts about its applicability in this area. However, it can be shown that in the case of electron energy distributions following the inverse power law, the method is applicable to both cases despite their differences.

In 1968, Jones derived exact formulas for the energy distribution of scattered photons for the case of an electron of energy $\varepsilon = E/m_e c^2$ (i.e., in units of its rest energy) moving through a region of space filled with a unit density of isotropically distributed photons with initial energy $a = \epsilon'/m_e c^2$.

Working under the assumption that the energy distributions of scattering particles (such as Axions or Axion-Like particles) follow the inverse power law, we will determine the Compton spec-

trum produced by an energy scattering particle $\gamma m_s c^2$ that scatters into a segment of the initial photon distribution that has energies within $d\epsilon$. The total Compton spectrum would then be obtained by integrating over $\epsilon$ and over the energy distribution of the scattering particles.

$$\frac{d^2 N_{\gamma,\epsilon}}{dt d\epsilon_1} = \iint_{(\epsilon',\Omega'_1)} \frac{d^5 N_{\gamma,\epsilon'}}{dt' d\epsilon' d\Omega'_1 d\epsilon'_1} \frac{dt'}{dt} \frac{d\epsilon' d\Omega'_1 d\epsilon'_1}{d\epsilon_1} \,. \tag{4.35}$$

The results have been derived in detail for the spectrum of Compton scattered photons in the case of low energies (Thomson limit, in the case of electrons). The derivation in the most general case that we propose follows exactly the same lines except that the corresponding cross-section must be used (Klein-Nishina cross-section for electrons).

# Chapter 5
# Compton-like Scattering with Axions

*"The miracle of the appropriateness of the language of mathematics for the formulation of the laws of physics is a wonderful gift which we neither understand nor deserve."*
—Eugene Wigner

## 5.1 Photon-Axion scattering

Due to the existing effective interaction between the Axion with two photons (see Ec. 3.68), it is possible to have the following scattering process:

$$\gamma(k,\lambda) + a(p) \longrightarrow \gamma(k',\lambda') + a(p')\,, \tag{5.1}$$

which in general terms follows the kinematics of generalized Compton scattering, with axion being the scattering particle.

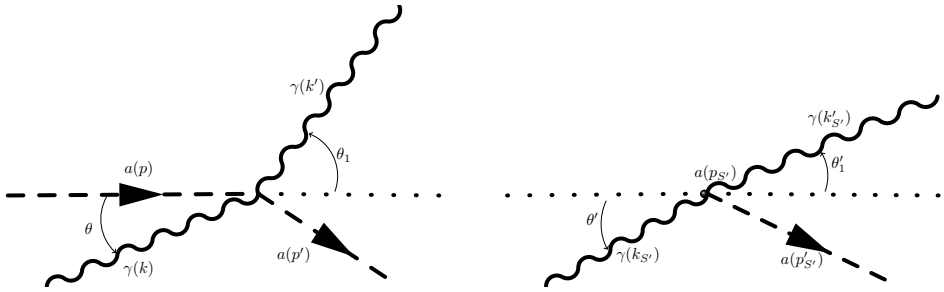


(a) (b)

Figure 5.1: Pictorial image of Compton scattering with axions: (a) Reference frame from the laboratory, (b) Reference frame where the axion is at rest.

### 5.1.1 Feynman rules in the photon-axion scattering process

i) For a (virtual) internal photon with 4-momentum $q$ the propagator to consider is $-i\frac{g_{\mu\nu}}{q^2}$ (In the Lorentz gauge $\partial_\mu A^\mu = 0$),

ii) An incoming (outgoing) photon with 4-momentum $k$ and spin polarization $\lambda$ has a contribution $\epsilon^\mu(\mathbf{k},\lambda)$ ($\epsilon^{\mu *}(\mathbf{k},\lambda)$),

iii) The absorption or emission of a scalar particle such as the axion contributes a factor equal to 1,

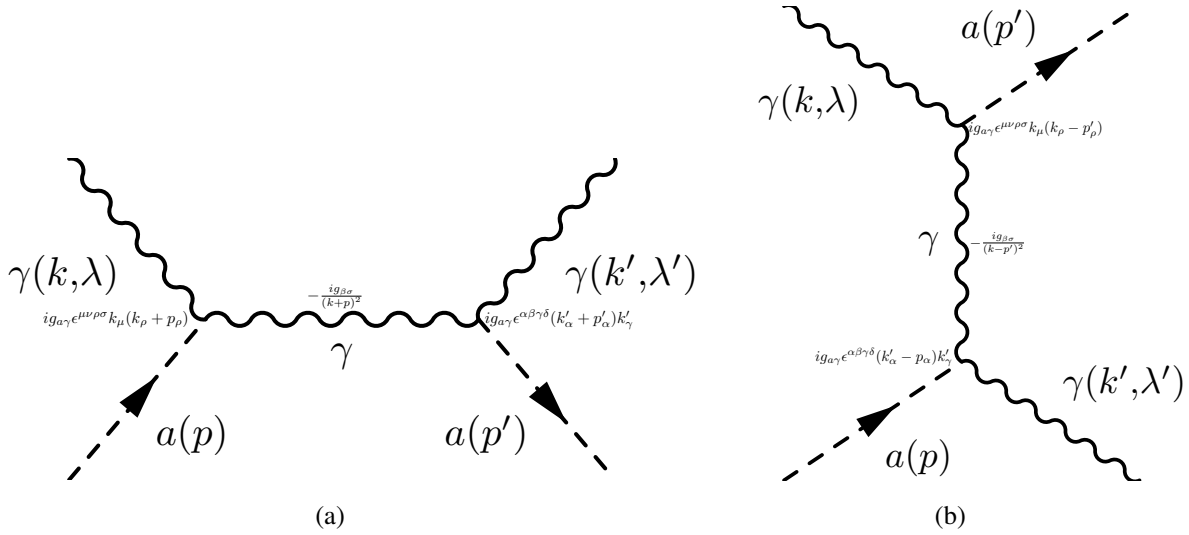


Figure 5.2: Effective contributions at tree level in the photon-axion scattering process: (a) s-channel; the incoming axion and the incoming photon have 4-momentum $p$ and $k$, respectively, so the virtual photon has 4-momentum $p+k=p'+k'$, (b) u-channel; the incoming axion and the incoming photon have 4-momentum $p$ and $k$, respectively, so the virtual photon has 4-momentum $k-p'=k'-p$.

iv) Since the Lagrangian density of interaction between a photon and axion takes the form

$$\mathcal{L}_{a\gamma\gamma}=-\frac{1}{4}g_{a\gamma\gamma}aF_{\mu\nu}\mathcal{F}^{\mu\nu}=-\frac{1}{2}g_{a\gamma\gamma}a\epsilon^{\mu\nu\rho\sigma}\partial_\mu A_\nu\partial_\rho A_\sigma\,, \tag{5.2}$$

Feynman's rule for the interaction vertex is (c.f. Appendix B.1)

$$ig_{a\gamma\gamma}\epsilon^{\mu\nu\rho\sigma}k^{(1)}_\mu k^{(2)}_\rho\,, \tag{5.3}$$

where $k^{(1)}$ and $k^{(2)}$ are the 4-momenta of the two photons, while the free indices $\nu$ and $\sigma$ correspond to photon 1 and 2, respectively.

v) Multiplying the above factors together we get the quantity $i\mathcal{M}$, where $\mathcal{M}$ is the Feynman invariant amplitude. For the case of dispersion, we place the terms from right to left, reading the diagrams from left to right.

### 5.1.2 Invariant amplitude and differential cross-section of the scattering process

For the $s$ channel following the Feynman rules mentioned above together with the diagram shown in Fig.5.2(a), we establish:

$$i\mathcal{M}_s=(ig_{a\gamma\gamma}\epsilon^{\alpha\beta\gamma\delta}(k'_\alpha+p'_\alpha)\epsilon^*_\delta(\mathbf{k}',\lambda')k'_\gamma)\left(-\frac{ig_{\beta\sigma}}{(k+p)^2}\right)(ig_{a\gamma\gamma}\epsilon^{\mu\nu\rho\sigma}k_\mu\epsilon_\nu(\mathbf{k},\lambda)(k_\rho+p_\rho))\,, \tag{5.4}$$

where to the right of the propagator we have the first vertex and to the left the second vertex. Taking into account the antisymmetry of the Levi-Civita symbol $\epsilon^{\alpha\beta\gamma\delta} = -\epsilon^{\alpha\delta\gamma\beta}$, we can use this property and change the indices $\beta \leftrightarrow \delta$, then

$$i\mathcal{M}_s = g_{a\gamma\gamma}^2 \epsilon^{\alpha\beta\gamma\delta}(k'_\alpha + p'_\alpha)\epsilon^*_\beta(\mathbf{k}', \lambda')k'_\gamma \left(-\frac{ig_{\delta\sigma}}{(k+p)^2}\right) \epsilon^{\mu\nu\rho\sigma} k_\mu \epsilon_\nu(\mathbf{k}, \lambda)(k_\rho + p_\rho)\,. \tag{5.5}$$

Using 4-momentum conservation and removing the common factor $i$, and noting that $\epsilon^{\mu\nu\rho\sigma}k_\mu k_\rho = 0$ (since we contract an antisymmetric "tensor" with a symmetric one), we find that

$$\mathcal{M}_s = -\frac{g_{a\gamma\gamma}^2}{(k+p)^2}(k_\alpha + p_\alpha)\epsilon^*_\beta(\mathbf{k}', \lambda')k'_\gamma \epsilon^{\alpha\beta\gamma\delta} g_{\delta\sigma}\epsilon^{\mu\nu\rho\sigma}k_\mu\epsilon_\nu(\mathbf{k}, \lambda)p_\rho\,. \tag{5.6}$$

Using the identity $\epsilon^{\alpha\beta\gamma\delta}g_{\delta\sigma}\epsilon^{\mu\nu\rho\sigma} = -3!\delta^{[\alpha}_{\mu'}\delta^{\beta}_{\nu'}\delta^{\gamma]}_{\rho'}g^{\mu'\mu}g^{\nu'\nu}g^{\rho'\rho}$ (to see a demonstration c.f. Appendix B.3), and using the index changes $\alpha \to \mu, \beta \to \nu$ and $\gamma \to \rho$, we rewrite

$$\mathcal{M}_s = \frac{3!g_{a\gamma\gamma}^2}{(k+p)^2}(k_\mu + p_\mu)\epsilon^*_\nu(\mathbf{k}', \lambda')k'_\rho k^{[\mu}\epsilon^{\nu}(\mathbf{k}, \lambda)p^{\rho]}\,. \tag{5.7}$$

We develop the previous expression taking antisymmetrization into account, using the Lorentz gauge (which implies that $k\cdot\epsilon = k_\mu\epsilon^\mu = 0$) and the free particle scattering relations for the photon and the ALP, respectively; $k\cdot k = k^2 = 0$ and $p\cdot p = p^2 = m_a^2$, leading to $(k+p)^2 = m_a^2 + 2k\cdot p$ (clearly $k\cdot p = p\cdot k$)

$$\begin{aligned}\mathcal{M}_s = \frac{g_{a\gamma\gamma}^2}{(m_a^2 + 2k\cdot p)}\big[&(k\cdot p)(k'\cdot p)\epsilon^*_\nu(\mathbf{k}', \lambda')\epsilon^\nu(\mathbf{k}, \lambda) - (k\cdot p)k'_\rho p^\nu \epsilon^*_\nu(\mathbf{k}', \lambda')\epsilon^\mu(\mathbf{k}, \lambda)\\ &+ (m_a^2 + k\cdot p)k'_\rho k^\nu \epsilon^*_\nu(\mathbf{k}', \lambda')\epsilon^\rho(\mathbf{k}, \lambda) - (k'\cdot p)p_\mu k^\nu \epsilon^*_\nu(\mathbf{k}', \lambda')\epsilon^\mu(\mathbf{k}, \lambda)\\ &+(k'\cdot k)p_\mu p^\nu \epsilon^*_\nu(\mathbf{k}', \lambda')\epsilon^\mu(\mathbf{k}, \lambda) - (m_a^2 + k\cdot p)(k'\cdot k)\epsilon^*_\nu(\mathbf{k}', \lambda')\epsilon^\nu(\mathbf{k}, \lambda)\big]\,,\end{aligned}$$

making the following changes on the dummy indices: in the first and last terms $\nu \to \mu$, in the second and third terms; $\rho \to \nu$ and $\nu \to \mu$, in the fourth term $\nu \leftrightarrow \mu$, we obtain

$$\begin{aligned}\mathcal{M}_s = \frac{g_{a\gamma\gamma}^2}{(m_a^2 + 2k\cdot p)}\big\{&\big[(k\cdot p)(k'\cdot p) - (m_a^2 + k\cdot p)(k'\cdot k)\big]\epsilon^*_\mu(\mathbf{k}', \lambda')\epsilon^\mu(\mathbf{k}, \lambda)\\ &+\big[(m_a^2 + k\cdot p)k^\mu k'_\nu - (k'\cdot p)k^\mu p_\nu - (k\cdot p)p^\mu k'_\nu + (k'\cdot k)p^\mu p_\nu\big]\epsilon^*_\mu(\mathbf{k}', \lambda')\epsilon^\nu(\mathbf{k}, \lambda)\big\}\,.\end{aligned} \tag{5.8}$$

On the other hand, we can determine an expression analogous to $\mathcal{M}_s$ for the channel $u$, following the Feynman rules established above but now for the diagram 5.2(b) we have that the invariant amplitude corresponding to the channel $u$ is determined by

$$i\mathcal{M}_u = (ig_{a\gamma\gamma}\epsilon^{\alpha\beta\gamma\delta}(k'_\alpha - p_\alpha)\epsilon^*_\delta(\mathbf{k}', \lambda')k'_\gamma)\left(-\frac{ig_{\beta\sigma}}{(k-p')^2}\right)(ig_{a\gamma\gamma}\epsilon^{\mu\nu\rho\sigma}k_\mu\epsilon_\nu(\mathbf{k}, \lambda)(k_\rho - p'_\rho))\,, \tag{5.9}$$

where to the right of the propagator we have the first vertex (the one above, see Fig.5.2(b)) and to the left the second vertex (the one below). Using the conservation of 4-momentum $k - p' = k' - p$ and the identity $\epsilon^{\alpha\beta\gamma\delta} = -\epsilon^{\alpha\delta\gamma\beta}$ with index change $\beta \leftrightarrow \delta$;

$$\mathcal{M}_u = -g_{a\gamma\gamma}^2\epsilon^{\alpha\beta\gamma\delta}(k_\alpha - p'_\alpha)\epsilon^*_\beta(\mathbf{k}', \lambda')k'_\gamma\frac{g_{\delta\sigma}}{(k-p')^2}\epsilon^{\mu\nu\rho\sigma}k_\mu\epsilon_\nu(\mathbf{k}, \lambda)(k_\rho - p'_\rho)\,.$$

Using the fact that the contraction $\epsilon^{\mu\nu\rho\sigma}k_\mu k_\rho = 0$

$$\mathcal{M}_u = -\frac{g_{a\gamma\gamma}^2}{(k-p')^2}(k_\alpha + (-p')_\alpha)\epsilon_\beta^*(\mathbf{k}',\lambda')k'_\gamma\epsilon^{\alpha\beta\gamma\delta}g_{\delta\sigma}\epsilon^{\mu\nu\rho\sigma}k_\mu\epsilon_\nu(\mathbf{k},\lambda)(-p'_\rho)\,. \tag{5.10}$$

We observe that this expression is similar to the one obtained previously for the $s$ channel in eq.(5.6), only that $p \to -p'$, thus we conclude that

$$\begin{aligned}\mathcal{M}_u = \frac{g_{a\gamma\gamma}^2}{(m_a^2 - 2k\cdot p')}\Big\{\big[(k\cdot p')(k'\cdot p') - (m_a^2 - k\cdot p')(k'\cdot k)\big]\,\epsilon_\mu^*(\mathbf{k}',\lambda')\epsilon^\mu(\mathbf{k},\lambda)\\ + \big[(m_a^2 - k\cdot p')k^\mu k'_\nu - (k'\cdot p')k^\mu p'_\nu - (k\cdot p')p'^\mu k'_\nu + (k'\cdot k)p'^\mu p'_\nu\big]\,\epsilon_\mu^*(\mathbf{k}',\lambda')\epsilon^\nu(\mathbf{k},\lambda)\Big\}\,.\end{aligned} \tag{5.11}$$

Then, the total amplitude of the process $\gamma + a \to \gamma + a$, $\mathcal{M}_{a\gamma}$ at the tree level is given by

$$\mathcal{M}_{a\gamma\gamma} = \mathcal{M}_s + \mathcal{M}_u\,. \tag{5.12}$$

Now, the squared modulus of the invariant amplitude of the process that we must use to calculate the cross-section is obtained by adding over all the polarizations of the photons involved (Axions are scalars) and dividing by the number of polarizations of the incident photon:

$$\overline{|\mathcal{M}|^2} = \frac{1}{2}\sum_{\lambda,\lambda'}|\mathcal{M}_{a\gamma\gamma}|^2 = \frac{1}{2}\sum_{\lambda,\lambda'}\left(|\mathcal{M}_s|^2 + |\mathcal{M}_u|^2 + 2\Re[\mathcal{M}_s\mathcal{M}_u^*]\right)\,. \tag{5.13}$$

Making use of the pseudo-completeness relation for the polarization vector of the photons

$$\sum_\lambda \epsilon^\mu(\mathbf{k},\lambda)\epsilon^{\alpha*}(\mathbf{k},\lambda) = -g^{\mu\alpha}\,, \tag{5.14}$$

we obtain:

$$\begin{aligned}\sum_{\lambda,\lambda'}|\mathcal{M}_s|^2 = \frac{g_{a\gamma\gamma}^4}{(m_a^2 + 2k\cdot p)^2}\big[2(k\cdot p)^2(k'\cdot p)^2 - 2(k\cdot p)(k'\cdot p)(k'\cdot k)m_a^2\\ + (m_a^2 + k\cdot p)^2(k'\cdot k)^2 + (k\cdot p)^2(k'\cdot k)^2\big]\,.\end{aligned} \tag{5.15}$$

We note that the calculation of $\sum_{\lambda,\lambda'}|\mathcal{M}_u|^2$ is the same as that of $\sum_{\lambda,\lambda'}|\mathcal{M}_s|^2$ by making the change of 4-moment $p^\mu \to -p'^\mu$ since $p'^2 = m_a^2$, so we conclude that

$$\begin{aligned}\sum_{\lambda,\lambda'}|\mathcal{M}_u|^2 = \frac{g_{a\gamma\gamma}^4}{(m_a^2 - 2k\cdot p')^2}\Big[2(k\cdot p')^2(k'\cdot p')^2 - 2(k\cdot p')(k'\cdot p')(k'\cdot k)m_a^2\\ + (m_a^2 - k\cdot p')^2(k'\cdot k)^2 + (k\cdot p')^2(k'\cdot k)^2\Big]\,.\end{aligned} \tag{5.16}$$

Now using the conservation of 4-momentum and the dispersion relations for photons and axions it can be shown that $k\cdot p = k'\cdot p'$ and $k\cdot p' = k'\cdot p$, using the above in eq. (5.16)

$$\begin{aligned}\sum_{\lambda,\lambda'}|\mathcal{M}_u|^2 = \frac{g_{a\gamma\gamma}^4}{(m_a^2 - 2k'\cdot p)^2}\Big[2(k\cdot p)^2(k'\cdot p)^2 - 2(k'\cdot p)(k\cdot p)(k'\cdot k)m_a^2\\ + (m_a^2 - k'\cdot p)^2(k'\cdot k)^2 + (k'\cdot p)^2(k'\cdot k)^2\Big]\,.\end{aligned} \tag{5.17}$$

While for the other term we get

$$\sum_{\lambda,\lambda'}\mathcal{M}_s\mathcal{M}_u^* = \frac{g_{a\gamma\gamma}^4}{(m_a^2+2k\cdot p)(m_a^2-2k'\cdot p)}\Big\{(m_a^2-k'\cdot p)(k\cdot p)(k'\cdot k)^2-(m_a^2+k\cdot p)(k'\cdot p)(k'\cdot k)^2 + 2(k\cdot p)(k'\cdot p)(k'\cdot k)m_a^2 - 2(k'\cdot p)^2(k'\cdot k)(m_a^2+k'\cdot k)+(k'\cdot p)^4 + (k\cdot p)^4 - 2(k\cdot p)^2(k'\cdot k)(m_a^2+k'\cdot k)+(k'\cdot k)^2(m_a^2+k'\cdot k)^2\Big\}. \quad (5.18)$$

To give an analytical expression of the scattering amplitude in any inertial reference frame, we define the following functions, which for illustration we will consider to be element dependent: $m_a, I_{k'p}=k'\cdot p, I_{kp}=k\cdot p$ and $I_{k',k}=k'\cdot k$.

$$F_s(m_a,I_{k'p},I_{kp},I_{k'k}) = \frac{1}{2g_{a\gamma\gamma}^4}\sum_{\lambda,\lambda'}|\mathcal{M}_s|^2 = \frac{1}{2(m_a^2+2I_{kp})^2}\Big[2I_{kp}^2I_{k'p}^2-2I_{kp}I_{k'p}I_{k'k}m_a^2 + (m_a^2+I_{kp})^2I_{k'k}^2+I_{kp}^2I_{k'k}^2\Big], \quad (5.19)$$

$$F_u(m_a,I_{k'p},I_{kp},I_{k'k}) = \frac{1}{2g_{a\gamma\gamma}^4}\sum_{\lambda,\lambda'}|\mathcal{M}_u|^2 = \frac{1}{2(m_a^2-2I_{k'p})^2}\Big[2I_{kp}^2I_{k'p}^2-2I_{kp}I_{k'p}I_{k'k}m_a^2 + (m_a^2-I_{k'p})^2I_{k'k}^2+I_{k'p}^2I_{k'k}^2\Big], \quad (5.20)$$

$$G_{su}(m_a,I_{k'p},I_{kp},I_{k'k}) = \frac{1}{g_{a\gamma\gamma}^4}\sum_{\lambda,\lambda'}\mathcal{M}_s\mathcal{M}_u^* = \frac{1}{(m_a^2+2I_{kp})(m_a^2-2I_{k'p})}\Big\{(m_a^2-I_{k'p})I_{kp}I_{k'k}^2 - (m_a^2+I_{kp})I_{k'p}I_{k'k}^2+2I_{kp}I_{k'p}I_{k'k}m_a^2+I_{k'p}^4-2(I_{k'p}^2+I_{kp}^2)I_{k'k}(m_a^2+I_{k'k})+I_{kp}^4+I_{k'k}^2(m_a^2+I_{k'k})^2\Big\}. \quad (5.21)$$

Given that the differential cross-section for a scattering process involving two non-massive particles is given by Eq.(C.7):

$$\frac{d^2\sigma}{d\Omega} = \frac{1}{64\pi^2}\frac{{k'}_0^2}{(p\cdot k)^2}\overline{|\mathcal{M}|^2}. \quad (5.22)$$

For the case studied, we conclude that

$$\frac{d^2\sigma}{d\Omega} = \frac{g_{a\gamma\gamma}^4}{64\pi^2}\frac{{k'}_0^2}{I_{kp}^2}\Big[F_s(m_a,I_{k'p},I_{kp},I_{k'k})+F_u(m_a,I_{k'p},I_{kp},I_{k'k})+G_{su}(m_a,I_{k'p},I_{kp},I_{k'k})\Big]. \quad (5.23)$$

It is the differential cross-section for the process studied in terms of the invariants $I_{k'p}=k'\cdot p, I_{kp}=k\cdot p, I_{k'k}=k'\cdot k$, the energy of the photon after being scattered (in ${k'}_0$) and the mass $m_a$ of the axion.

## 5.2 Photon-Axion scattering at low energies

To obtain the energy distribution of the scattered photons through Compton-like scattering with axions, we need to find the cross-section of the scattering process at the Rest Frame (RF) $S$ (where the axion is at rest), in this frame we meet the following:

$$p^{\nu} = (m_a, 0, 0, 0)\,, \tag{5.24}$$
$$k^{\nu} = k_0(1, \cos\theta', \sin\theta', 0) = \epsilon'(1, \cos\theta', \sin\theta', 0)\,, \tag{5.25}$$
$$k'^{\nu} = k'_0(1, \cos\theta'_1, \sin\theta'_1, 0) = \epsilon'_1(1, \cos\theta'_1, \sin\theta'_1, 0)\,. \tag{5.26}$$

This implies that

$$I_{k'p} = k' \cdot p = m_a\epsilon'_1\,, \tag{5.27}$$
$$I_{kp} = k \cdot p = m_a\epsilon'\,, \tag{5.28}$$
$$I_{k'k} = k' \cdot k = \epsilon'_1\epsilon'(1 - \cos(\theta'_1 - \theta'))\,. \tag{5.29}$$

Given that, for this frame of reference we have the relationship between the energy $\epsilon'$ of the incident photon and $\epsilon'_1$ of the scattered photon.

$$\epsilon'_1 = \frac{\epsilon'}{\left[1 + \left(\frac{\epsilon'}{m_a}\right)(1 - \cos(\theta'_1 - \theta'))\right]}\,, \tag{5.30}$$

writing the invariants in terms of the energy of the incident photon

$$I_{k'p} = k' \cdot p = \frac{m_a^2(\epsilon'/m_a)}{\left[1 + \left(\frac{\epsilon'}{m_a}\right)(1 - \cos(\theta'_1 - \theta'))\right]}\,, \tag{5.31}$$
$$I_{kp} = k \cdot p = m_a^2(\epsilon'/m_a)\,, \tag{5.32}$$
$$I_{k'k} = k' \cdot k = m_a^2\frac{(\epsilon'/m_a)^2(1 - \cos(\theta'_1 - \theta'))}{\left[1 + \left(\frac{\epsilon'}{m_a}\right)(1 - \cos(\theta'_1 - \theta'))\right]}\,. \tag{5.33}$$

Under these conditions we can considerably simplify the functions $F_s$, $F_u$ and $G_{su}$, in particular we take $b = \frac{\epsilon'}{m_a}$ and a scattering angle $\theta'_1 - \theta' \to \theta'_1$, taking $b = \frac{\epsilon'}{m_a}$, the invariants can be rewritten as:

$$I_{k'p} = m_a^2\frac{b}{[1 + b(1 - \cos\theta'_1)]}\,,$$
$$I_{kp} = m_a^2 b\,,$$
$$I_{k'k} = m_a^2\frac{b^2(1 - \cos\theta'_1)}{[1 + b(1 - \cos\theta'_1)]}\,.$$

We can write $F_s(m_a, I_{k'p}, I_{kp}, I_{k'k}) \to F_S^R(m_a, b, \theta_1')$

$$F_S^R(m_a,b,\theta_1') = \frac{1}{2(m_a^2+2m_a^2b)^2}\left[2\left(m_a^2b\right)^2\left(m_a^2\frac{b}{[1+b(1-\cos\theta_1')]}\right)^2\right.$$
$$-2m_a^2b\left(m_a^2\frac{b}{[1+b(1-\cos\theta_1')]}\right)\left(m_a^2\frac{b^2(1-\cos\theta_1')}{[1+b(1-\cos\theta_1')]}\right)m_a^2$$
$$\left.+(m_a^2+m_a^2b)^2\left(m_a^2\frac{b^2(1-\cos\theta_1')}{[1+b(1-\cos\theta_1')]}\right)^2+\left(m_a^2b\right)^2\left(m_a^2\frac{b^2(1-\cos\theta_1')}{[1+b(1-\cos\theta_1')]}\right)^2\right].$$

After some algebra

$$F_S^R(m_a,b,\theta_1') = \frac{m_a^4b^4}{2(1+2b)^2[1+b(1-\cos\theta_1')]^2}\Big[2\cos\theta_1'+(1+2b+2b^2)(1-\cos\theta_1')^2\Big]. \quad (5.34)$$

Similarly $F_u(m_a, I_{k'p}, I_{kp}, I_{k'k}) \to F_u^R(m_a, b, \theta_1')$, we get

$$F_u^R(m_a,b,\theta_1') = \frac{m_a^4b^4}{2[1-b(1+\cos\theta_1')]^2}\left[2\cos\theta_1'\right.$$
$$\left.+\frac{(1-b)^2+2(1-b)b(1-\cos\theta_1')+2b^2(1-\cos\theta_1')^2)}{[1+b(1-\cos\theta_1')]^2}(1-\cos\theta_1')^2\right]. \quad (5.35)$$

For the last function $G_{su}(m_a, I_{k'p}, I_{kp}, I_{k'k}) \to G_{su}^R(m_a, b, \theta_1')$

$$G_{su}^R(m_a,b,\theta_1') = \frac{1}{(1+2b)}\frac{1}{[1-b(1+\cos\theta_1')]}\frac{m_a^4b^4}{[1+b(1-\cos\theta_1')]}\left[\left(1-\frac{1+2b}{[1+b(1-\cos\theta_1')]}\right)\times\right.$$
$$b(1-\cos\theta_1')^2+2(1-\cos\theta_1')+\frac{1}{[1+b(1-\cos\theta_1')]^2}+[1+b(1-\cos\theta_1')]^2$$
$$-2(1-\cos\theta_1')\left(\frac{1+[1+b(1-\cos\theta_1')]^2}{[1+b(1-\cos\theta_1')]}\right)\left(1+\frac{b^2(1-\cos\theta_1')}{[1+b(1-\cos\theta_1')]}\right)$$
$$\left.+(1-\cos\theta_1')^2\left(1+\frac{b^2(1-\cos\theta_1')}{[1+b(1-\cos\theta_1')]}\right)^2\right]. \quad (5.36)$$

In short, we can write

$$F_s^R(m_a,b,\theta_1') = m_a^4b^4f_s(b,\theta_1'), \quad (5.37)$$
$$F_u^R(m_a,b,\theta_1') = m_a^4b^4f_u(b,\theta_1'), \quad (5.38)$$
$$G_{su}^R(m_a,b,\theta_1') = m_a^4b^4g_{su}(b,\theta_1'), \quad (5.39)$$

where the functions $f_s(b,\theta_1')$, $f_u(b,\theta_1')$ and $g_{su}(b,\theta_1')$ are

$$f_s(b,\theta_1') = \frac{1}{2(1+2b)^2}\frac{1}{[1+b(1-\cos\theta_1')]^2}\Big[2\cos\theta_1'+(1+2b+2b^2)(1-\cos\theta_1')^2\Big], \quad (5.40)$$

$$f_u(b,\theta_1') = \frac{1}{2[1-b(1+\cos\theta_1')]^2}\Big[2\cos\theta_1' + \frac{(1-b)^2+2(1-b)b(1-\cos\theta_1')+2b^2(1-\cos\theta_1')^2}{[1+b(1-\cos\theta_1')]^2}(1-\cos\theta_1')^2\Big], \quad (5.41)$$

$$g_{su}(b,\theta_1') = \frac{1}{(1+2b)}\frac{1}{[1-b(1+\cos\theta_1')]}\frac{1}{[1+b(1-\cos\theta_1')]}\Bigg[\left(1-\frac{1+2b}{[1+b(1-\cos\theta_1')]}\right)\times b(1-\cos\theta_1')^2+2(1-\cos\theta_1')+\frac{1}{[1+b(1-\cos\theta_1')]^2}+[1+b(1-\cos\theta_1')]^2 - 2(1-\cos\theta_1')\left(\frac{1+[1+b(1-\cos\theta_1')]^2}{[1+b(1-\cos\theta_1')]}\right)\left(1+\frac{b^2(1-\cos\theta_1')}{[1+b(1-\cos\theta_1')]}\right) + (1-\cos\theta_1')^2\left(1+\frac{b^2(1-\cos\theta_1')}{[1+b(1-\cos\theta_1')]}\right)^2\Bigg]. \quad (5.42)$$

We observe that the functions $f_u(b,\theta_1')$ and $g_{su}(b,\theta_1')$ have a point where they diverge, due to the term $1-b(1+\cos\theta_1')$ in its denominator, such a point lies in

$$\cos\theta'^{*}_1 = x^* = \frac{1-b}{b} = \frac{1-(\epsilon'/m_a)}{(\epsilon'/m_a)} = \frac{m_a-\epsilon'}{\epsilon'}. \quad (5.43)$$

On the other hand, when taking into account that $p\cdot k = m_a\epsilon'$ and that $k_0' = \epsilon_1'$, the differential cross section turns out to be

$$\frac{d^2\sigma}{d\Omega_1'} = \frac{g_{a\gamma\gamma}^4 m_a^2}{64\pi^2}\left(\frac{b^2}{[1+b(1-\cos\theta_1')]}\right)^2\Big[f_s(b,\theta_1')+f_u(b,\theta_1')+g_{su}(b,\theta_1')\Big]. \quad (5.44)$$

### 5.2.1 Cross-section at low energies

As previously discussed for $b<0.5$, we can establish the cross-section without finding any divergence in the differential cross section $d^2\sigma/d\Omega$, this contains the low energies $\epsilon'\ll m_a$.

Since we treat the dispersion process collinearly we can easily integrate the equation (5.44) into the azimuthal angle $\phi_1'$ and note that the functions $f_s$, $f_u$ and $g_{su}$ depend on $\cos\theta_1'$

$$-\frac{d\sigma}{d(\cos\theta_1')} = \frac{g_{a\gamma\gamma}^4 m_a^2}{32\pi}\left(\frac{b^2}{[1+b(1-\cos\theta_1')]}\right)^2\left[f_s(b,\cos\theta_1')+f_u(b,\cos\theta_1')+g_{su}(b,\cos\theta_1')\right]. \quad (5.45)$$

Using the change of variable $x=\cos\theta_1'$ when considering that the integral is made of $x\in[-1,1]$ we can write

$$\frac{d\sigma}{dx} = \frac{g_{a\gamma\gamma}^4 m_a^2}{32\pi}\left(\frac{b^2}{[1+b(1-x)]}\right)^2\Big[f_s(b,x)+f_u(b,x)+g_{su}(b,x)\Big], \quad (5.46)$$

where

$$f_s(b,x) = \frac{1}{2(1+2b)^2}\frac{1}{[1+b(1-x)]^2}\left[2x + (1+2b+2b^2)(1-x)^2\right], \tag{5.47}$$

$$f_u(b,x) = \frac{1}{2[1-b(1+x)]^2}\left[2x + \frac{(1-b)^2+2(1-b)b(1-x)+2b^2(1-x)^2}{[1+b(1-x)]^2}(1-x)^2\right], \tag{5.48}$$

$$g_{su}(b,x) = \frac{1}{(1+2b)[1-b(1+x)]}\frac{1}{[1+b(1-x)]}\left[\left(1-\frac{1+2b}{[1+b(1-x)]}\right)b(1-x)^2 + 2(1-x)\right.$$
$$+\frac{1}{[1+b(1-x)]^2} + [1+b(1-x)]^2 - 2(1-x)\left(\frac{1+[1+b(1-x)]^2}{[1+b(1-x)]}\right)\left(1+\frac{b^2(1-x)}{[1+b(1-x)]}\right)$$
$$\left. + (1-x)^2\left(1+\frac{b^2(1-x)}{[1+b(1-x)]}\right)^2\right]. \tag{5.49}$$

Integrating, we observe that the last two integrals are only valid for $b < 0.5$, with this we restrict ourselves to the case of low energies.

$$H_s(b) = \int_{-1}^{1}\left(\frac{b^2}{[1+b(1-x)]}\right)^2 f_s(b,x)dx = \frac{3}{4}\frac{b^4}{(1+2b)^3} \tag{5.50}$$

$$H_u(b) = \int_{-1}^{1}\left(\frac{b^2}{[1+b(1-x)]}\right)^2 f_u(b,x)dx = \frac{1}{48b^4(1-2b)(1+2b)^3}\times$$
$$\left\{4b^2[3+b(-1+2b)(6+b(42+b(9+2b(-62+b(-39+4b)))))]\right.$$
$$\left. + 3(1+2b)^3[1+b(-8+b(24+b(-27+4b(1+b))))]\ln\left[\frac{1-2b}{1+2b}\right]\right\} \tag{5.51}$$

$$H_{su}(b) = \int_{-1}^{1}\left(\frac{b^2}{[1+b(1-x)]}\right)^2 g_{su}(b,x)dx = -\frac{1}{48b^2(1+2b)}\times$$
$$\left\{\frac{4b^2[3+2b(6+b(3+2b)^2)]}{(1+2b)^2} + 3\ln\left[\frac{1-2b}{1+2b}\right]\right\}. \tag{5.52}$$

In this way the cross-section multiplied by $\frac{32\pi}{g_{q\gamma}^4 m_a^2}$ turns out to be the sum of the previous functions and we can see the qualitative change that happens with the total cross-section at low energies.

$$\sigma(b) = \frac{g_{q\gamma\gamma}^4 m_a^2}{32\pi}H(b), \quad \text{where} \quad H(b) := H_s(b) + H_u(b) + H_{su}(b). \tag{5.53}$$

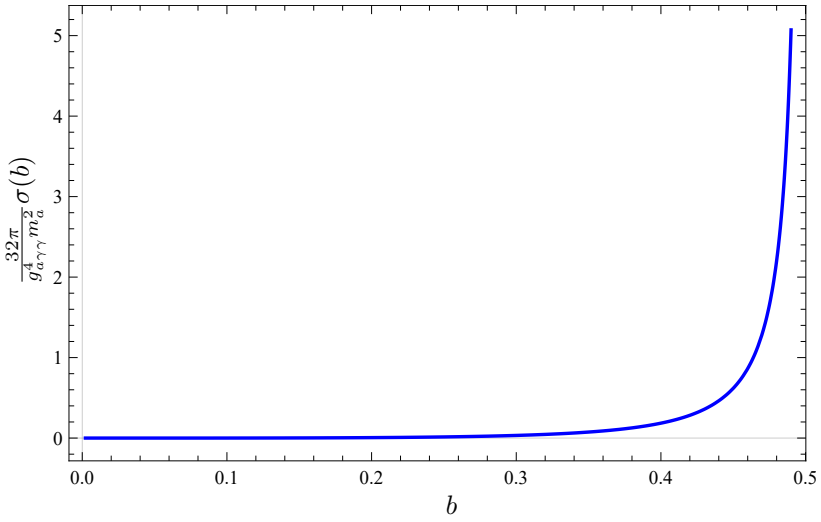


Figure 5.3: Plot of the cross-section at low energies for the Compton-like scattering process with axions as a function of $b = \frac{\epsilon'}{m_a}$.

We observe that the function $H(b)$ is dimensionless since $b$ is also dimensionless. Therefore, we make a graph that illustrates the behavior of the cross-section for a specific mass value, noting that this is negligible or not depending on the value of $g_{a\gamma\gamma}^4 m_a^2$.

In contrast to the usual Compton scattering process (with electrons), the cross-section does not remain constant at low energies. To describe this behavior, a logarithmic graphical representation is generally used. In this context, we highlight the differences in behavior, where $a = \frac{\epsilon'}{m_e}$ and $b = \frac{\epsilon'}{m_a}$.

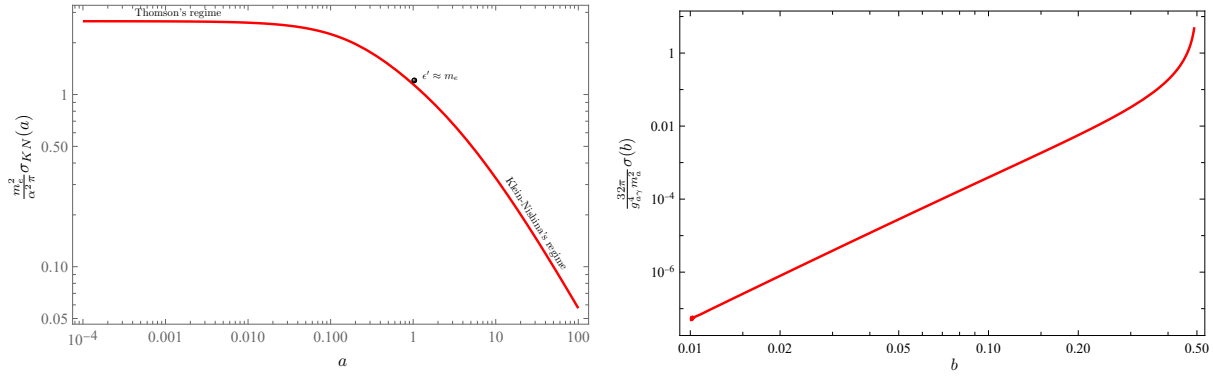


(a) (b)

Figure 5.4: Compton scattering plot on logarithmic scale: (a) with electrons the Klein-Nishina cross-section is shown, which includes the low energy and high energy case, (b) with axions, only the low energy case is included.

Consequently, we conclude that the Compton scattering process depends on the scattering particle. This variability is expected, since the theory that models the process at a fundamental level is different.

# Chapter 6
# Some Physical Results

*"Whatever the final laws of nature may be, there is no reason to suppose that they are designed to make physicists happy."*
**—Steven Weinberg**

In this section we discuss some physical situations in which the photon-axion scattering process could occur.

## 6.1 On the kinematics in Axion-Photon scattering

As discussed in chapter 4, the kinematics of Compton scattering does not depend on the nature of the scattering particle. The interest in studying the photon-axion dispersion process lies in the fact that the energy transfer is considered very different when working at low energies or high energies in Compton dispersion. As we saw previously, it is argued that the maximum energy with which a photon can come out when scattered in the low energy regime is given by Eq. (4.33) and at high energies given by Eq. (4.34), respectively.

$$\epsilon_{1\max} \approx 4\gamma^2\epsilon\,, \quad \epsilon_{1\max} \sim \gamma mc^2\,. \tag{6.1}$$

At low energies in Compton scattering with electrons, the maximum corresponds to a head-on collision between the electron and the photon. However, the energy of the scattered photon is still small compared to the energy of the electron (see Fig. 4.3), so the electron loses little energy. However, as seen in the following graph when working with an axion, this does not necessarily happen. Taking the upper bound $m_a < 10^{-2}$ eV, it is observed that only for masses close to this does the result remain valid, that is, the "Thomson limit" corresponding to the case of the axion has different effects due to the small mass of these particles.

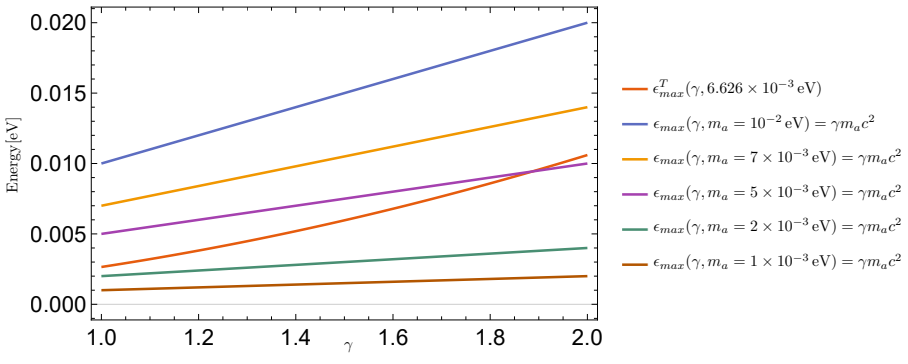


Figure 6.1: Maximum energy of a photon comes from the CMB (Mean energy per CMB photon $E_{ph} \approx 6.626\times10^{-4}$eV, [158]) scattered at high energies $\epsilon_{max}(\gamma, m_a)$ vs that found at low energies $\epsilon^T_{max}(\gamma, \epsilon)$ in $S$ for scattering by axions.

Of course, this result is interesting, since we can infer the following phenomenological result (even from kinematics): the large energy loss behavior in Compton scattering depends on the mass of the scattering particle in question. We should not be surprised by the abrupt change we experience when considering electrons and axions, since $m_e \approx 511\,\text{keV} \gg 10^{-2}\,\text{eV} > m_a$.

## 6.2 Angular distribution

We can study what happens with the Compton dispersion from the differential cross section established in Eq. (5.44). To do this, we make a graph in polar coordinates to observe how the distribution of the dispersion angles of photons coming from the CMB is as a function of the masses that we use for the axions, essentially varying $b$.

Note that, since we are in the reference system where the axion is at rest, it is enough to analyze what happens with the angle $\theta_1'$, therefore we integrate in $\phi_1'$

$$\frac{d\sigma}{d(\cos\theta_1')} = \frac{g_{a\gamma\gamma}^4 m_a^2}{32\pi}\left(\frac{b^2}{[1+b(1-\cos\theta_1')]}\right)^2\left[f_s(b,\theta_1') + f_u(b,\theta_1') + g_{su}(b,\theta_1')\right]. \tag{6.2}$$

Where $f_s(b,\theta_1')$, $f_u(b,\theta_1')$ and $g_{su}(b,\theta_1')$ are given by Eqs. (5.40), (5.41) and (5.42), respectively. We use photons with energy $E_{ph} = 6.626 \times 10^{-4}\,\text{eV}$.

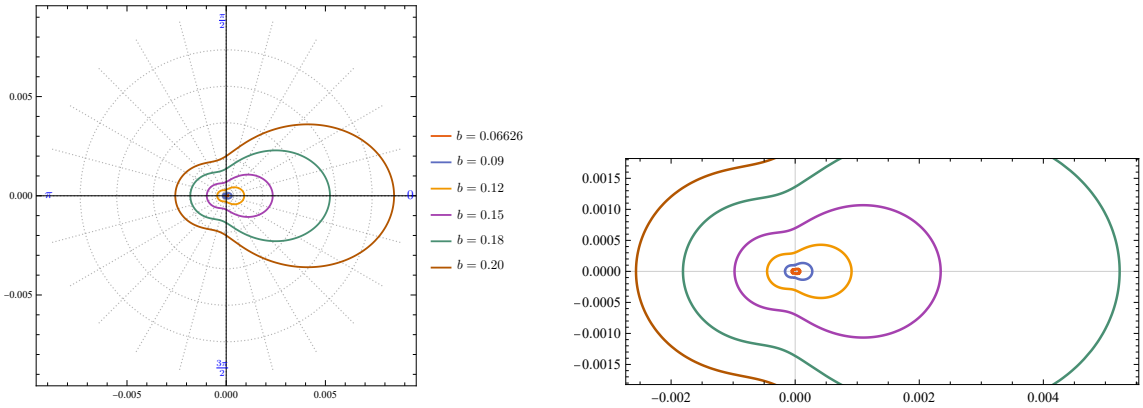


(a) (b)

Figure 6.2: Angular distribution for photons from the CMB scattered by axions.

We observe that photons preferentially exit forward, and this preference increases as the mass of the axions decreases.

### 6.2.1 Mean free path of photons in an axion dark matter halo

As discussed in detail in chapter 2, the interest in searching for axions in astrophysical situations is that these are good candidates for dark matter and in particular could be treated as cold dark matter when their production is non-thermal. Under this scenario, it is clear that we can have dark matter halos formed by axions, and we will be able to estimate the mean free path that a photon that crosses the halo will travel and see whether its interaction, even if suppressed, should be taken into

account or not. To do this, we will use the conditions established in various cosmological studies (see Chapter 2), where it is established that the local density of dark matter can be estimated as $\rho_0 = (0.550.17)\,\mathrm{GeV/cm^3}$ in the SHM model (see section 2.4), then we can assume that the axions are distributed isotropically and homogeneously, under this condition the local number density of axions is given by

$$n = \frac{\rho_0}{m_a} = (0.55 \pm 0.17)\,\frac{\mathrm{GeV}}{m_a \mathrm{cm}^3}\,. \tag{6.3}$$

The following graph shows $n$ for $10^{-6}\,\mathrm{eV} < m_a < 10^{-2}\,\mathrm{eV}$, having a dotted line in the mean value.

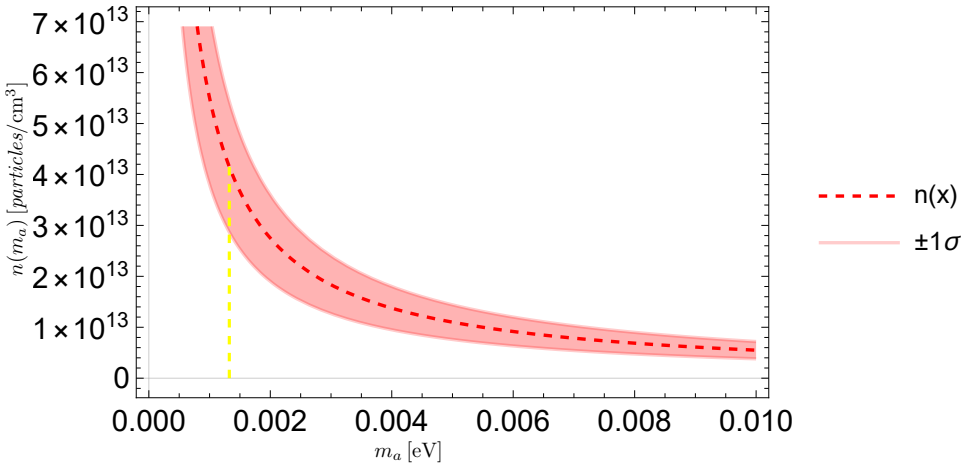


Figure 6.3: Axion number density in the galactic halo. A cut in the mass corresponding to $b = 0.5$ is shown for photos that come from the CMB.

In different estimates of the speed of local dark matter, a relativistic parameter is obtained at $\beta \approx 7.77 \times 10^{-4} - 1.76 \times 10^{-3}$ [85]. To provide a clear idea, we select the circular velocity values $v_\odot = 233\,\mathrm{km/s}$ and $v_{esc} = 528\,\mathrm{km/s}$. This circular speed is valid in a radius of $r_\odot \approx 8\,\mathrm{kpc}$ [159]. Taking into account that it is proposed that they follow a Maxwell-Boltzmann distribution and a cut is made at $v > v_{esc}$ [160]. This distribution is given by

$$f(v) = \frac{4N}{\sqrt{\pi} v_\odot}\left(\frac{v}{v_\odot}\right)^2 \exp\left(-\frac{v_{esc}^2}{v_\odot^2}\right)\,, \quad v < v_{esc}\,, \tag{6.4}$$

where $N$ is a normalization constant.

We see that $\beta \sim 10^{-3}$. This does not drastically affect the energy of the outgoing photon in the Compton scattering process, so the calculations can be done in the reference frame where the axion is at rest.

Knowing the cross-section, we can estimate the mean free path of the photon

$$\langle l_\nu \rangle = \frac{1}{n(m_a)\sigma(m_a)} \tag{6.5}$$

Choosing the best of the scenarios $g_{a\gamma\Gamma} \approx \frac{2}{3} \times 10^{-10}\,\mathrm{GeV}^{-1}$. Using the result we obtained in the

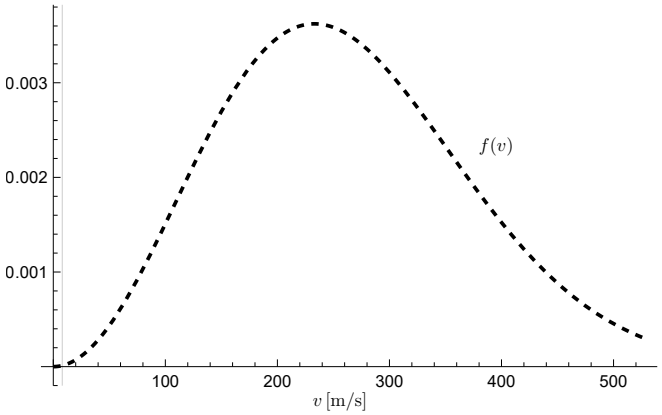


Figure 6.4: Velocity distribution of dark matter particles in the galactic halo, with $N = 1.01667$.

previous section $b = \frac{\epsilon_{th}}{m_a}$, with $\epsilon_{ph} \approx 1.168\,\text{eV}$[1]

$$\sigma(b) \approx \bar{g}_{a\gamma\gamma}^4 \bar{m_a}^2 \left(\frac{H(b)}{32\pi}\right) (3.894 \times 10^{-46})\,\text{cm}^2\,, \tag{6.6}$$

Here $\bar{g}_{a\gamma\gamma}$ is the value of the coupling constant measured in GeV, and its units have already been considered, similarly $\bar{m}_a$, is measured in eV, and we could take the best case $\bar{g}_{a\gamma\gamma} \approx \frac{2}{3} \times 10^{-10}$

$$\sigma(b) \approx \bar{m_a}^2 \left(\frac{H(b)}{72\pi}\right) (3.894 \times 10^{-86})\,\text{cm}^{\,2}\,. \tag{6.7}$$

It is evident that this cross-section will turn out to be too small, which may well be ignored since $H(b) < 5$ agrees with the graph shown in Fig. 5.3. Furthermore, as we saw in the graph 6.3 the local axion number density must be $\sim 10^{12} - 10^{13}\,\frac{\text{Axions}}{cm^3}$. And that will not be enough to offset the small cross-section, in fact the mean free path exceeds the observable size of the universe is approximately $46.5$ billion light years $\approx 1.425 \times 10^4$ Mpc. Since by choosing the best of the cases $\bar{m}_a = 10^{-2}$ therefore $H(b) \approx 0.000709$, we obtain

$$\sigma \approx 1.22 \times 10^{-95}\,\text{cm}^2\,. \tag{6.8}$$

This produces $l = 8.197 \times 10^{81}$ cm $\approx 2.656 \times 10^{57}$Mpc.

So "cold" axions of this type have not yet interacted anywhere in the observable Universe with CMB photons.

## 6.3 On the possibility of having inverse Compton scattering with Axions and Total Compton Spectrum

What we have left to see is whether we can have Inverse Compton scattering with axions, that is, that an axion has somehow obtained enough energy to be considered relativistic and, when

[1]This value is obtained by considering that the CMB radiates as a black body and corresponds to the peak energy emission that follows Wien's displacement law and the temperature of the CMB.

scattered with a low-energy photon, the axion gives up its energy to the photon, making it high energy. As discussed in chapter 4, this situation is of great interest in astrophysics. In the case that our scattering particle is an electron, this case is the extreme Klein-Nishina limit and is considered when determining the total Compton spectrum.

As we analyzed in section 6.1, in the scattering of photons through very relativistic particles, they acquire much more energy when the high energy case of electrons is taken into account. However, for axions, this is not always the case, since the effect is suppressed by the small mass they have. A difference is observed for masses $5 \times 10^{-3}\,\text{eV} < m_a < 10^{-2}\,\text{eV}$, and for smaller masses it is interesting to note that it is not acquired higher energy (see Fig. 6.1), which rules out studying the process at high energies in accordance with the limits for ALPs that are in Table 3.1.

A problem that we found when determining the cross section of the photon-axion scattering process at the tree level is that the term corresponding to the $u$ channel causes a divergence from $b = 0.5$. In the following figure we show that divergence occurs for an angle $\theta_1' \to \pi$ as $b$ increases.

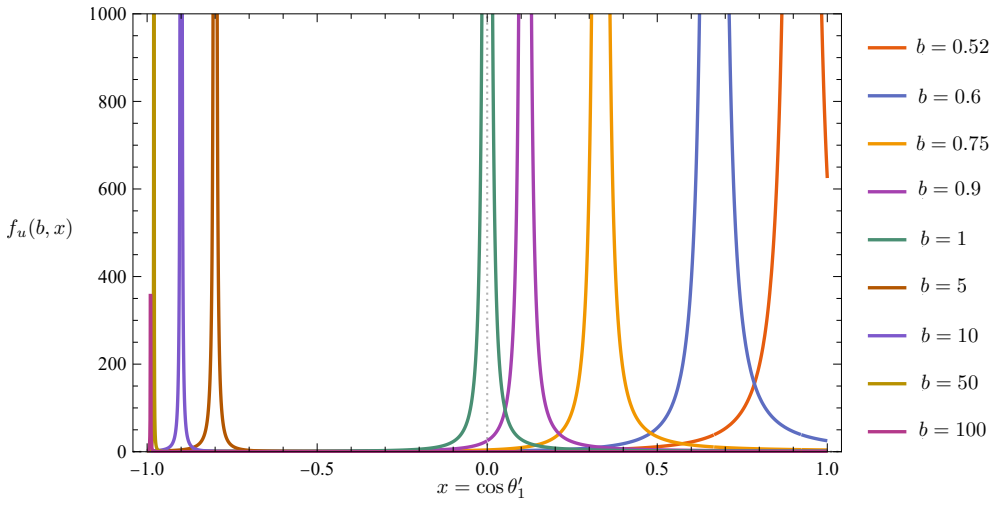


Figure 6.5: Graph of the function $f_u(b, x)$ for values of $b > 0.5$.

The divergence is caused by the zero-momentum divergent photon propagator and is typical of any infinite-range interaction. This phenomenon occurs in various processes such as dispersion $e^-e^- \to e^-e^-$ or $e^+e^+ \to e^+e^+$, known as Bhabha scattering. Usually, radiative corrections are expected to cure this [161][162]. In the latter case, the solution to this divergence is still being debated: some say it is "false" and others say it has a physical interpretation. However, it is generally accepted that the question is well posed for a finite angle and has been verified by experiments [163] [164].

In the situation studied, we face the same problem, but when dealing with an effective theory it is possible that some contribution is not being considered. We can study a little more in detail where we find the divergences for $b > 0.5$, trying to work directly in the laboratory reference system. The problem with this is that we have a parameter $\theta$, which is the angle of incidence of the photon with

respect to the direction of propagation of the axion in this situation.

$$m_a^2 - 2I_{k'p} = m_a^2\left(1 - 2\gamma\frac{\epsilon_1}{m_a}(1-\beta\cos\theta_1)\right) \tag{6.9}$$

$$= m_a^2\left(1 - 2\gamma\frac{\epsilon/m_a(1-\beta\cos\theta)(1-\beta\cos\theta_1)}{\left[(1-\beta\cos\theta_1) + \left(\frac{\epsilon}{\gamma m_a}\right)(1-\cos(\theta_1-\theta))\right]}\right) \tag{6.10}$$

So it is enough to determine if there are values for which $(m_a^2 - 2I_{k'p}) \neq 0$. This can be verified with computational tools. Choosing $m_a \approx 10^{-6} - 10^{-4}$, eV, no values were found for which there were no divergences in the differential cross section.

Trying to regularize the integral goes beyond the scope of the present work. As mentioned, in the case of low-energy axions, despite their abundance as dark matter, we would not have a significant cross section. Therefore, for the mass range allowed for axions, we can conclude that the scattering process is irrelevant.

For this reason, trying to establish the total Compton scattering spectrum, as discussed in chapter 3, does not go beyond an academic work due to the few physical implications that we could find.

## 6.4 Axion effects on propagation of gamma-rays

Since the gamma rays-bursts (GRB) delay produced by a charged plasma was found proportional to the inverse of the particle mass, $\tau \propto m^{-1}$ [165], it is natural to look for particles of mass much smaller than the electron's.

In this context, we will consider a model where dark matter consists of axions. However, since an electrically charged axion is not consistent with experiments and observations, the plasma frequency formula for a charged plasma is no longer valid. Despite this, given the activity in axion-electrodynamics with its connection to topological insulators, the assumption of a photon-axionic plasma coupling seems appropriate.

We consider scattering of unpolarized light and emerging time delays depending on the photon energy, which is the relevant case for the current GRB experiments. A theoretical quantum calculation of the plasma frequency range $\omega_p^2$ is presented below. The calculation is valid for high-energy photons, when the photon energy is much greater than the axion mass $m_a$. A plasma can support both longitudinal and transverse waves. We are interested in transverse waves. Dispersion relation for light in a plasma is

$$\omega^2 = |\mathbf{k}|^2 + \omega_p^2\,, \tag{6.11}$$

Where $\omega_p$ is the plasma frecuency, which is due to the plasma oscillations called Langmuir waves [165]. On the other hand, we have already determined the contributions to the scattering amplitude of the form

$$\mathcal{M}_s = \frac{g_{a\gamma\gamma}^2}{(m_a^2 + 2k\cdot p)}\left\{\left[(k\cdot p)(k'\cdot p) - (m_a^2 + k\cdot p)(k'\cdot k)\right]\epsilon_\mu^*(\mathbf{k}',\lambda')\epsilon^\mu(\mathbf{k},\lambda)\right.$$
$$\left. + \left[(m_a^2 + k\cdot p)k^\mu k'_\nu - (k'\cdot p)k^\mu p_\nu - (k\cdot p)p^\mu k'_\nu + (k'\cdot k)p^\mu p_\nu\right]\epsilon_\mu^*(\mathbf{k}',\lambda')\epsilon^\nu(\mathbf{k},\lambda)\right\}\,, \tag{6.12}$$

$$\mathcal{M}_u = \frac{g_{a\gamma\gamma}^2}{(m_a^2 - 2k\cdot p')}\left\{\left[(k\cdot p')(k'\cdot p') - (m_a^2 - k\cdot p')(k'\cdot k)\right]\epsilon_\mu^*(\mathbf{k}',\lambda')\epsilon^\mu(\mathbf{k},\lambda)\right.$$
$$\left. + \left[(m_a^2 - k\cdot p')k^\mu k'_\nu - (k'\cdot p')k^\mu p'_\nu - (k\cdot p')p'^\mu k'_\nu + (k'\cdot k)p'^\mu p'_\nu\right]\epsilon_\mu^*(\mathbf{k}',\lambda')\epsilon^\nu(\mathbf{k},\lambda)\right\} . \quad (6.13)$$

In accordance with what was previously explained for low energies, we note that the scattering of photons occurs preferentially forward, even more with the most energetic photons, we extrapolate this idea. When the momenta of the initial and final photons are parallel (with an angle $\theta = 0$ between $k$ and $k'$), we have $k\cdot k' = 0$, and also $k_\mu\cdot\epsilon^\mu(k,\lambda) = 0$ and $k_\mu^*\epsilon^\mu(k,\lambda) = 0$ from the gauge condition. Thus, only the first term of eqs. (6.12)-(6.13), survives on forward dispersal. Furthermore, since the momenta of the initial and final photons are parallel, their polarization can be described by the same vectors, which are taken as orthonormal, $\epsilon_\mu^*(k,\lambda)\epsilon_\mu(k,\lambda) = \delta_{\lambda\lambda}$. Therefore we obtain (considering $k\cdot p' = k'\cdot p$ and $k'\cdot p' = k\cdot p$)

$$\mathcal{M}_s = \frac{g_{a\gamma\gamma}^2}{(m_a^2 + 2k\cdot p)}(k\cdot p)(k'\cdot p)\delta_{\lambda,\lambda'} , \quad (6.14)$$

$$\mathcal{M}_u = \frac{g_{a\gamma\gamma}^2}{(m_a^2 - 2k'\cdot p)}(k\cdot p)(k'\cdot p)\delta_{\lambda,\lambda'} . \quad (6.15)$$

For cold axions they can be the cold dark matter particle ($\beta\sim 10^{-3}$). In forward scatter $\theta = 0$ and $k^{0\prime}\approx k^0$. Then the differential cross-section is determined by

$$\frac{d\sigma(0)}{d\Omega} = \frac{1}{64\pi^2 m_a^2}\left(\frac{1}{2}\sum_{\lambda,\lambda'}|\mathcal{M}(0)|\right) = \frac{g_{a\gamma\gamma}^4}{16\pi^2}\left|\frac{k_0^2 m_a}{m_a^2 - 4k_0^2}\right|^2 = \left(\frac{g_{a\gamma\gamma}^2}{4\pi}\right)^2\left|\frac{k_0^2 m_a}{m_a^2 - 4k_0^2}\right|^2 . \quad (6.16)$$

The differential cross-section is given in terms of the scattering amplitude as

$$|f(\theta)|^2 = \frac{d\sigma}{d\Omega} . \quad (6.17)$$

So the absolute value of the forward scattering amplitude is given as

$$|f(0)| = \frac{g_{a\gamma\gamma}^2}{4\pi}\frac{k_0^2 m_a}{|m_a^2 - 4k_0^2|} . \quad (6.18)$$

We can show that the plasma frequency when the photon frequency is large compared to the plasma frequency, $w \gg w_p$, is

$$w_p^2 = 4\pi n \mathrm{Re}|f(0)| . \quad (6.19)$$

Thus, the frequency of the axion plasma is determinated by

$$w_p^2 = g_{a\gamma\gamma}^2 n\frac{\omega^2 m_a}{|4\omega^2 - m_a^2|} . \quad (6.20)$$

Note that $\omega_p$ is proportional to the average mass density of the axions, $\rho_a = nm_a$, as ($\omega \gg \omega_p$)

$$w_p^2 = g_{a\gamma\gamma}^2\frac{\omega^2\rho_a}{|4\omega^2 - m_a^2|} = \frac{g_{a\gamma\gamma}^2\rho_a}{4}\left(1 + \sum_{n=1}^{\infty}\left(\frac{m_a^2}{4\omega^2}\right)^n\right) \approx \frac{1}{4}g_{a\gamma\gamma}^2\rho_a . \quad (6.21)$$

Thus only the density of axionic dark matter determines the dispersion of light in the cosmic axion medium. The plasma frequency is nearly constant, i.e. independent of the frequency of the incoming light.

The group velocity can be taken as the signal velocity. If the plasma frequency is independent of $\mathbf{k}$, which is the case in a usual plasma with charged particles, and the photon momentum is large compared to the plasma frequency ($|\mathbf{k}|^2 \gg \omega_p^2$), we obtain that the group velocity is only slightly lower than $c$.

$$v_{GRB} = 1 - d = 1 - \frac{1}{2}\frac{\omega_p^2}{\omega^2} = 1 - g_{a\gamma\gamma}^2 \frac{\rho_a}{8\omega^2} \tag{6.22}$$

Assume now that $D(z)$ is the effective distance traveled by the photons taking into account the expansion of the Universe. In principle, the photon transit time is [166]

$$t = \frac{D(Z)}{v_{GRB}}\,. \tag{6.23}$$

The time delay between two signals traveling at the speeds $v_{GRB}$ and $c$ is obtained as:

$$\tau = \frac{Dd}{c(1-d)} \approx \frac{Dd}{c}\,. \tag{6.24}$$

For estimation purposes, we ignore the dependence of $D$ on redshift. The CAST experiment established the limits $\gamma_{a\gamma\gamma} < 0.66 \times 10^{-10}$ GeV$^{-1}$ and $m_a \lesssim 0.02$ eV [152]. In the optimistic scenario, $d = 4.27 \times 10^{-63}\,(\overline{p}_a)\,/\left(\overline{E}_{\rm GR}^2\right)$, where $(\overline{p}_a)$ is the axion DM density in units GeV/cm$^3$ and $\overline{E}_{\rm GR}$ is gamma-ray energy in GeV.

Let us consider the Galactic Halo (GH) where DM is assumed to consist of axions. The energy density of GH is $\rho_a = 0.55$ GeV/(cm$^3$) [85], and the radius of GH is $D = 8$ kpc $\approx 2.47 \times 10^{20}$ m [159]. The delay of GRB propagating through the GH is

$$\tau = \frac{1.93 \times 10^{-51}}{\overline{E}_{\rm GR}^2}\,\text{s}\,. \tag{6.25}$$

As a second example, we consider a massive galaxy filament. The average axion density is estimated as $\rho_a = 10^{-3}$ GeV/cm$^3$, and the effective distance is $D = 3$ Gpc $\approx 9.26 \times 10^{25}$ m. The delay of GRB is obtained as

$$\tau = \frac{1.32 \times 10^{-48}}{\overline{E}_{\rm GR}^2}\,\text{s}\,. \tag{6.26}$$

We conclude that only the density of axionic DM determines the dispersion of light in the cosmic axion medium and the delay is negligible for high-energy photons in massive galaxy filament, as it also is in the case of GH.

# Chapter 7
# Conclusions and discussion

The Standard Model of Elementary Particles has demonstrated remarkable success in its phenomenological and experimental predictions. However, the presence of various challenges, such as the strong $CP$ problem and observations that suggest the existence of DM, this compels us to expand this model to explain the composition of the Universe. The challenge lies in developing a theoretical framework that builds on the explanations already offered by the SM.

In this work, an extension to the SM was explored that adds a new symmetry $U(1)_{PQ}$. With this addition, the strong $CP$ problem is addressed and a candidate to be the DM particle is presented: the QCD axion. To address more general cases, the incorporation of axion-like particles that arise in other scenarios intended to extend the SM or that appear in more general theories than the latter was proposed. The new symmetries considered in these cases are not detailed, since, in general, we work with an effective coupling between an axion and two photons.

Since the initial proposal of axions, their search through this coupling has focused on axion-photon conversion in media with intense magnetic fields. The fundamental purpose of this work was to explore the possibility of having an interaction between photons and axions through a scattering process that we call "Compton-like scattering". Below, we present the conclusions obtained:

- Guided by the usual Compton scattering process, the kinematics present in generalized Compton scattering have been generally discussed (without establishing the nature of the scattering particle). It is shown that the significant energy loss behavior of scattering particles in inverse Compton scattering depends mainly on the mass of the scattering particle [1], which makes this phenomenon more pronounced at as the mass of the particle increases. Therefore, for axions, this behavior begins to be notable when the mass of the axion is greater than $0.5 \times 10^{-2}$ eV, when working with photons from the CMB.

- When analyzing the angular distribution of the differential cross-section, the presence of an infrared divergence is noted that makes it difficult to calculate the cross-section at the tree level in a wide range of energies. Furthermore, preferential forward emission is observed as the energy increases in the reference frame where the axion is at rest. This behavior is analogous to Compton scattering with electrons, at least in the allowed parameter space, defined by $b = \frac{\epsilon'}{m_a}$.

- The cross-section at low energies is determined, revealing that it is considerably small for light axions, which are candidates for CDM. Therefore, we can rule out the search for these particles through this process.

- In attempting to address the "high energy" limit, it was shown that in no scenario is it possible to eliminate infrared divergence. Therefore, we cannot speak with certainty about what will happen in this case. However, as we have concluded from the kinematics, no significant energy loss is expected.

[1] Eletrons, in usual Compton scattering.

- By modeling the structures formed by DM as a plasma, we examine the possibility of distinguishing the signal of a photon that has interacted with the plasma by the corresponding group velocity of the beam, compared to other photons that have not interacted. It is shown that the associated delay time is also negligible.

Unfortunately, the search for axions through photon scattering is extremely difficult because the interaction is practically negligible, and we can only count on the search for axions through the axion-photon conversion. The results of section 4 of [121] indicate that in grand unification theories (GUTs), the expectation is that ALPs have a relation $g_{a\gamma\gamma} = \frac{g_a}{m_a}$ smaller than the QCD prediction, making it impossible to explore that region. The lack of experimental access to this region of parameter space highlights the need for experimental approaches that do not rely on axion-photon coupling. Of particular interest in this direction are the couplings of axions to fermions, which have recently been sought to be explored [167].

# Appendix A

## A.1 Friedmann-Robertson-Walker (FRW) Universe

It is reasonable, from an observational point of view, to assume that the Universe is almost isotropic and homogeneous. Mathematically, an isotropic and homogeneous universe is described by the Friedmann-Robertson-Walker (FRW) metric:

$$ds^2 = -dt^2 + R^2(t)\left[d\mathbf{r}^2 + \frac{(\mathbf{r}\cdot d\mathbf{r})^2}{1-kr^2}\right], \tag{A.1}$$

where $R(t)$ is known as *scale factor* and here has dimensions of length, so the radial coordinate $r = |\mathbf{r}|$ has no units. The constant $k$ represents the type of curvature of space and can acquire the following values:

$$k = \begin{cases} +1 & \text{closed universe,} \\ 0 & \text{flat universe,} \\ -1 & \text{open universe.} \end{cases} . \tag{A.2}$$

The dynamics of cosmic expansion is determined by Einstein's equation [1]

$$R_{\mu\nu} - \frac{1}{2}g_{\mu\nu}\mathcal{R} = 8\pi T_{\mu\nu}\,. \tag{A.3}$$

Here $R_{\mu\nu}$ is the Ricci tensor, $\mathcal{R}$ is the Ricci scalar, and $T_{\mu\nu}$ is the energy-momentum tensor. Due to the assumption of isotropy and homogeneity, the energy-momentum tensor can be modeled as a perfect fluid, that is

$$T_{00} = \rho(t), \quad T_{i0} = 0, \quad T_{ij} = F^2(t)p(t)\left(\delta_{ij} + \frac{kr_ir_j}{1-kr^2}\right), \tag{A.4}$$

where $i$ and $j$ run through the three spatial directions, and $\rho$ and $p$ are the energy density and pressure of the fluid. The non-zero components of the Ricci tensor and the Ricci scalar are given by:

$$R_{00} = -3\frac{\ddot{R}}{R}, \quad R_{ij} = -\left[\frac{\ddot{R}}{R} + 2\left(\frac{\dot{R}}{R}\right)^2 + 2\frac{k}{R^2}\right]g_{ij}, \quad \mathcal{R} = -6\left[\frac{\ddot{R}}{R} + \left(\frac{\dot{R}}{R}\right)^2 + \frac{k}{R^2}\right]. \tag{A.5}$$

Using (A.3), the component $(\mu,\nu) = (0,0)$ of the Einstein field equations (A.3) when using (A.4)

$$\left(\frac{\dot{R}}{R}\right)^2 + \frac{k}{R^2} = \frac{8\pi}{3}\rho\,, \tag{A.6}$$

[1] We use natural units where $G = 1$.

The *Hubble parameter* is usually defined

$$H := \frac{\dot{R}}{R}\,, \tag{A.7}$$

we obtain the *Friedman Equation*

$$H^2 + \frac{k}{R^2} = \frac{8\pi}{3}\rho\,. \tag{A.8}$$

On the other hand, due to the homogeneity of the FRW space–time, the spatial components $(\mu,\nu) = (i,i)$ of the Einstein field equations (A.3) under the metric of FRW lead to the same equation. For example, taking $\mu = \nu = 2$ we find

$$\left[\frac{\ddot{R}}{R} + 2\left(\frac{\dot{R}}{R}\right)^2 + \frac{k}{2R^2}\right] R^2 r^2 - 3\left[\frac{\ddot{R}}{R} + \left(\frac{\dot{R}}{R}\right)^2 + \frac{k}{R^2}\right] r^2 R^2 = 8\pi(-p)(-R^2 r^2)\,, \tag{A.9}$$

which, after a little algebra, leads to the cosmological acceleration equation

$$\frac{\ddot{R}}{R} = -\frac{4\pi}{3}(\rho + 3p)\,. \tag{A.10}$$

Combining the Friedmann equation and (A.10), or, using $D_\mu T^{\mu 0} = 0$, we obtain the expression of the equation of continuity and conservation of energy in the universe by FRW

$$D_\mu T^{\mu 0} = T^{\mu 0}{}_{,\mu} + \Gamma^\mu_{\lambda\mu} T^{\lambda 0} - \Gamma^\lambda_{\mu 0} T^{\mu\lambda} = \dot{\rho} + 3H(\rho + p) = 0\,. \tag{A.11}$$

Various energy components contribute to the right side of Eq. (A.8), such as matter $\rho_M \propto R^{-3}$, radiation $\rho_R \propto R^{-4}$, and dark energy $\rho_\Lambda =$ constant. Putting these three contributions together, we observe that the energy density behaves as follows:

$$\rho = \rho_{M,0}\left(\frac{R_0}{R}\right)^3 + \rho_{R,0}\left(\frac{R_0}{R}\right)^4 + \rho_\Lambda\,. \tag{A.12}$$

Where the subscript $0$ represents the amount in the present time. We define the density parameters:

$$\Omega_M \equiv \frac{\rho_{M,0}}{\rho_{c,0}}, \quad \Omega_R \equiv \frac{\rho_{R,0}}{\rho_{c,0}}, \quad \Omega_\Lambda \equiv \frac{\rho_{\Lambda,0}}{\rho_{c,0}}, \quad \Omega_k \equiv -\frac{k}{R_0^2 H_0^2}\,. \tag{A.13}$$

Where $\rho_{c,0} \equiv \frac{3H_0^2}{8\pi}$ is the critical density at present, and $H_0 = 100h\,\mathrm{kms}^{-1}\mathrm{Mpc}^{-1}$ is the Hubble parameter at the present time. The parameter $h$ parameterizes the Hubble parameter measurements, and the current measurements indicate $h \approx 0.674$ [168]. Combining Eqs. (A.8), (A.12), (A.7) and (A.13), we obtain

$$\frac{H(t)^2}{H_0^2} = \Omega_M\left(\frac{R_0}{R}\right)^3 + \Omega_R\left(\frac{R_0}{R}\right)^4 + \Omega_\Lambda + \Omega_k\left(\frac{R_0}{R}\right)^2\,. \tag{A.14}$$

Seven years of data from WMAP measurements indicate $\Omega_M h^2 = 0.11161$ and $\Omega_\Lambda = 0.729$ [169]. Furthermore, from the observed temperature of the cosmic microwave background $T_0 = 2.7250.002\,\mathrm{K}$ [170], the radiation density parameter is estimated as $\Omega_R h^2 = 4.15 \times 10^{-5}$. Using this result, the epoch of equality between matter and radiation is estimated, where the energy density of matter is equal to that of radiation, as $\frac{F_{eq}}{F_0} = 4.15 \times 10^{-5}(\Omega_M h^2)^{-1}$.

# Appendix B

## B.1 Feynman's rule for the vertex of interaction between a photon and an axion

To establish what happens at the vertex of the interaction of the axion (or ALP) with two photons, it is convenient to rewrite the Lagrangian density given in (3.68), noting that

$$\begin{aligned} F_{\mu\nu}\widetilde{F}^{\mu\nu} &= (\partial_\mu A_\nu - \partial_\nu A_\mu)\frac{1}{2}\epsilon^{\mu\nu\rho\sigma}(\partial_\rho A_\sigma - \partial_\rho A_\sigma) \\ &= \frac{1}{2}\epsilon^{\mu\nu\rho\sigma}(\partial_\mu A_\nu \partial_\rho A_\sigma - \partial_\mu A_\nu \partial_\sigma A_\rho - \partial_\nu A_\mu \partial_\rho A_\sigma + \partial_\nu A_\mu \partial_\sigma A_\rho) \\ &= \frac{1}{2}(\epsilon^{\mu\nu\rho\sigma}\partial_\mu A_\nu \partial_\rho A_\sigma - \epsilon^{\mu\nu\rho\sigma}\partial_\mu A_\nu \partial_\sigma A_\rho - \epsilon^{\mu\nu\rho\sigma}\partial_\nu A_\mu \partial_\rho A_\sigma + \epsilon^{\mu\nu\rho\sigma}\partial_\nu A_\mu \partial_\sigma A_\rho)\,, \end{aligned}$$

making the changes on the dummy sum indices $\rho \leftrightarrow \sigma$, $\nu \leftrightarrow \mu$ and $\nu \leftrightarrow \mu$ with $\sigma \leftrightarrow \rho$ in the second, third, and fourth term, respectively. In addition to using the fact that the Levi-Civita symbol $\epsilon^{\mu\nu\rho\sigma}$ is antisymmetric under the exchange of two indices it is concluded that

$$F_{\mu\nu}\widetilde{F}^{\mu\nu} = \frac{1}{2}(4)\epsilon^{\mu\nu\rho\sigma}\partial_\mu A_\nu \partial_\rho A_\sigma\,. \tag{B.1}$$

Then, the Lagrangian density of interaction given in (3.68) takes the form

$$\mathcal{L}_{a\gamma\gamma} = -\frac{1}{2}g_{a\gamma\gamma}a\epsilon^{\mu\nu\rho\sigma}\partial_\mu A_\nu \partial_\rho A_\sigma\,, \tag{B.2}$$

We express the preceding term in the momentum space, omitting the constant factor $\frac{g_{a\gamma\gamma}}{2}$, so

$$\begin{aligned} L &= -a(k^{(3)})\epsilon^{\mu\nu\rho\sigma}(-ik_\mu^{(1)})A_\nu(k^{(1)})(-ik_\rho^{(2)})A_\sigma(k^{(1)}) \\ &= a(k^{(3)})\epsilon^{\mu\nu\rho\sigma}k_\mu^{(1)}A_\nu(k^{(1)})k_\rho^{(2)}A_\sigma(k^{(1)}) \\ &= a(k^{(3)})\epsilon^{\mu\nu\rho\sigma}A_\nu(k^{(1)})A_\sigma(k^{(1)})k_\mu^{(1)}k_\rho^{(2)}\,, \end{aligned}$$

we take the functional derivative of $L$ with the term $(-i)^3$, and since second-degree terms appear in the component of the field $A_\mu$, we multiply by the factor $2! = 2$

$$\begin{aligned} 2\frac{(-i)^3\delta^3 L}{\delta a(k^{(3)})\delta A^\alpha(k^{(1)})\delta A^\beta(k^{(2)})} &= 2i\frac{\delta a(k^{(3)})}{\delta a(k^{(3)})}\epsilon^{\mu\nu\rho\sigma}\frac{\delta A_\nu(k^{(1)})}{\delta A^\alpha(k^{(1)})}\frac{\delta A_\sigma(k^{(2)})}{\delta A^\beta(k^{(2)})}k_\mu^{(1)}k_\rho^{(2)} \\ &= 2i\epsilon^{\mu\nu\rho\sigma}g_{\gamma\nu}\frac{\delta A^\gamma(k^{(1)})}{\delta A^\alpha(k^{(1)})}g_{\delta\sigma}\frac{\delta A^\delta(k^{(2)})}{\delta A^\beta(k^{(2)})}k_\mu^{(1)}k_\rho^{(2)} \\ &= 2i\epsilon^{\mu\nu\rho\sigma}g_{\gamma\nu}\delta^{\gamma\alpha}g_{\delta\sigma}\delta^{\delta\beta}k_\mu^{(1)}k_\rho^{(2)} \\ &= 2i\epsilon^{\mu\nu\rho\sigma}\delta_\nu^\alpha\delta_\sigma^\beta k_\mu^{(1)}k_\rho^{(2)} \\ &= 2i\epsilon^{\mu\alpha\rho\beta}k_\mu^{(1)}k_\rho^{(2)}\,. \end{aligned}$$

Finally, multiplying by the factor $\frac{g_{a\gamma}}{2}$ we obtain Feynman's rule for the interaction vertex

$$ig_{a\gamma\gamma}\epsilon^{\mu\nu\rho\sigma}k^{(1)}_{\mu}k^{(2)}_{\rho}\,, \tag{B.3}$$

where $k^{(1)}$ and $k^{(2)}$ are the 4-momenta of the two photons, while the free indices $\nu$ and $\sigma$ correspond to the photon 1 and 2, respectively.

## B.2 Axion decay in two photons

It can be shown that the rate decay of a particle of mass $M$ to two particles of mass $m_1$ and $m_2$, respectively is given by the differential decay width (in the system reference where the particle of mass $M$ is at rest [23]

$$\frac{d^2\Gamma}{d\Omega} = \frac{1}{64\pi^2 M^2}\overline{|\mathcal{M}|^2}\sqrt{\left[1-\left(\frac{m_1+m_2}{M}\right)^2\right]+\left[1-\left(\frac{m_1-m_2}{M}\right)^2\right]}\,, \tag{B.4}$$

where $\overline{|\mathcal{M}|^2}$ is the square of the Feynman amplitude containing the sum over all polarizations of the particles involved (averaged where necessary) and indistinguishability fractions.

To calculate the two-photon axion decay width, we use Feynman's rule for the interaction vertex derived in the previous section. Additionally, we consider the following Feynman rules:

1. An incoming (outgoing) photon with 4-momentum $k$ and spin polarization $\lambda$ has a contribution $\epsilon^{\mu}(\mathbf{k},\lambda)$ ($\epsilon^{\mu *}(\mathbf{k},\lambda)$),

2. The absorption or emission of a scalar particle such as the axion contributes a factor equal to 1.

3. Multiplying the above factors together we obtain the quantity $i\mathcal{M}$, where $\mathcal{M}$ is the invariant Feynman amplitude.

In the case studied

$$i\mathcal{M} = ig_{a\gamma\gamma}\epsilon^{\mu\nu\rho\sigma}k^{(1)}_{\mu}k^{(2)}_{\rho}\epsilon^{*}_{\nu}(\mathbf{k}_1,\lambda_1)\epsilon^{*}_{\sigma}(\mathbf{k}_2,\lambda_2)\,. \tag{B.5}$$

Then the invariant amplitude squared is

$$\begin{aligned}
|\mathcal{M}|^2 &= [g_{a\gamma\gamma}\epsilon^{\alpha\beta\gamma\delta}k^{(1)}_{\alpha}k^{(2)}_{\gamma}\epsilon^{*}_{\beta}(\mathbf{k}_1,\lambda_1)\epsilon^{*}_{\delta}(\mathbf{k}_2,\lambda_2)][g_{a\gamma\gamma}\epsilon^{\mu\nu\rho\sigma}k^{(1)}_{\mu}k^{(2)}_{\rho}\epsilon^{*}_{\nu}(\mathbf{k}_1,\lambda_1)\epsilon^{*}_{\sigma}(\mathbf{k}_2,\lambda_2)]^{*}\\
&= g^2_{a\gamma\gamma}\epsilon^{\alpha\beta\gamma\delta}\epsilon^{\mu\nu\rho\sigma}k^{(1)}_{\alpha}k^{(2)}_{\gamma}k^{(1)}_{\mu}k^{(2)}_{\rho}\epsilon^{*}_{\beta}(\ bfk_1,\lambda_1)\epsilon^{*}_{\delta}(\mathbf{k}_2,\lambda_2)\epsilon_{\nu}(\mathbf{k}_1,\lambda_1)\epsilon_{\sigma}(\mathbf{k}_2,\lambda_2)\\
&= g^2_{a\gamma\gamma}\epsilon^{\alpha\beta\gamma\delta}\epsilon^{\mu\nu\rho\sigma}k^{(1)}_{\alpha}k^{(2)}_{\gamma}k^{(1)}_{\mu}k^{(2)}_{\rho}\epsilon^{*}_{\beta}(\mathbf{k}_1,\lambda_1)\epsilon_{\nu}(\mathbf{k}_1,\lambda_1)\epsilon^{*}_{\delta}(\mathbf{k}_2,\lambda_2)\epsilon_{\sigma}(\mathbf{k}_2,\lambda_2)\,.
\end{aligned}$$

Adding over the polarizations of the outgoing photons, and using the identities, adding the factor

of 1/2 because the outgoing photons are indistinguishable.

$$\begin{aligned}
\overline{|\mathcal{M}|^2} &= \frac{1}{2} g_{a\gamma\gamma}^2 \epsilon^{\alpha\beta\gamma\delta}\epsilon^{\mu\nu\rho\sigma} k_\alpha^{(1)} k_\gamma^{(2)} k_\mu^{(1)} k_\rho^{(2)} \sum_{\lambda_1,\lambda_2} \epsilon_\beta^*(\mathbf{k}_1,\lambda_1)\epsilon_\nu(\mathbf{k}_1,\lambda_1)\epsilon_\delta^*(\mathbf{k}_2,\lambda_2)\epsilon_\sigma(\mathbf{k}_2,\lambda_2) \\
&= \frac{1}{2} g_{a\gamma\gamma}^2 \epsilon^{\alpha\beta\gamma\delta}\epsilon^{\mu\nu\rho\sigma} k_\alpha^{(1)} k_\gamma^{(2)} k_\mu^{(1)} k_\rho^{(2)} \sum_{\lambda_1} \epsilon_\beta^*(\mathbf{k}_1,\lambda_1)\epsilon_\nu(\mathbf{k}_1,\lambda_1) \sum_{\lambda_2} \epsilon_\delta^*(\mathbf{k}_2,\lambda_2)\epsilon_\sigma(\mathbf{k}_2,\lambda_2) \\
&= \frac{1}{2} g_{a\gamma\gamma}^2 \epsilon^{\alpha\beta\gamma\delta}\epsilon^{\mu\nu\rho\sigma} k_\alpha^{(1)} k_\gamma^{(2)} k_\mu^{(1)} k_\rho^{(2)} (-g_{\beta\nu})(-g_{\delta\sigma}) \\
&= \frac{1}{2} g_{a\gamma\gamma}^2 \epsilon^{\alpha\beta\gamma\delta} g_{\delta\sigma}\epsilon^{\mu\nu\rho\sigma} g_{\beta\nu} k_\alpha^{(1)} k_\gamma^{(2)} k_\mu^{(1)} k_\rho^{(2)} \,.
\end{aligned}$$

Now, noting that when using the identity (B.15)

$$\begin{aligned}
\epsilon^{\alpha\beta\gamma\delta} g_{\delta\sigma}\epsilon^{\mu\nu\rho\sigma} g_{\beta\nu} &= -3!\delta^{[\alpha}_{\mu'}\delta^{\beta}_{\nu'}\delta^{\gamma]}_{\rho'} g^{\mu'\mu} g^{\nu'\nu} g^{\rho'\rho} g_{\beta\nu} \\
&= -3!\delta^{[\alpha}_{\mu'}\delta^{\beta}_{\nu'}\delta^{\gamma]}_{\rho'} g^{\mu'\mu} g^{\rho'\rho} \delta^{\nu'}_{\beta} \,.
\end{aligned}$$

By applying the previous identity in the calculation of $\overline{|\mathcal{M}|^2}$

$$\begin{aligned}
\overline{|\mathcal{M}|^2} &= \frac{1}{2} g_{a\gamma\gamma}^2 \left(-3!\delta^{[\alpha}_{\mu'}\delta^{\beta}_{\nu'}\delta^{\gamma]}_{\rho'} g^{\mu'\mu} g^{\rho'\rho} \delta^{\nu'}_{\beta}\right) k_\alpha^{(1)} k_\gamma^{(2)} k_\mu^{(1)} k_\rho^{(2)} \\
&= \frac{1}{2} g_{a\gamma\gamma}^2 (-1) \left[\left(\delta^\alpha_{\mu'}\delta^\beta_{\nu'}\delta^\gamma_{\rho'} - \delta^\alpha_{\mu'}\delta^\gamma_{\nu'}\delta^\beta_{\rho'} + \delta^\beta_{\mu'}\delta^\gamma_{\nu'}\delta^\alpha_{\rho'} - \delta^\beta_{\mu'}\delta^\alpha_{\nu'}\delta^\gamma_{\rho'} + \delta^\gamma_{\mu'}\delta_{\nu'}^{alpha}\delta^\beta_{\rho'} - \delta^\gamma_{\mu'}\delta^\beta_{\nu'}\delta^\alpha_{\rho'}\right)\delta^{\nu'}_{\beta}\right] \times \\
&\quad g^{\mu'\mu} g^{\rho'\rho} k_\alpha^{(1)} k_\gamma^{(2)} k_\mu^{(1)} k_\rho^{(2)} \\
&= \frac{1}{2} g_{a\gamma\gamma}^2 (-1) \left(2\delta^\alpha_{\mu'}\delta^\gamma_{\rho'} - 2\delta^\gamma_{\mu'}\delta^\alpha_{\rho'}\right) k_\alpha^{(1)} k_\gamma^{(2)} k^{(1)\mu'} k^{(2)\rho'} \\
&= g_{a\gamma\gamma}^2 (\delta^\gamma_{\mu'}\delta^\alpha_{\rho'} - \delta^\alpha_{\mu'}\delta^\gamma_{\rho'}) k_\alpha^{(1)} k_\gamma^{(2)} k^{(1)\mu'} k^{(2)\rho'} \\
&= g_{a\gamma\gamma}^2 \left(k_\alpha^{(1)} k^{(2)\alpha} k_\gamma^{(1)} k^{(2)\gamma} - k_\alpha^{(1)} k^{(1)\alpha} k_\gamma^{(2)} k^{(2)\gamma}\right) \,.
\end{aligned}$$

Using the dispersion relation for photons $k^{(i)2} = k_\alpha^{(i)} k^{(i)\alpha} = 0$ with $i = 1.2$ , we get

$$\overline{|\mathcal{M}|^2} = g_{a\gamma}^2 \left(k^{(1)} \cdot k^{(2)}\right)^2 \,, \tag{B.6}$$

but of the conservation of 4-momentum, considering that $P^\mu$ is the 4-momentum of the ALP $P^\mu = k^{(1)\mu} + k^{(2)\mu}$, thus $P^2 = m_a^2 = 2k^{(1)} \cdot k^{(2)}$, therefore

$$\overline{|\mathcal{M}|^2} = g_{a\gamma}^2 \frac{m_a^4}{4} \,. \tag{B.7}$$

Finally, by the equation (B.4) with $m_1 = m_2 = 0$ and $M = m_a$

$$\frac{d^2\Gamma_{a\gamma\gamma}}{d\Omega} = \frac{1}{64\pi^2 m_a^2}\overline{|\mathcal{M}|^2} = \frac{g_{a\gamma}^2}{64\pi^2 m_a^2}\left(\frac{m_a^4}{4}\right) = \frac{g_{a\gamma}^2}{64\pi}\left(\frac{m_a^3}{4\pi}\right) \,, \tag{B.8}$$

integrating over the solid angle we conclude that

$$\Gamma_{a\gamma\gamma} = \frac{g_{a\gamma}^2 m_a^3}{64\pi} \,. \tag{B.9}$$

This result is well known in the literature.

## B.3 Some mathematical results

We define the Levi-Civita symbol for n-indices as

$$\epsilon^{\alpha_0\alpha_1\cdots\alpha_{n-1}} := \begin{cases} 1 & \textit{if the permutation of } \alpha_0,\alpha_1,\ldots,\alpha_{n-1} \textit{ is even} \\ -1 & \textit{if the permutation of } \alpha_0,\alpha_1,\ldots,\alpha_{n-1} \textit{ is odd} \\ 0 & \textit{otherwise} \end{cases} \tag{B.10}$$

The Levi-Civita symbol is that it can be written in terms of Kronecker Deltas

$$\epsilon^{\alpha_0\alpha_1\cdots\alpha_{n-1}} = \begin{vmatrix} \delta_0^{\alpha_0} & \delta_0^{\alpha_1} & \cdots & \delta_0^{\alpha_{n-1}} \\ \delta_1^{\alpha_0} & \delta_1^{\alpha_1} & \cdots & \delta_1^{\alpha_{n-1}} \\ \vdots & \vdots & \ddots & \vdots \\ \delta_{n-1}^{\alpha_0} & \delta_{n-1}^{\alpha_1} & \cdots & \delta_{n-1}^{\alpha_{n-1}} \end{vmatrix} . \tag{B.11}$$

A relevant quantity to determine is $\epsilon^{\alpha\beta\gamma\delta} g_{\delta\sigma} \epsilon^{\mu\nu\rho\sigma}$, where $g_{\delta\sigma}$ is the component of the metric tensor. We observed that

$$\epsilon^{\alpha\beta\gamma\delta} g_{\delta\sigma} \epsilon^{\mu\nu\rho\sigma} = \epsilon^{\alpha\beta\gamma\delta} g_{\delta\sigma} \epsilon_{\mu'\nu'\rho'}{}^{\sigma} g^{\mu'\mu} g^{\nu'\nu} g^{\rho'\rho} = \epsilon^{\alpha\beta\gamma\delta} \epsilon_{\mu'\nu'\rho'\delta} g^{\mu'\mu} g^{\nu'\nu} g^{\rho'\rho} , \tag{B.12}$$

Now, by employing the definition of the Levi-Civita symbol in terms of a determinant with Kronecker deltas

$$\begin{aligned} \epsilon^{\alpha\beta\gamma\delta} \epsilon_{\mu'\nu'\rho'\delta} &= \left| \begin{pmatrix} \delta_0^\alpha & \delta_1^\alpha & \delta_2^\alpha & \delta_3^\alpha \\ \delta_0^\beta & \delta_1^\beta & \delta_2^\beta & \delta_3^\beta \\ \delta_0^\gamma & \delta_1^\gamma & \delta_2^\gamma & \delta_3^\gamma \\ \delta_0^\delta & \delta_1^\delta & \delta_2^\delta & \delta_3^\delta \end{pmatrix} \begin{pmatrix} \delta_{\mu'}^0 & \delta_{\nu'}^0 & \delta_{\rho'}^0 & \delta_\delta^0 \\ \delta_{\mu'}^1 & \delta_{\nu'}^1 & \delta_{\rho'}^1 & \delta_\delta^1 \\ \delta_{\mu'}^2 & \delta_{\nu'}^2 & \delta_{\rho'}^2 & \delta_\delta^2 \\ \delta_{\mu'}^3 & \delta_{\nu'}^3 & \delta_{\rho'}^3 & \delta_\delta^3 \end{pmatrix} \right| \\ &= \begin{vmatrix} \delta_{\mu'}^\alpha & \delta_{\nu'}^\alpha & \delta_{\rho'}^\alpha & \delta_\delta^\alpha \\ \delta_{\mu'}^\beta & \delta_{\nu'}^\beta & \delta_{\rho'}^\beta & \delta_\delta^\beta \\ \delta_{\mu'}^\gamma & \delta_{\nu'}^\gamma & \delta_{\rho'}^\gamma & \delta_\delta^\gamma \\ \delta_{\mu'}^\delta & \delta_{\nu'}^\delta & \delta_{\rho'}^\delta & 4 \end{vmatrix} = \delta_{\mu'}^\delta \begin{vmatrix} \delta_{\nu'}^\alpha & \delta_{\rho'}^\alpha & \delta_\delta^\alpha \\ \delta_{\nu'}^\beta & \delta_{\rho'}^\beta & \delta_\delta^\beta \\ \delta_{\nu'}^\gamma & \delta_{\rho'}^\gamma & \delta_\delta^\gamma \end{vmatrix} - \delta_{\nu'}^\delta \begin{vmatrix} \delta_{\mu'}^\alpha & \delta_{\rho'}^\alpha & \delta_\delta^\alpha \\ \delta_{\mu'}^\beta & \delta_{\rho'}^\beta & \delta_\delta^\beta \\ \delta_{\mu'}^\gamma & \delta_{\rho'}^\gamma & \delta_\delta^\gamma \end{vmatrix} + \delta_{\rho'}^\delta \begin{vmatrix} \delta_{\mu'}^\alpha & \delta_{\nu'}^\alpha & \delta_\delta^\alpha \\ \delta_{\mu'}^\beta & \delta_{\nu'}^\beta & \delta_\delta^\beta \\ \delta_{\mu'}^\gamma & \delta_{\nu'}^\gamma & \delta_\delta^\gamma \end{vmatrix} \\ &\quad - 4 \begin{vmatrix} \delta_{\mu'}^\alpha & \delta_{\nu'}^\alpha & \delta_{\rho'}^\alpha \\ \delta_{\mu'}^\beta & \delta_{\nu'}^\beta & \delta_{\rho'}^\beta \\ \delta_{\mu'}^\gamma & \delta_{\nu'}^\gamma & \delta_{\rho'}^\gamma \end{vmatrix} \\ &= \delta_{\mu'}^\delta \epsilon^{\alpha\beta\gamma} \epsilon_{\nu'\rho'\delta} - \delta_{\nu'}^\delta \epsilon^{\alpha\beta\gamma} \epsilon_{\mu'\rho'\delta} + \delta_{rho'}^\delta \epsilon^{\alpha\beta\gamma} \epsilon_{\mu'\nu'\delta} - 4\epsilon^{\alpha\beta\gamma} \epsilon_{\mu'\nu'\rho'} \\ &= \epsilon^{\alpha\beta\gamma} \epsilon_{\nu'\rho'\mu'} - \epsilon^{\alpha\beta\gamma} \epsilon_{\mu'\rho'\nu'} + \epsilon^{\alpha\beta\gamma} \epsilon_{\mu'\nu'\rho'} - 4\epsilon^{\alpha\beta\gamma\delta} \epsilon_{\mu'\nu'\rho'} = -\epsilon^{\alpha\beta\gamma} \epsilon_{\mu'\nu'\rho'} , \end{aligned}$$

therefore

$$\epsilon^{\alpha\beta\gamma\delta} g_{\delta\sigma} \epsilon^{\mu\nu\rho\sigma} = -\epsilon^{\alpha\beta\gamma} \epsilon_{\mu'\nu'\rho'} g^{\mu'\mu} g^{\nu'\nu} g^{\rho'\rho} . \tag{B.13}$$

The term $\epsilon^{\alpha\beta\gamma}\epsilon_{\mu'\nu'\rho'}$ can be expressed in terms of products of Kronecker Deltas, using the expressions of the determinants

$$\begin{aligned}\epsilon^{\alpha\beta\gamma}\epsilon_{\mu'\nu'\rho'} &= \left|\begin{pmatrix}\delta^\alpha_0 & \delta^\beta_0 & \delta^\gamma_0\\ \delta^\alpha_1 & \delta^\beta_1 & \delta^\gamma_1\\ \delta^\alpha_2 & \delta^\beta_2 & \delta^\gamma_2\end{pmatrix}\right|\left|\begin{pmatrix}\delta^0_{\mu'} & \delta^0_{\nu'} & \delta^0_{\rho'}\\ \delta^1_{\mu'} & \delta^1_{\nu'} & \delta^1_{\rho'}\\ \delta^2_{\mu'} & \delta^2_{\nu'} & \delta^2_{\rho'}\end{pmatrix}\right| = \left|\begin{pmatrix}\delta^\alpha_0 & \delta^\alpha_1 & \delta^\alpha_2\\ \delta^\beta_0 & \delta^\beta_1 & \delta^\beta_2\\ \delta^\gamma_0 & \delta^\gamma_1 & \delta^\gamma_2\end{pmatrix}\begin{pmatrix}\delta^0_{\mu'} & \delta^0_{\nu'} & \delta^0_{\rho'}\\ \delta^1_{\mu'} & \delta^1_{\nu'} & \delta^1_{\rho'}\\ \delta^2_{\mu'} & \delta^2_{\nu'} & \delta^2_{\rho'}\end{pmatrix}\right| \\ &= \begin{vmatrix}\delta^\alpha_{\mu'} & \delta^\alpha_{\nu'} & \delta^\alpha_{\rho'}\\ \delta^\beta_{\mu'} & \delta^\beta_{\nu'} & \delta^\beta_{\rho'}\\ \delta^\gamma_{\mu'} & \delta^\gamma_{\nu'} & \delta^\gamma_{\rho'}\end{vmatrix} = \delta^{\alpha\beta\gamma}_{\mu'\nu'\rho'}(\textit{Generalized Kronecker delta}) \\ &= \delta^\alpha_{\mu'}\delta^\beta_{\nu'}\delta^\gamma_{\rho'} - \delta^\alpha_{\mu'}\delta^\gamma_{\nu'}\delta^\beta_{\rho'} + \delta^\beta_{\mu'}\delta^\gamma_{\nu'}\delta^\alpha_{\rho'} - \delta^\beta_{\mu'}\delta^\alpha_{\nu'}\delta^\gamma_{\rho'} + \delta^\gamma_{\mu'}\delta^\alpha_{\nu'}\delta^\beta_{\rho'} - \delta^\gamma_{\mu'}\delta^\beta_{\nu'}\delta^\alpha_{\rho'}\,.\end{aligned}$$

Now, since the antisymmetrization of a tensor $\begin{pmatrix}p\\ q\end{pmatrix}$ in $k$ contravariant indices is defined in its components by

$$A^{[m_1m_2\cdots m_k]m_{k+a}\cdots m_p}_{n_1n_2\cdots n_q} = \frac{1}{k!}\sum_{\sigma(m_1m_2\cdots m_k)}(-1)^{\operatorname{sgn}\sigma}A^{\sigma(m1)\sigma(m_2)\cdots\sigma(m_k)m_{k+1}\cdots m_p}_{n_1n_2\cdots n_q}\,, \tag{B.14}$$

where $\operatorname{sgn}\sigma$ is the sign of the permutation of the given indices. In the case of three indices we have

$$\delta^{[\alpha}_{\mu'}\delta^\beta_{\nu'}\delta^{\gamma]}_{\rho'} = \frac{1}{3!}\left(\delta^\alpha_{\mu'}\delta^\beta_{\nu'}\delta^\gamma_{\rho'} - \delta^\alpha_{\mu'}\delta^\gamma_{\nu'}\delta^\beta_{\rho'} + \delta^\beta_{\mu'}\delta^\gamma_{\nu'}\delta^\alpha_{\rho'} - \delta^\beta_{\mu'}\delta^\alpha_{\nu'}\delta^\gamma_{\rho'} + \delta^\gamma_{\mu'}\delta^\alpha_{\nu'}\delta^\beta_{\rho'} - \delta^\gamma_{\mu'}\delta^\beta_{\nu'}\delta^\alpha_{\rho'}\right)\,.$$

From the above in the equation (B.13) we can write

$$\epsilon^{\alpha\beta\gamma\delta}g_{\delta\sigma}\epsilon^{\mu\nu\rho\sigma} = -\epsilon^{\alpha\beta\gamma}\epsilon_{\mu'\nu'\rho'}g^{\mu'\mu}g^{\nu'\nu}g^{\rho'\rho} = -3!\delta^{[\alpha}_{\mu'}\delta^\beta_{\nu'}\delta^{\gamma]}_{\rho'}g^{\mu'\mu}g^{\nu'\nu}g^{\rho'\rho}\,. \tag{B.15}$$

# Appendix C

## C.1 Differential Cross-section in Compton scattering

In a $2 \to 2$ scattering process, the differential cross-section is determined by

$$d^6\sigma = \frac{1}{4\sqrt{(k\cdot p)^2 - m_k^2 m_p^2}} |\mathcal{M}|^2 d^6 Lips(s, k', p') \,, \tag{C.1}$$

where $k^\mu$ and $p^\mu$ are the 4-momentum components of the initial particles in the scattering process, and $k'^\mu$ and $p'^\mu$ are the 4-momentum components of the two particles after the scattering process. Furthermore, $m_k$ is the mass of the particle with 4-momentum $k$, while $m_p$ is the mass of the particle with 4-momentum $p$. We also have the square of the invariant amplitude $\mathcal{M}$ of the process in question. In this expression there appears the differential Lorentz invariant phase space element.

$$d^6 Lips(s, k', p') = (2\pi)^4 \delta^{(4)}(k + p - k' - p') \frac{d^3\mathbf{k}'}{(2\pi)^3 2k'_0} \frac{d^3\mathbf{p}'}{(2\pi)^3 2p'_0} \,, \tag{C.2}$$

here $s := (k+p)^2$, with $k'^\mu = (k'^0 = k'_0, \mathbf{k}')$ and $p'^\mu = (p'^0 = p'_0, \mathbf{p}')$ [1]. In the Compton scattering process, $k'^\mu$ and $p'^\mu$ are the $4$-momentum of the photon and $p'^\mu$ the $4$-momentum of the scattering particle at the end. Additionally $m_k$ = 0 (photons are massless particles). Observe that the $4$-dimensional Dirac Delta in Eq.(C.2) contains the conservation of $4$-momentum, that is, the energy conservation and linear momentum in the process, then the cross-section $\sigma$ can be obtained by integrating over phase space since the invariant amplitude $\mathcal{M}$ is a function depending on the $4$-momenta $p^\mu, k^\mu, p'^\mu$ and $k'^\mu$ when integrating with the Dirac delta, must be evaluated taking into account the conservation of $4$-momentum in the process. Then without loss of information, you can do the integral over the phase space. Noting that $\delta^{(4)}(k + p - k' - p') = \delta^{(3)}(\mathbf{k} + \mathbf{p} - \mathbf{k}' - \mathbf{p}')\delta(k_0 + p_0 - k'_0 - p'_0)$ integrates easily into $\mathbf{p}'$;

$$d^3 Lips = \frac{1}{(2\pi)^2 4k'_0 p'_0} \delta(k_0 + p_0 - k'_0 - p'_0) d^3\mathbf{k}' \,. \tag{C.3}$$

Using spherical coordinates in momentum space $\mathbf{k}'$, we have that $d^3\mathbf{k}' = |\mathbf{k}'|^2 d|\mathbf{k}'| d\Omega$, where $d\Omega$ is the solid angle element. Since $k'^\mu$ is the $4$-momentum of a photon propagating in a "vacuum", it satisfies the dispersion relation $k'^2 = k'_\mu k'^\mu = k'^2_0 - |\mathbf{k}'|^2 = 0$, so $k'_0 = |\mathbf{k}'|$, so in the expression given in (C.3) we can integrate and apply the following Dirac Delta property within the integral, where it is taken into account that $d^3 Lips(s, k', p')$ is a Lorentz invariant when integrating.

$$\delta[f(|\mathbf{k}'|)] = \frac{\delta(|\mathbf{k}'| - k'_0)}{\left| \frac{df}{d|\mathbf{k}'|} \right|_{\mathbf{k}' = k'_0}} \,.$$

[1] It is usual in the literature to use the components as a notation to refer to the $4$-moment, which is understood by the context.

If we do the integral in the center of mass system (center of moments, $|\mathbf{p}'| = |\mathbf{k}'|$), given that ${p'}_0 = \sqrt{|\mathbf{p}'|^2 + m_e^2}$;

$$\delta(k_0 + p_0 - k'_0 - p'_0) = \delta\left(k_0 + p_0 - |\mathbf{k}'| - \sqrt{|\mathbf{k}'|^2 + m_p^2}\right) .$$

Let $f(|\mathbf{k}'|) = k_0 + p_0 - |\mathbf{k}'| - |\sqrt{|\mathbf{k}'|^2 + m_e^2}$, we find that

$$\left|\frac{df}{d|\mathbf{k}'|}\bigg|_{\mathbf{k}'=k'_0}\right| = \left|1 + \frac{|\mathbf{k}'|}{\sqrt{|\mathbf{k}'|^2 + m_e^2}}\bigg|_{\mathbf{k}'=k'_0}\right| = \left|\frac{\sqrt{|\mathbf{k}'|^2 + m_e^2}k'_0 + |\mathbf{k}'|k'_0}{\sqrt{|\mathbf{k}'|^2 + m_e^2}k'_0}\right| = \frac{p'_0k'_0 + |\mathbf{k}'||\mathbf{k}'|}{p'_0k'_0}$$
$$= \frac{p'_0k'_0 + |\mathbf{p}'||\mathbf{k}'|}{p'_0k'_0} = \frac{p'_0k'_0 - \mathbf{p}'\cdot\mathbf{k}'}{p'_0k'_0} = \frac{p'\cdot k'}{p'_0k'_0} .$$

Note that even before the last line in the series of equalities we work with a particular result, but at the end the form of the expression is established in any inertial reference frame [2]. Then, for the case of study

$$\delta(k_0 + p_0 - k'_0 - p'_0) = \frac{p'_0k'_0\delta(|\mathbf{k}'| - k'_0)}{p'\cdot k'} . \tag{C.4}$$

Taking the above into account, by applying the Dirac delta property to the integral, the phase space element is reduced to

$$d^2Lips = \frac{1}{(2\pi)^2 4k'_0p'_0}\frac{p'_0k'_0}{p'\cdot k'}{k'}_0^2 d\Omega = \frac{{k'}_0^2}{(2\pi)^2 4(p'\cdot k')}d\Omega . \tag{C.5}$$

Thus, the differential cross-section for the Compton scattering process is given by

$$\frac{d^2\sigma}{d\Omega} = \frac{1}{64\pi^2}\frac{1}{(p\cdot k)}\frac{{k'}_0^2}{(k'\cdot p')}\overline{|\mathcal{M}|^2} , \tag{C.6}$$

or equivalently, by taking the account that $p\cdot k = k'\cdot p'$;

$$\frac{d^2\sigma}{d\Omega} = \frac{1}{64\pi^2}\frac{{k'}_0^2}{(p\cdot k)^2}\overline{|\mathcal{M}|^2} , \tag{C.7}$$

where $\overline{|\mathcal{M}|^2}$ indicates that the unpolarized or unpolarized process has been taken into account, and therefore is averaged over the possible polarizations of the particles involved, in addition to that conservation of 4-momentum is used. Note that it has been possible to integrate because $\mathcal{M}$ is an invariant.

[2] Sometimes when only working on the center of mass system it is not necessary to generalize, also in some articles erroneously $d^3Lips = \frac{1}{(2\pi)^2 4k'_0p'_0}\delta(k_0 + p_0 - k'_0 - p'_0)d^3\mathbf{k}' = \frac{1}{(2\pi)^2 4k'_0p'_0}(p_0 - k'_0 - p'_0)^2 d\Omega = \frac{k'_0}{(2\pi)^2 4p'_0}d\Omega$ is used, ignoring the important role played by $p'_0$ in the integration.

## C.2 Mean optical depth and mean free path of radiation

The probability that the photon travels at least one optical depth $\tau_\nu$ is $e^{-\tau_\nu}$. Therefore, the average optical depth traveled must be calculated as

$$\langle \tau_\nu \rangle := \int_0^\infty t_\nu e^{-\tau_\nu} d\tau_\nu = 1\,. \tag{C.8}$$

Then, the average distance a photon can travel without being absorbed, denoted as the mean free path $\langle i_\nu \rangle$, is determined by

$$\langle \tau_\nu \rangle = n\sigma_\nu \langle l_\nu \rangle = 1\,, \tag{C.9}$$

where $n$ is the number density of scattering particle and $\sigma_\nu$ is the cross-section for scattering process. Therefore the **mean free path** is defined by

$$i = \langle l_\nu \rangle := \frac{1}{n\sigma_\nu}\,. \tag{C.10}$$

## C.3 Mathematica code

In this part we present the code used to explore the possibility of evading the divergence of the differential cross-section in the studied process.

```
\[Beta] = 0.01;
a = (1 - \[Beta]^2)^(-1/2);
NumberForm[a, 15]
Eph = 1.168*10^(-3);
ma = 10^(-6);
b = Eph/ma;
NumberForm[b, 15]

Clear[U2]

U2[a_, b_, \[Theta]1_, \[Theta]_, \[Beta]_] :=
 1 - 2 a b ((1 - \[Beta] Cos[\[Theta]]) (1 - \[Beta] \
Cos[\[Theta]1])/((1 - \[Beta] Cos[\[Theta]1]) + (b/a) (1 -
           Cos[\[Theta]1 - \[Theta]])))

U2AlwaysPositiveQ[\[Theta]_] :=
 Resolve[ForAll[\[Theta]1, 0 <= \[Theta]1 <= 2 Pi,
   U2[a, b, \[Theta]1, \[Theta], \[Beta]] > 0], Reals]

(* Find the values of \[Theta] for which U2 is always positive *)
positiveThetaValues =
  Select[Range[0, 2 Pi, 0.1], U2AlwaysPositiveQ[#] &];
```

```
(* Show results *)
If[Length[positiveThetaValues] == 0,
 Print["There are no values of \[Theta] for which U2 is always positive."],
 Print["Values of \[Theta] for which U2 is always positive:",
  positiveThetaValues]]

Clear[U2]

U2[a_, b_, \[Theta]1_, \[Theta]_, \[Beta]_] :=
 1 - 2 a b ((1 - \[Beta] Cos[\[Theta]]) (1 - \[Beta] \
Cos[\[Theta]1])/((1 - \[Beta] Cos[\[Theta]1]) + (b/a) (1 -
           Cos[\[Theta]1 - \[Theta]])))

(* Plot cross sections of U2 as a function of \[Theta]1 and \[Theta] *)
Manipulate[
 Plot[U2[a, b, \[Theta]1, \[Theta], \[Beta]], {\[Theta]1, 0, 2 Pi},
  PlotRange -> {-1, 1},
  PlotLabel -> Row[{"\[Theta] = ", \[Theta]}]], {\[Theta], 0, 2 Pi,
  Pi/10}]
```

# Bibliography


[1] Sabine Schindler. $\omega$ m—different ways to determine the matter density of the universe. In *Matter in the Universe: Proceedings of an ISSI Workshop 19–23 March 2001, Bern, Switzerland*, pages 299–309. Springer, 2002.

[2] Particle Data Group, RL Workman, VD Burkert, V Crede, E Klempt, U Thoma, L Tiator, K Agashe, G Aielli, BC Allanach, et al. Review of particle physics. *Progress of theoretical and experimental physics*, 2022(8):083C01, 2022.

[3] Maria Krawczyk, Dorota Sokołowska, Paweł Swaczyna, and Bogumiła Świeżewska. Constraining inert dark matter by r $\gamma\gamma$ and wmap data. *Journal of High Energy Physics*, 2013(9):1–20, 2013.

[4] Steven Weinberg. A new light boson? *Physical Review Letters*, 40(4):223, 1978.

[5] Frank Wilczek. Problem of strong p and t invariance in the presence of instantons. *Physical Review Letters*, 40(5):279, 1978.

[6] Jihn E Kim and Gianpaolo Carosi. Axions and the strong c p problem. *Reviews of Modern Physics*, 82(1):557, 2010.

[7] Laurence F Abbott and P Sikivie. A cosmological bound on the invisible axion. *Physics Letters B*, 120(1-3):133–136, 1983.

[8] Michael Dine and Willy Fischler. The not-so-harmless axion. *Physics Letters B*, 120(1-3):137–141, 1983.

[9] George R Blumenthal, SM Faber, Joel R Primack, and Martin J Rees. Formation of galaxies and large-scale structure with cold dark matter. *Nature*, 311(5986):517–525, 1984.

[10] Alexander Vilenkin and E Paul S Shellard. *Cosmic strings and other topological defects*. Cambridge University Press, 1994.

[11] Gordon Kane. *Modern Elementary Particle Physics: Explaining and Extending the Standard Model*. Cambridge University Press, 2017.

[12] Cliff Burgess and Guy Moore. *The standard model: A primer*. Cambridge University Press, 2007.

[13] W Noel Cottingham and Derek A Greenwood. *An introduction to the standard model of particle physics*. Cambridge university press, 2007.

[14] Patrick Janot and Stanisław Jadach. Improved bhabha cross section at lep and the number of light neutrino species. *Physics Letters B*, 803:135319, 2020.

[15] James D Wells. The once and present standard model of elementary particle physics. In *Discovery Beyond the Standard Model of Elementary Particle Physics*, pages 51–69. Springer, 2020.

[16] Yoshiyuki Fukuda, T Hayakawa, E Ichihara, K Inoue, K Ishihara, Hirokazu Ishino, Y Itow, T Kajita, J Kameda, S Kasuga, et al. Evidence for oscillation of atmospheric neutrinos. *Physical review letters*, 81(8):1562, 1998.

[17] Jean Iliopoulos. Physics beyond the standard model. *arXiv preprint arXiv:0807.4841*, 2008.

[18] Carlo Giunti and Chung W Kim. *Fundamentals of neutrino physics and astrophysics*. Oxford university press, 2007.

[19] Georges Aad, Tatevik Abajyan, B Abbott, J Abdallah, S Abdel Khalek, Ahmed Ali Abdelalim, R Aben, B Abi, M Abolins, OS AbouZeid, et al. Observation of a new particle in the search for the standard model higgs boson with the atlas detector at the lhc. *Physics Letters B*, 716(1):1–29, 2012.

[20] Cms Collaboration et al. Observation of a new boson at a mass of 125 gev with the cms experiment at the lhc. *arXiv preprint arXiv:1207.7235*, 2012.

[21] Ta-Pei Cheng and Ling-Fong Li. *Gauge theory of elementary particle physics*. Oxford university press, 1994.

[22] Jorge C Romao and Joao P Silva. A resource for signs and feynman diagrams of the standard model. *International Journal of Modern Physics A*, 27(26):1230025, 2012.

[23] Palash B Pal. *An introductory course of particle physics*. Taylor & Francis, 2014.

[24] Sally Dawson, Christoph Englert, and Tilman Plehn. Higgs physics: It ain't over till it is over. *Physics Reports*, 816:1–85, 2019.

[25] Gerald S Guralnik, C Richard Hagen, and Thomas WB Kibble. Broken symmetries and the goldstone theorem. *Advances in particle physics*, 2:567–708, 1968.

[26] Gino Isidori. Flavor physics and cp violation. *arXiv preprint arXiv:1302.0661*, 2013.

[27] Matthew D Schwartz. *Quantum field theory and the standard model*. Cambridge university press, 2014.

[28] OF PARITY. Question of parity conservation in weak interactions [56hl. *Selected Papers (1945-1980) Of Chen Ning Yang (With Commentary)*, 36:189, 2005.

[29] Lev Landau. On the conservation laws for weak interactions. *Nuclear Physics*, 3(1):127–131, 1957.

[30] Giles David Barr, P Buchholz, R Carosi, D Coward, D Cundy, N Doble, L Gatignon, V Gibson, P Grafström, R Hagelberg, et al. A new measurement of direct cp violation in the neutral kaon system. *Physics Letters B*, 317(1-2):233–242, 1993.

[31] LK Gibbons, AR Barker, RA Briere, G Makoff, V Papadimitriou, JR Patterson, B Schwingenheuer, SV Somalwar, YW Wah, B Winstein, et al. Measurement of the cp-violation parameter re $(\epsilon'/\epsilon)$. *Physical Review Letters*, 70(9):1203, 1993.

[32] Planck Collaboration. Aghanim n et al. 2018 planck 2018 results. vi. cosmological parameters. In *Journal of Physics: Conference Series*, volume 1390, page 012048, 2019.

[33] Julian B Muñoz and Abraham Loeb. A small amount of mini-charged dark matter could cool the baryons in the early universe. *Nature*, 557(7707):684–686, 2018.

[34] Ikaros I Bigi and A Ichiro Sanda. Cp violation, 2001.

[35] Samoil M Bilenky, C Giunti, and W Grimus. Long-baseline neutrino oscillation experiments and cp violation in the lepton sector. *Physical Review D*, 58(3):033001, 1998.

[36] EM Purcell and NF Ramsey. On the possibility of electric dipole moments for elementary particles and nuclei. *Physical Review*, 78(6):807, 1950.

[37] Norman F Ramsey. Earliest criticisms of assumed p and t symmetries. In *AIP Conference Proceedings*, volume 270, pages 179–183. American Institute of Physics, 1991.

[38] WW Havens Jr, II Rabi, and LJ Rainwater. Interaction of neutrons with electrons in lead. *Physical Review*, 72(7):634, 1947.

[39] Enrico Fermi and L Marshall. On the interaction between neutrons and electrons. *Physical Review*, 72(12):1139, 1947.

[40] Tsung-Dao Lee and Chen Ning Yang. Elementary particles and weak interactions. Technical report, Brookhaven National Lab.(BNL), Upton, NY (United States), 1957.

[41] W Pauli. Exclusion principle, lorentz group, and reversal of space-time and charge. *Niels Bohr and the Development of Physics, W. Pauli (ed.) New York: Pergamon*, 1955.

[42] Hilary Greaves and Teruji Thomas. On the cpt theorem. *Studies in History and Philosophy of Science Part B: Studies in History and Philosophy of Modern Physics*, 45:46–65, 2014.

[43] Gerard t Hooft. Symmetry breaking through bell-jackiw anomalies. *Physical Review Letters*, 37(1):8–11, 1976.

[44] Anson Hook. Tasi lectures on the strong cp problem and axions. *arXiv preprint arXiv:1812.02669*, 2018.

[45] Steven Weinberg. The $u(1)_a$ problem. *Physical Review D*, 11(12):3583, 1975.

[46] Stephen L Adler. Axial-vector vertex in spinor electrodynamics. *Physical Review*, 177(5):2426, 1969.

[47] John Stewart Bell and Roman W Jackiw. A pcac puzzle: $\pi^0 \to \gamma\gamma$ in the $\sigma$-model. *Nuovo cimento*, 60(CERN-TH-920):47–61, 1969.

[48] William A Bardeen. Anomalous ward identities in spinor field theories. *Physical Review*, 184(5):1848, 1969.

[49] Benjamin P Abbott, Richard Abbott, TDe Abbott, MR Abernathy, Fausto Acernese, Kendall Ackley, Carl Adams, Thomas Adams, Paolo Addesso, RX Adhikari, et al. Observation of gravitational waves from a binary black hole merger. *Physical review letters*, 116(6):061102, 2016.

[50] Joshua D Simon. The faintest dwarf galaxies. *Annual Review of Astronomy and Astrophysics*, 57:375–415, 2019. https://arxiv.org/abs/1901.05465.

[51] Paolo Salucci. The distribution of dark matter in galaxies. *The Astronomy and Astrophysics Review*, 27:1–60, 2019. https://arxiv.org/abs/1811.08843.

[52] Steven W Allen, August E Evrard, and Adam B Mantz. Cosmological parameters from observations of galaxy clusters. *Annual Review of Astronomy and Astrophysics*, 49:409–470, 2011. https://arxiv.org/abs/1103.4829.

[53] Vera C Rubin and W Kent Ford Jr. Rotation of the andromeda nebula from a spectroscopic survey of emission regions. *Astrophysical Journal, vol. 159, p. 379*, 159:379, 1970.

[54] CB Netterfield, Peter AR Ade, James J Bock, JR Bond, J Borrill, A Boscaleri, K Coble, CR Contaldi, BP Crill, P De Bernardis, et al. A measurement by boomerang of multiple peaks in the angular power spectrum of the cosmic microwave background. *The Astrophysical Journal*, 571(2):604, 2002.

[55] Vinicius Miranda, Mariana Carrillo González, Elisabeth Krause, and Mark Trodden. Finding structure in the dark: Coupled dark energy, weak lensing, and the mildly nonlinear regime. *Physical Review D*, 97(6):063511, 2018.

[56] Adam G Riess, Alexei V Filippenko, Peter Challis, Alejandro Clocchiatti, Alan Diercks, Peter M Garnavich, Ron L Gilliland, Craig J Hogan, Saurabh Jha, Robert P Kirshner, et al. Observational evidence from supernovae for an accelerating universe and a cosmological constant. *The astronomical journal*, 116(3):1009, 1998.

[57] Ewa L Łokas and Gary A Mamon. Dark matter distribution in the coma cluster from galaxy kinematics: breaking the mass–anisotropy degeneracy. *Monthly Notices of the Royal Astronomical Society*, 343(2):401–412, 2003.

[58] G Kauffmann, Simon DM White, and B Guiderdoni. The formation and evolution of galaxies within merging dark matter haloes. *Monthly Notices of the Royal Astronomical Society*, 264(1):201–218, 1993.

[59] Yong Du, Fei Huang, Hao-Lin Li, Yuan-Zhen Li, and Jiang-Hao Yu. Revisiting dark matter freeze-in and freeze-out through phase-space distribution. *Journal of Cosmology and Astroparticle Physics*, 2022(04):012, 2022.

[60] Kimberly K Boddy, Mariangela Lisanti, Samuel D McDermott, Nicholas L Rodd, Christoph Weniger, Yacine Ali-Haïmoud, Malte Buschmann, Ilias Cholis, Djuna Croon, Adrienne L Erickcek, et al. Snowmass2021 theory frontier white paper: Astrophysical and cosmological probes of dark matter. *Journal of High Energy Astrophysics*, 35:112–138, 2022.

[61] WB Lin, DH Huang, X Zhang, and R Brandenberger. Nonthermal production of weakly interacting massive particles and the subgalactic structure of the universe. *Physical Review Letters*, 86(6):954, 2001.

[62] S Nussinov. Technocosmology—could a technibaryon excess provide a "natural" missing mass candidate? *Physics Letters B*, 165(1-3):55–58, 1985.

[63] Kathryn M Zurek. Asymmetric dark matter: theories, signatures, and constraints. *Physics Reports*, 537(3):91–121, 2014.

[64] James S Bullock and Michael Boylan-Kolchin. Small-scale challenges to the $\lambda$cdm paradigm. *Annual Review of Astronomy and Astrophysics*, 55:343–387, 2017. https://arxiv.org/abs/1707.04256.

[65] Julio F Navarro, Aaron Ludlow, Volker Springel, Jie Wang, Mark Vogelsberger, Simon DM White, Adrian Jenkins, Carlos S Frenk, and Amina Helmi. The diversity and similarity of simulated cold dark matter haloes. *Monthly Notices of the Royal Astronomical Society*, 402(1):21–34, 2010.

[66] WJG De Blok et al. The core-cusp problem. *Advances in Astronomy*, 2010, 2010.

[67] JAMES Bullock. Notes on the missing satellites problem. *Local Group Cosmology*, 20:95, 2013.

[68] Mark R Lovell, Violeta Gonzalez-Perez, Sownak Bose, Alexey Boyarsky, Shaun Cole, Carlos S Frenk, and Oleg Ruchayskiy. Addressing the too big to fail problem with baryon physics and sterile neutrino dark matter. *Monthly Notices of the Royal Astronomical Society*, 468(3):2836–2849, 2017.

[69] David N Spergel and Paul J Steinhardt. Observational evidence for self-interacting cold dark matter. *Physical review letters*, 84(17):3760, 2000.

[70] Justin I Read. The local dark matter density. *Journal of Physics G: Nuclear and Particle Physics*, 41(6):063101, 2014. https://arxiv.org/abs/1404.1938.

[71] Philip J Humphrey, David A Buote, Claude R Canizares, Andrew C Fabian, and Jon M Miller. A census of baryons and dark matter in an isolated, milky way sized elliptical galaxy. *The Astrophysical Journal*, 729(1):53, 2011.

[72] Paolo Salucci, Fabrizio Nesti, Gianfranco Gentile, and C Frigerio Martins. The dark matter density at the sun's location. *Astronomy & Astrophysics*, 523:A83, 2010.

[73] Riccardo Catena and Piero Ullio. A novel determination of the local dark matter density. *arXiv preprint arXiv:0907.0018*, 2009.

[74] Markus Weber and Wim de Boer. Determination of the local dark matter density in our galaxy. *Astronomy & Astrophysics*, 509:A25, 2010.

[75] Fabio Iocco, Miguel Pato, Gianfranco Bertone, and Philippe Jetzer. Dark matter distribution in the milky way: microlensing and dynamical constraints. *Journal of Cosmology and Astroparticle Physics*, 2011(11):029, 2011.

[76] Paul J McMillan. Mass models of the milky way. *Monthly Notices of the Royal Astronomical Society*, 414(3):2446–2457, 2011.

[77] Til Piffl, Cecilia Scannapieco, James Binney, Matthias Steinmetz, R-D Scholz, Mary EK Williams, Roelof S De Jong, Georges Kordopatis, Gal Matijevič, Olivier Bienayme, et al. The rave survey: the galactic escape speed and the mass of the milky way. *Astronomy & Astrophysics*, 562:A91, 2014. https://arxiv.org/abs/1309.4293.

[78] Lina Necib, Mariangela Lisanti, and Vasily Belokurov. Inferred evidence for dark matter kinematic substructure with sdss–gaia. *The Astrophysical Journal*, 874(1):3, 2019.

[79] Nassim Bozorgnia, Francesca Calore, Matthieu Schaller, Mark Lovell, Gianfranco Bertone, Carlos S Frenk, Robert A Crain, Julio F Navarro, Joop Schaye, and Tom Theuns. Predictions of hydrodynamic simulations for direct dark matter detection. In *Journal of Physics: Conference Series*, volume 718, page 042007. IOP Publishing, 2016.

[80] Anne M Green. Astrophysical uncertainties on the local dark matter distribution and direct detection experiments. *Journal of Physics G: Nuclear and Particle Physics*, 44(8):084001, 2017. https://arxiv.org/abs/1703.10102.

[81] Chris Kelso, Christopher Savage, Monica Valluri, Katherine Freese, Gregory S Stinson, and Jeremy Bailin. The impact of baryons on the direct detection of dark matter. *Journal of Cosmology and Astroparticle Physics*, 2016(08):071, 2016.

[82] Nassim Bozorgnia, Francesca Calore, Matthieu Schaller, Mark Lovell, Gianfranco Bertone, Carlos S Frenk, Robert A Crain, Julio F Navarro, Joop Schaye, and Tom Theuns. Simulated milky way analogues: implications for dark matter direct searches. *Journal of Cosmology and Astroparticle Physics*, 2016(5):024, 2016.

[83] Jonathan D Sloane, Matthew R Buckley, Alyson M Brooks, and Fabio Governato. Assessing astrophysical uncertainties in direct detection with galaxy simulations. *The Astrophysical Journal*, 831(1):93, 2016.

[84] Amina Helmi, Carine Babusiaux, Helmer H Koppelman, Davide Massari, Jovan Veljanoski, and Anthony GA Brown. The merger that led to the formation of the milky way's inner stellar halo and thick disk. *Nature*, 563(7729):85–88, 2018.

[85] N Wyn Evans, Ciaran AJ O'Hare, and Christopher McCabe. Refinement of the standard halo model for dark matter searches in light of the gaia sausage. *Physical Review D*, 99(2):023012, 2019. https://arxiv.org/abs/1810.11468.

[86] Michio Kaku. *Quantum field theory: a modern introduction*. Oxford University Press, 1993.

[87] EC Marino. Chern-simons theory from first principles. 1994.

[88] RJ Crewther, P Di Vecchia, G Veneziano, and Edward Witten. Chiral estimate of the electric dipole moment of the neutron in quantum chromodynamics. *Physics Letters B*, 88(1-2):123–127, 1979.

[89] Heinz Pagels. Dynamical chiral symmetry breaking in quantum chromodynamics. *Physical Review D*, 19(10):3080, 1979.

[90] CA Baker, DD Doyle, P Geltenbort, K Green, MGD Van der Grinten, PG Harris, P Iaydjiev, SN Ivanov, DJR May, JM Pendlebury, et al. Improved experimental limit on the electric dipole moment of the neutron. *Physical review letters*, 97(13):131801, 2006.

[91] John Ellis and Mary K Gaillard. Strong and weak cp violation. *Nuclear Physics B*, 150:141–162, 1979.

[92] Marco Serone. Notes on quantum field theory. *Lecture notes from SISSA*, 2015.

[93] Ann Nelson. Naturally weak cp violation. *Physics Letters B*, 136(5-6):387–391, 1984.

[94] Stephen M Barr. Solving the strong cp problem without the peccei-quinn symmetry. *Physical Review Letters*, 53(4):329, 1984.

[95] Kaluza Theodor. Zum unitätsproblem in der physik. *Sitzungsber. Preuss. Akad. Wiss. Berlin.(Math. Phys.)*, 1921:966–972, 1921.

[96] Roberto D Peccei and Helen R Quinn. Cp conservation in the presence of pseudoparticles. *Physical Review Letters*, 38(25):1440, 1977.

[97] Roberto D Peccei and Helen R Quinn. Constraints imposed by cp conservation in the presence of pseudoparticles. *Physical Review D*, 16(6):1791, 1977.

[98] M Sivertz, J Lee-Franzini, JE Horstkotte, C Klopfenstein, RD Schamberger Jr, LJ Spencer, PM Tuts, T Böhringer, P Franzini, K Han, et al. Upper limit for axion production in radiative $\upsilon$ decay. *Physical Review D*, 26(3):717, 1982.

[99] Y Asano, M Miyajima, E Kikutani, S Sugimoto, Y Nagashima, S Kurokawa, T Miyachi, Y Yoshimura, and T Shinkawa. Search for a rare decay mode $k^+ \to \pi^+\nu\nu$ approximately and axion. *Phys. Lett. B*, 107:159–162, 1981.

[100] TW Donnelly, SJ Freedman, RS Lytel, RD Peccei, and M Schwartz. Do axions exist? *Physical Review D*, 18(5):1607, 1978.

[101] Roberto D Peccei, Tai Tsun Wu, and Tsutomu Yanagida. A viable axion model. *Physics Letters B*, 172(3-4):435–440, 1986.

[102] Lawrence M Krauss and Frank Wilczek. A short-lived axion variant. *Physics Letters B*, 173(2):189–192, 1986.

[103] R Eichler, L Felawka, N Kraus, C Niebuhr, HK Walter, S Egli, R Engfer, Ch Grab, EA Hermes, HS Pruys, et al. Limits for short-lived neutral particles emitted in $\mu$+ or $\pi$+ decay. *Physics Letters B*, 175(1):101–104, 1986.

[104] M Davier, J Jeanjean, and H Nguyen Ngoc. Search for axion-like particles in electron bremsstrahlung. *Physics Letters B*, 180(3):295–298, 1986.

[105] Jihn E Kim. Weak-interaction singlet and strong cp invariance. *Physical Review Letters*, 43(2):103, 1979.

[106] Mikhail A Shifman, AI Vainshtein, and Valentin I Zakharov. Can confinement ensure natural cp invariance of strong interactions? *Nuclear Physics B*, 166(3):493–506, 1980.

[107] David J Gross, Robert D Pisarski, and Laurence G Yaffe. Qcd and instantons at finite temperature. *Reviews of Modern Physics*, 53(1):43, 1981.

[108] AR Zhitnitskij. On possible suppression of the axion-hadron interactions. *Yadernaya Fizika*, 31(2):497–504, 1980.

[109] Michael Dine, Willy Fischler, and Mark Srednicki. A simple solution to the strong cp problem with a harmless axion. *Physics letters B*, 104(3):199–202, 1981.

[110] Stefan Scherer and Matthias R Schindler. *A primer for chiral perturbation theory*, volume 830. Springer Science & Business Media, 2011.

[111] Howard Georgi and Lisa Randall. Flavor conserving cp violation in invisible axion models. *Nuclear Physics B*, 276(1):241–252, 1986.

[112] Marc Kamionkowski and John March-Russell. Planck-scale physics and the peccei-quinn mechanism. *Physics Letters B*, 282(1-2):137–141, 1992.

[113] Stephen M Barr and D Seckel. Planck-scale corrections to axion models. *Physical Review D*, 46(2):539, 1992.

[114] James Alvey and Miguel Escudero. The axion quality problem: global symmetry breaking and wormholes. *Journal of High Energy Physics*, 2021(1):1–28, 2021.

[115] Riccardo Penco. An introduction to effective field theories. *arXiv preprint arXiv:2006.16285*, 2020.

[116] Edward Witten. Some properties of o (32) superstrings. *Physics Letters B*, 149(4-5):351–356, 1984.

[117] Mark Srednicki. Axion couplings to matter:(i). cp-conserving parts. *Nuclear Physics B*, 260(3-4):689–700, 1985.

[118] Gian F Giudice, Riccardo Rattazzi, and Alessandro Strumia. Unificaxion. *Physics Letters B*, 715(1-3):142–148, 2012.

[119] David B Kaplan. Opening the axion window. *Nuclear Physics B*, 260(1):215–226, 1985.

[120] Luca Di Luzio, Federico Mescia, and Enrico Nardi. Window for preferred axion models. *Physical Review D*, 96(7):075003, 2017.

[121] Prateek Agrawal, Michael Nee, and Mario Reig. Axion couplings in grand unified theories. *Journal of High Energy Physics*, 2022(10):1–35, 2022.

[122] Daniel Aloni, Yotam Soreq, and Mike Williams. Coupling qcd-scale axionlike particles to gluons. *Physical Review Letters*, 123(3):031803, 2019.

[123] Asimina Arvanitaki, Savas Dimopoulos, Sergei Dubovsky, Nemanja Kaloper, and John March-Russell. String axiverse. *Physical Review D*, 81(12):123530, 2010.

[124] Michael S Turner. Thermal production of not so invisible axions in the early universe. Technical report, Fermi National Accelerator Lab., 1986.

[125] Eduard Masso, Francesc Rota, and Gabriel Zsembinszki. Axion thermalization in the early universe. *Physical Review D*, 66(2):023004, 2002.

[126] DH Lyth. Axions and inflation: Vacuum fluctuations. *Physical Review D*, 45(10):3394, 1992.

[127] Lawrence J Hall, Keisuke Harigaya, et al. Qcd axion dark matter with a small decay constant. *Physical review letters*, 120(21):211602, 2018.

[128] Masahiro Kawasaki, Eisuke Sonomoto, and Tsutomu T Yanagida. Cosmologically allowed regions for the axion decay constant fa. *Physics Letters B*, 782:181–184, 2018.

[129] Anupam Mazumdar, Saleh Qutub, and Ken'ichi Saikawa. Nonthermal axion dark radiation and constraints. *Physical Review D*, 94(6):065030, 2016.

[130] Paola Arias, Nicolas Bernal, Dimitrios Karamitros, Carlos Maldonado, Leszek Roszkowski, and Moira Venegas. New opportunities for axion dark matter searches in nonstandard cosmological models. *Journal of Cosmology and Astroparticle Physics*, 2021(11):003, 2021.

[131] Renata Kallosh, Andrei Linde, Dmitri Linde, and Leonard Susskind. Gravity and global symmetries. *Physical Review D*, 52(2):912, 1995.

[132] Olivier Wantz and EPS Shellard. Axion cosmology revisited. *Physical Review D*, 82(12):123508, 2010.

[133] Olivier Wantz. *The instanton liquid and the axion*. PhD thesis, University of Cambridge, 2010.

[134] Minos Axenides, Robert Brandenberger, and Michael Turner. Development of axion perturbations in an axion dominated universe. *Physics Letters B*, 126(3-4):178–182, 1983.

[135] Andrei D Linde. Generation of isothermal density perturbations in the inflationary universe. *Physics Letters B*, 158(5):375–380, 1985.

[136] Alexander Vilenkin and Allen E Everett. Cosmic strings and domain walls in models with goldstone and pseudo-goldstone bosons. *Physical Review Letters*, 48(26):1867, 1982.

[137] P Sikivie. Axions, domain walls, and the early universe. *Physical Review Letters*, 48(17):1156, 1982.

[138] Richard Lynn Davis. Goldstone bosons in string models of galaxy formation. *Physical Review D*, 32(12):3172, 1985.

[139] Pierre Sikivie. Experimental tests of the" invisible" axion. *Physical Review Letters*, 51(16):1415, 1983.

[140] Pierre Sikivie. Detection rates for "invisible"-axion searches. *Physical Review D*, 32(11):2988, 1985.

[141] Richard Bradley, John Clarke, Darin Kinion, Leslie J Rosenberg, Karl van Bibber, Seishi Matsuki, Michael Mück, and Pierre Sikivie. Microwave cavity searches for dark-matter axions. *Reviews of Modern Physics*, 75(3):777, 2003.

[142] Javier Redondo and Andreas Ringwald. Light shining through walls. *Contemporary Physics*, 52(3):211–236, 2011.

[143] SL Cheng, CQ Geng, and W-T Ni. Axion-photon couplings in invisible axion models. *Physical Review D*, 52(5):3132, 1995.

[144] Georg G Raffelt. Axions—motivation, limits and searches. *Journal of Physics A: Mathematical and Theoretical*, 40(25):6607, 2007.

[145] Attila Abramowski, Fabio Acero, F Aharonian, F Ait Benkhali, AG Akhperjanian, E Angüner, Gisela Anton, Shangkari Balenderan, Agnès Balzer, Anna Barnacka, et al. Constraints on axionl-ike particles with hess from the irregularity of the pks 2155- 304 energy spectrum. *Physical Review D*, 88(10):102003, 2013. https://arxiv.org/abs/1311.3148.

[146] M Ajello, A Albert, Brandon Anderson, L Baldini, G Barbiellini, D Bastieri, R Bellazzini, E Bissaldi, RD Blandford, ED Bloom, et al. Search for spectral irregularities due to photon–axionlike-particle oscillations with the fermi large area telescope. *Physical Review Letters*, 116(16):161101, 2016. https://arxiv.org/abs/1603.06978.

[147] David JE Marsh. Axions and alps: a very short introduction. *arXiv preprint arXiv:1712.03018*, 2017. https://arxiv.org/abs/1712.03018.

[148] Cun Zhang, Yun-Feng Liang, Shang Li, Neng-Hui Liao, Lei Feng, Qiang Yuan, Yi-Zhong Fan, and Zhong-Zhou Ren. New bounds on axionlike particles from the fermi large area telescope observation of pks 2155- 304. *Physical Review D*, 97(6):063009, 2018.

[149] Hai-Jun Li, Jun-Guang Guo, Xiao-Jun Bi, Su-Jie Lin, and Peng-Fei Yin. Limits on axionlike particles from mrk 421 with 4.5-year period observations by argo-ybj and fermi-lat. *Physical Review D*, 103(8):083003, 2021.

[150] Hai-Jun Li. Relevance of vhe blazar spectra models with axion-like particles. *Journal of Cosmology and Astroparticle Physics*, 2022(02):025, 2022.

[151] Christopher S Reynolds, MC David Marsh, Helen R Russell, Andrew C Fabian, Robyn Smith, Francesco Tombesi, and Sylvain Veilleux. Astrophysical limits on very light axion-like particles from chandra grating spectroscopy of ngc 1275. *The Astrophysical Journal*, 890(1):59, 2020.

[152] New cast limit on the axion–photon interaction. *Nature Physics*, 13(6):584–590, 2017. https://arxiv.org/abs/1705.02290.

[153] Adrian Ayala, Inma Domínguez, Maurizio Giannotti, Alessandro Mirizzi, and Oscar Straniero. Revisiting the bound on axion-photon coupling from globular clusters. *Physical review letters*, 113(19):191302, 2014.

[154] Eugene Feenberg and Henry Primakoff. Interaction of cosmic-ray primaries with sunlight and starlight. *Physical Review*, 73(5):449, 1948.

[155] TM Donahue. The significance of the absence of primary electrons for theories of the origin of the cosmic radiation. *Physical Review*, 84(5):972, 1951.

[156] MP Savedoff. The crab and cygnus a as gamma ray sources. *Il Nuovo Cimento (1955-1965)*, 13:12–18, 1959.

[157] JE Felten and P Morrison. Recoil photons from scattering of starlight by relativistic electrons. *Physical Review Letters*, 10(10):453, 1963.

[158] Barbara Ryden. *Introduction to cosmology*. Cambridge University Press, 2017.

[159] DG Cerdeno and AM Green. Particle dark matter: Observations, models and searches, 2010.

[160] Anton N Baushev. Principal properties of the velocity distribution of dark matter particles on the outskirts of the solar system. *Monthly Notices of the Royal Astronomical Society: Letters*, 417(1):L83–L87, 2011.

[161] AB Arbuzov, VV Bytev, EA Kuraev, E Tomasi-Gustafsson, and Yu M Bystritskiy. Radiative corrections to the bhabha scattering. *Physics of Particles and Nuclei*, 41:636–689, 2010.

[162] Stefano Actis, Pierpaolo Mastrolia, and Giovanni Ossola. Nlo qed corrections to hard-bremsstrahlung emission in bhabha scattering. *Physics Letters B*, 682(4-5):419–427, 2010.

[163] Ahmad Borzou, Gerald Cleaver, and Behrouz Mirza. Lorentz gauge theory of gravity in electron–positron colliders. *Classical and Quantum Gravity*, 34(22):225013, 2017.

[164] Jiang Min, Fang Zhen-Yun, Sang Wen-Long, and Gao Fei. Accurate calculation of the differential cross section of bhabha scattering with photon chain loops contribution in qed. *Chinese Physics Letters*, 23(10):2681, 2006.

[165] John David Jackson. Classical electrodynamics, 1999.

[166] Silvia Adrián-Martínez, Andreas Albert, Michel André, Marco Anghinolfi, G Anton, M Ardid, J-J Aubert, B Baret, J Barrios-Marti, S Basa, et al. Stacked search for time shifted high energy neutrinos from gamma ray bursts with the antares neutrino telescope. *The European Physical Journal C*, 77:1–10, 2017.

[167] Giovanni Grilli di Cortona and Enrico Nardi. Probing light mediators at the muone experiment. *Physical Review D*, 105(11):L111701, 2022.

[168] Nabila Aghanim, Yashar Akrami, Mark Ashdown, J Aumont, C Baccigalupi, M Ballardini, AJ Banday, RB Barreiro, N Bartolo, S Basak, et al. Planck 2018 results-vi. cosmological parameters. *Astronomy & Astrophysics*, 641:A6, 2020.

[169] CL Bennett, RS Hill, G Hinshaw, D Larson, KM Smith, J Dunkley, B Gold, M Halpern, N Jarosik, A Kogut, et al. Seven-year wilkinson microwave anisotropy probe (wmap) observations: Are there cosmic microwave background anomalies? *The Astrophysical journal supplement series*, 192(2):17, 2011.

[170] John C Mather, DJ Fixsen, RA Shafer, C Mosier, and DT Wilkinson. Calibrator design for the cobe far infrared absolute spectrophotometer (firas). *The Astrophysical Journal*, 512(2):511, 1999.